Albrecht Miletzky

Adding value to cellulose fibers by the addition of xylan

Doctoral Thesis
submitted at the
Technical University of Graz

for obtaining the academic degree of
Doctor of technology
(Dr.techn.)
Doctoral School of Process Engineering

Supervisor:
Ao.Univ.-Prof. Mag. Dr.rer.nat. Robert Schennach
Institute of Solid State Physics

Graz, October 30, 2014

Deutsche Fassung:
Beschluss der Curricula-Kommission für Bachelor-, Master- und Diplomstudien vom 10.11.2008
Genehmigung des Senates am 1.12.2008

EIDESSTATTLICHE ERKLÄRUNG

Ich erkläre an Eides statt, dass ich die vorliegende Arbeit selbstständig verfasst, andere als die angegebenen Quellen/Hilfsmittel nicht benutzt, und die den benutzten Quellen wörtlich und inhaltlich entnommenen Stellen als solche kenntlich gemacht habe.

Graz, am …… ……..
(Unterschrift)

Englische Fassung:

STATUTORY DECLARATION

I declare that I have authored this thesis independently, that I have not used other than the declared sources / resources, and that I have explicitly marked all material which has been quoted either literally or by content from the used sources.

…… ……..
date (signature)

Adding value to cellulose fibers by the addition of xylan

Albrecht Miletzky

Acknowledgements

The following thesis was carried out between November 2011 and October 2014 within the *"'Christian Doppler Laboratory for Surface Chemical and Physical Fundamentals of Paper Strength"'* at the Graz University of Technology (Austria).

At first, I want to gratefully thank **Prof. Dr. Robert Schennach** (Institute of Solid State Physics, Graz University of Technology) for the great possibility to work and write my doctoral thesis within this Christian Doppler Laboratory. He was an excellent mentor and inspired me with constructive advises and discussions and I have greatly benefited from him. Moreover, I would like to express my gratitude to **Prof. Dr. Wolfgang Bauer** (Institute of Paper, Pulp and Fibre Technology, Graz University of Technology) for his support and the opportunity to perform most of the experiments at his institute in a very familiar, pleasant, and cooperative environment.

I want to acknowledge the **Lenzing AG**, **Mondi Frantschach GmbH**, **Kelheim Fibres GmbH**, the **Austrian Federal Ministry of Economy, Family and Youth** and the **National Foundation for Research, Technology and Development** for their financial support.

I am indebted to **Dr. Andrea Borgards** and **Dr. Gabriele Schild** (Lenzing AG, Lenzing, Austria) as well as **Dr. Petra Wollboldt** (Kompetenzzentrum Holz GmbH, Linz, Austria) for their support and encouragement.

I owe a very important debt to the following people, who helped me and performed measurements:

- **Adelheid Bakshi**, **Manuela Hartner**, **Karin Holzer**, **Kerstin Roschitz**, and **Irmgard Windisch** (Institute of Paper, Pulp and Fibre Technology, Graz University of Technology), investigations and support in the laboratories of the institute,
- **Dr. Wolfgang Fischer** (Institute of Paper, Pulp and Fibre Technology, Graz University of Technology) being also a great colleague and friend, measurements of individual fiber-fiber joints,
- **Dr. Georg Koller** (Institute of Physics, University of Graz), investigations of the surface chemistry by XPS,

- **Regina Krasser** (Kompetenzzentrum Holz GmbH, St. Veit an der Glan, Austria), surface charge measurements,
- **Walter Millacher** and **Manuel Punz** (Lenzing AG, Lenzing, Austria), chemical analysis by HPLC,
- **Dr. Hansjörg Weber** (Institute for Organic Chemistry, Graz University of Technology), chemical analysis by NMR spectroscopy, and
- **Dr. Armin Zankel** (Institute for Electron Microscopy and Nanoanalysis, Graz University of Technology), investigations of the surface morphology by SEM methods.

I would particularly like to thank **Caterina Czibula**, **Christian Ganser**, and **Prof. Dr. Christian Teichert** (Institute of Physics, Montanuniversität Leoben, Austria) for the performance of AFM measurements and their persistent patience during the investigations.

I would like to offer my thanks to **Dr. Stefan Spirk** (Institute for Chemistry and Technology of Materials, Graz University of Technology) for the analyses via QCM-D and his comments and support.

I want to thank **Claudia Bäumel** and **Kerstin Schefzik** (Institute for Paper, Pulp and Fibre Technology, Graz University of Technology) as well as **Esther Schennach** for their help with administrative tasks. In addition, I thank **Harald Streicher** (Institute of Paper, Pulp and Fibre Technology, Graz University of Technology) for IT support.

I would like to show my appreciation to **Wolfgang Fuchs**, **Lukas Jagiello**, **Christian Lorbach**, **Wolfgang Pacher**, **Christian Probst**, **Matthias Trimmel**, and **Dr. Frederik Weber** for being great colleagues and friends.

Special thanks also to my friends for having a wonderful time in Graz and spending great adventures in the mountains and at the water—*Hang Loose!*

Last but not least, I owe my deepest gratitude to my family and girlfriend.

Graz, *A. Miletzky*
September 2014

Abstract

Xylan is one of the most abundant biopolymers in higher plants and wood. Hardwoods contain up to 35% of xylan. Compared to cellulose, xylans can exhibit a highly branched structure. During delignification and the production of pulp, lignin but also short-chained sugar polymers and part of the xylan present in the wood is being removed, which have a strong impact on the yield. In general, pulp and paper with a lower amount of xylan feature lower strength properties.

Xylan is able to take up water resulting in fiber swelling and an increased wet flexibility. This enables the fibers to conform to each other more easily leading to a higher amount fiber-fiber joints within a paper network. Due to the swelling behavior of xylan, larger areas in molecular contact can be achieved and additional coulomb force can be generated by the carboxylic groups present on the backbone of xylan. Thus, it is of great importance to achieve pulps with a high yield as well as to increase the value added chain of xylan by an enhanced material utilization.

The aim of this work was to treat various pulp samples with different xylans. In total, six variables were investigated regarding an efficient increase in the amount of xylan on the fibers. Moreover, the influence of additional xylan on strength properties of handsheets and individual fiber-fiber joints of the pulp samples were analyzed. Additionally, the quantitative and qualitative characterization of the distribution of xylan on the fiber surface was of great interest.

The amount of xylan of the fiber samples could be significantly increased during an adsorption step. However, an influence on strength properties of handsheets of xylan-treated pulp could not be observed. This may be due to the fact, that paper is a network. A network will always fail at its weakest point. Thus, xylan-enriched bonds between fibers could be present, but they may not be predominant to enhance strength properties. A statistical significant increase in the breaking load of individual fiber-fiber joints was noticed. In general, a higher force was needed to break fiber crossings of fibers with additional xylan. This is also influenced by the distribution of xylan on the fiber surface which is heterogeneous and nonuniform. Last but not least, the use of functionalized tips for atomic force microscopy has the advantage of generating a higher phase contrast between cellulose and xylan and to determine adhesive forces between the functionalized tip and the surface. Thus, it could be a key role in quantifying the bonding mechanisms within paper as well.

Kurzfassung

Xylan ist eines der am häufigsten vorkommenden Biopolymeren in höher entwickelten Pflanzen und Holz. Laubholz kann bis zu 35% Xylan aufweisen. Im Vergleich zu Cellulose können Xylane eine stark verzweigte Struktur aufweisen. Bei der Delignifizierung von Holz und Herstellung von Zellstofffasern werden neben Lignin auch anderer kurzkettige Zuckerpolymere sowie ein Teil des Xylans im Holz herausgelöst. Dies hat einen Ausbeuteverlust zur Folge. Des Weiteren weisen Zellstoffe mit einem geringeren Xylangehalt und daraus produzierte Papiere im Allgemeinen verringerte Festigkeitseigenschaften auf.

Xylan kann Wasser aufnehmen, was zu einer stärkeren Faserquellung und damit zu einer höheren Faserflexibilität führt. Dadurch können sich Fasern bei der Papierherstellung besser aneinander legen und die Anzahl von Faser-Faserbindungen steigern. Durch die Quellfähigkeit von Xylan können aber auch größere Flächen im molekularen Kontakt erzielt werden. Zusätzlich können wegen des Vorhandenseins von Carboxylgruppen Coulomb-Kräfte ausgebildet werden. Das Resultat sind stärkere Faser-Faserbindungen. Aus diesem Grund ist es von größter Bedeutung die Ausbeute nach der Zellstoffkochung zu erhöhen, aber auch die Wertschöpfungskette von Xylan durch eine gesteigerte stoffliche Nutzung zu erhöhen.

Ziel dieser Arbeit war es, verschiedene Zellstoffe mit unterschiedlichen Xylanen zu behandeln. Dabei wurden insgesamt sechs Einflussparameter auf die Xylananreicherung an den Faserstoffen untersucht, um einen möglichst effektiven Anstieg der Xylanmenge zu erzielen. Darüber hinaus wurde von diesen Zellstoffen der Einfluss von zusätzlichem Xylan auf die Festigkeitseigenschaften von Laborblättern sowie einzelnen Faser-Faserbindungen untersucht. Ein weiterer Schwerpunkt lag in der quantitativen und qualitativen Charakterisierung der Xylanverteilung auf der Faseroberfläche.

Der Xylangehalt der Zellstoffe konnte durch einen Adsorptionsschritt deutlich gesteigert werden. Jedoch konnte keine festigkeitssteigernde Wirkung an den hergestellten Laborblättern feststellt werden. Dies könnte auf das Fasernetzwerk selbst zurückzuführen sein. Es gibt sicherlich Faser-Faserbindungen, in denen Xylan eingearbeitet ist, jedoch versagt ein Netzwerk immer an der schwächsten Stelle, so dass diese Faser-Faserbindungen nicht in das Gewicht fallen. Bei der Bestimmung der Bindungsstärke von einzelnen Faser-Faserbindungen konnte hingegen

ein statistisch signifikanter Anstieg festgestellt werden. Bei den Faserstoffen mit einem gesteigerten Xylangehalt war tendenziell eine größere Kraft nötig, um Faser-Faserbindungen zu brechen. Allerdings ist dies auch von der Verteilung von adsorbierten Xylan auf der Faseroberfläche abhängig, welche sehr inhomogen und ungleichförmig ist. Die Verwendung von funktionalisierten Spitzen bei der Rasterkraftmikroskopie hat nicht nur den Vorteil eines höheren Phasenkontrastes zwischen Cellulose und Xylan sowie der Bestimmung der Adhäsionskraft zwischen der funktionalisierten Spitze und der Oberfläche, sondern könnte auch eine Schlüsselrolle in der Quantifizierung der Bindungsmechanismen im Papier spielen.

Contents

Abstract **vii**

Kurzfassung **viii**

1 Introduction **1**
1.1 Motivation . . . 2
1.2 CD Laboratory for paper strength . . . 2
1.3 Outline . . . 3
1.4 List of publications . . . 4

2 Background and State of Research **7**
2.1 Chemical composition of wood fibers . . . 8
2.1.1 Cellulose . . . 9
2.1.2 Hemicelluloses . . . 12
2.1.3 Lignin . . . 15
2.2 Anatomy of the cell wall structure . . . 16
2.2.1 Molecular models . . . 17
2.3 Xylan . . . 19
2.3.1 Reaction during chemical pulping . . . 19
2.3.2 Xylan adsorption . . . 21
2.3.3 Mechanism(s) of xylan deposition . . . 25
2.3.4 Location of adsorbed xylan . . . 27
2.3.5 Influence on fiber properties . . . 27
2.4 Bonding mechanisms within paper . . . 32

3 Materials and Methods **35**
3.1 Characterization of the pulp samples . . . 36
3.2 Composition of the xylan samples . . . 36
3.3 Adsorption experiments . . . 37
3.3.1 Overall process . . . 38
3.4 Chemical analysis . . . 40
3.4.1 Analysis via HPLC . . . 40
3.4.2 Analysis via ^{1}H NMR spectroscopy . . . 41

3.5 Xylan distribution on the surface . . . 42
3.5.1 IR spectroscopy . . . 42
3.5.2 XPS . . . 43
3.5.3 SEM . . . 44
3.5.4 AFM . . . 46
3.6 Pulp and paper properties . . . 51
3.6.1 Adsorption conditions . . . 51
3.6.2 Pulp properties . . . 52
3.6.3 Paper properties . . . 53
3.7 Fiber properties . . . 54
3.7.1 Bond strength on individual fiber-fiber joints . . . 54
3.7.2 Elastic modulus of single fibers . . . 56

4 Results and Discussion 61
4.1 Characterization of the pulp samples . . . 62
4.2 Chemical analysis . . . 63
4.2.1 Factors influencing xylan adsorption . . . 63
4.2.2 Comparison between HPLC and NMR . . . 68
4.3 Distribution of attached xylan . . . 70
4.3.1 Attenuated total reflection spectroscopy . . . 70
4.3.2 X-ray photoelectron spectroscopy . . . 72
4.3.3 Scanning electron microscopy . . . 74
4.3.4 Atomic force microscopy . . . 78
4.3.5 Summary . . . 89
4.4 Influence of xylan on pulp and paper properties . . . 90
4.4.1 Fiber charge . . . 90
4.4.2 Water retention value . . . 93
4.4.3 Strength properties . . . 98
4.5 Influence of xylan on properties of individual fibers . . . 105
4.5.1 Individual fiber-fiber joints . . . 105
4.5.2 Elastic modulus of individual fibers . . . 109
4.5.3 Summary . . . 113

5 Conclusion and Outlook 114
5.1 Conclusion . . . 115
5.2 Outlook . . . 116

References 118

Appendices 130
A High pressure liquid chromatography . . . 130
B Nuclear magnetic resonance spectroscopy . . . 133

C Infrared spectroscopy 135
D X-ray photoelectron spectroscopy 138
E Fiber charge 140
F QCM-D measurements 141
G Strength properties vs. sheet density 143
H Fiber-fiber joint 145

List of Figures **146**

List of Tables **149**

Chapter 1

Introduction

1.1 Motivation

Xylan is one of the most abundant biopolymers in higher plants and wood. During utilization of wood for the production of pulp and paper as well as man-made (viscose) fibers, part of the xylan present in the used wood source is removed from the wood matrix due to dissolution. The dissolved xylan is accumulating in the cooking liquor (chemical pulping) or in the alkaline environment before spinning of viscose fibers. In case of pulp fibers, the dissolution of xylan has an impact on the yield but also on the strength properties of paper which is in general decreasing at lower yields. Moreover, the porosity is increasing and defects are introduced within the fiber wall during chemical pulping which has an impact on single fiber properties.

Xylan is able to take up water, thus influencing the swelling behavior and wet flexibility of fibers. Thus, the indentation hardness is reduced (Ganser et al. 2014; Persson et al. 2013) and higher areas in molecular contact between adjacent fibers can be achiecht. Therefore, a suggested area of application of xylan is papermaking. Furthermore, instead of a thermal utilization of dissolved xylan, it is of interest to increase added value of xylan by material utilization.

Aim of this work was to add value to cellulose fibers by the addition of xylan. Therefore, pulp fibers were treated with aqueous solutions of two different xylans. Six variables (temperature, pH, salt concentration, pulp consistency, xylan input, and time) were analyzed regarding an efficient increase in the amount of xylan present on the fibers. Moreover, the influence of additional xylan on pulp and paper properties, such as tensile strength and tear resistance, were studied. Due to the fact that paper is a network of many fibers, the influence of xylan was investigated regarding the breaking load of individual fiber-fiber joints and on single fiber tensile strength to calculate the modulus of elasticity. This was done to avoid the complication of the fiber network. Last but not least, the quantitative and qualitative analysis of the distribution of adsorbed or precipitated xylan was of interest. Therefore

1.2 Christian Doppler Laboratory for paper strength

The scientific research of this thesis was done within the "Christian Doppler (CD) Laboratory for Surface Chemical and Physical Fundamentals of Paper Strength", which was established in 2007. The CD Laboratory is a collaboration between the Institute of Solid State Physics and the Institute of Paper-, Pulp- and Fiber Technology (Graz University of Technology, Austria), the Institute of Physics (Montanuniversität Leoben, Austria) and three industry partners, i.e. Lenzing AG (Lenz-

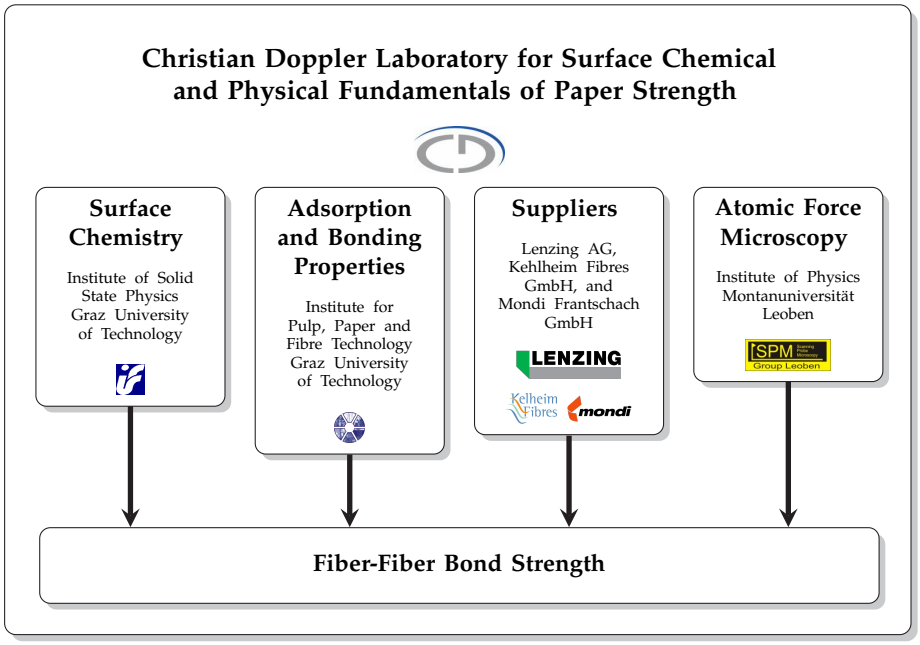

Figure 1.1 Distribution of responsibilities within the "Christian Doppler Laboratory for Surface Chemical and Physical Fundamentals of Paper Strength".

ing, Austria), Kelheim Fibres GmbH (Kelheim, Germany), and Mondi Frantschach GmbH (Frantschach-St. Gertraud, Austria). The individual tasks of the participating members and their joint synergy is shown in Figure 1.1.

Both, fiber and xylan samples were provided from the industry partners. The treatments of the fibers samples with xylan as well as the investigation of the morphology and strength of fiber-fiber bonds were performed at the Institute of Solid State Physics and the Institute of Paper-, Pulp- and Fiber Technology. Surface and bulk chemistry was determined at the Institute of Solid State Physics. The Institute of Physics was responsible for the detection of the surface morphology via atomic force microscopy.

The main intention of the CD Laboratory is the investigation of paper strength, i.e. to determine the characteristics of individual fibers and fiber-fiber joints to understand the various bonding mechanisms taking place between adjacent fibers in a paper network. It is also of interest to analyze the influence of charges and hemicelluloses, especially xylan, on fiber properties and their effect on bond strength. This helps to understand a variety of factors on the strength properties of paper.

1.3 Outline

Besides the introductory chapter, this thesis is divided into the following four chapters:

Chapter 2 *Background* gives an overview of the chemical composition and morphology of wood fibers which are the main resource for papermaking. Moreover, the behavior of xylan under pulping conditions is described found in the literature...

Chapter 3 *Materials and Methods* present the resources and methods used for the investigations for this work. The adsorption step of xylans on cellulosic materials, chemical composition of the samples, characterization of the surfaces, and the influence of addition xylan on fiber and paper properties are described.

Chapter 4 *Results and Discussion* presents the obtained results from the different investigations. They are compared to other results found in the literature and critically discussed.

Chapter 5 In *Conclusion and Outlook* the most important results are briefly discussed including examples for further work for this field of research.

1.4 List of publications

Papers

1) Miletzky, A., Punz, M., Zankel, A., Schlader, S., Ganser, C., Czibula, C., Teichert, C., Spirk, S., Zöhrer, S., Bauer, W., Schennach, R.: (2014). Modifying cellulose fibers by adsorption/precipitation of xylan, *Cellulose*. **21**(5): DOI: 10.1007/s10570-014-0472-3.

2) Miletzky, A., Fischer, W. J., Czibula, C., Teichert, C., Bauer, W., Schennach, R.: (2014). How xylan effects the breaking load of individual fiber-fiber joints and the single fiber tensile strength. *Cellulose*, submitted on 08.10.2014 (manuscript number CELS-D-14-00576).

Contribution to Conference Proceedings

1) Miletzky, A., Punz, M., Weber, H., Wollboldt, P., Krasser, R., Bauer, W., Schennach, R.: (2013). Improvement of paper strength by increasing the xylan content. In: *Advances in Pulp and Paper Research, Cambridge 2013, Trans XVth Fund. Res. Symp. Cambridge, UK, 2013 (S.J.I'Anson, ed.)*, pp. 887–906.

Contribution to Conference Proceedings, Book of Abstracts

1) Miletzky, A., Punz, M., Wollboldt, P., Krasser, R., Weber, H., Bauer, W., Schennach, R.: (2013). Adsorption of xylans onto softwood kraft pulp. In: *Minisymposium Verfahrenstechnik*, pp. 164–170 , April 18th, 2013, Leoben, Austria.

2) Czibula, C., Ganser, C., Miletzky, A., Spirk, S., Bauer, W., Schennach, R., Teichert, C.: (2014). Spatial localization of xylan on cellulose model films by AFM using functionalized tips. In: *Progress in Paper Physics Seminar*, #6007, September 8th, 2014, Raleigh, NC, USA.

Oral Presentations

1) Miletzky, A., Punz, M., Weber, H., Wollboldt, P., Bauer, W., Schennach, R.: (2012). Adsorption of xylan onto cellulosic surfaces. In: *European Paper Week*, November 13th, 2012, Brussels, Belgium.

2) Miletzky, A., Punz, M., Wollboldt, P., Krasser, R., Weber, H., Bauer, W., Schennach, R.: (2013). Adsorption of xylans onto softwood kraft pulp. In: *Minisymposium der Verfahrenstechnik*, April 18th, 2013, Leoben, Austria.

3) Miletzky, A., Punz, M., Weber, H., Wollboldt, P., Krasser, R., Bauer, W., Schennach, R.: (2013). Improvement of paper strength by increasing the xylan content. In: *15th Fundamental Research Symposium*, September 13th, 2013, Cambridge, UK.

4) Miletzky, A., Punz, M., Wollboldt, P., Krasser, R., Weber, H., Bauer, W., Schennach, R.: (2013). Adsorption of xylans onto softwood kraft pulp. In: *Minisymposium der Verfahrenstechnik*, April 18th, 2013, Leoben, Austria.

5) Czibula, C., Ganser, C., Miletzky, A., Spirk, S., Bauer, W., Schennach, R., Teichert, C.: (2014). Spatial localization of xylan on cellulose model films by AFM using functionalized tips. In: *Progress in Paper Physics Seminar*, September 8th, 2014, Raleigh, NC, USA.

6) Czibula, C., Ganser, C., Miletzky, A., Spirk, S., Schennach, R., Teichert, C.: (2014). Charakterisierung von Xylan auf amorphen Cellulose-Modellfilmen mittels Rasterkraftmikroskopiemethoden. In: *Österreichische Papierfachtagung*, June 5th, 2014, Graz, Austria.

Posters

1) Miletzky, A., Punz, M., Weber, H., Wollboldt, P., Bauer, W., Schennach, R.: (2012). *Adsorption of xylan onto bleached softwood fibers*. In: 62nd Annual Meeting of the Austrian Phyisical Society, September 19th, 2012, Graz, Austria.

2) Miletzky, A., Punz, M., Weber, H., Wollboldt, P., Bauer, W., Schennach, R.: (2013). *Adsorption of xylan onto softwood kraft pulp*. In: 9. Minisymposium der Verfahrenstechnik, April 18th, 2013, Leoben, Austria.

3) Miletzky, A., Punz, M., Weber, H., Krasser, R., Zankel, A., Ganser, C., Bauer, W., Schennach, R.: (2013). *Xylan adsorption onto cellulosic surfaces*. In: Advanced Material Science Day, October 24th, 2013, Graz, Austria.

4) Czibula, C., Ganser, C., Miletzky, A., Spirk, S., Schennach, R., Teichert, C.: (2014). *AFM studies of adsorbed xylan on amorphous cellulose films using functionalized tips*. In: 64nd Annual Meeting of the Austrian Phyisical Society, September 25th, 2014, Pöllau, Austria.

Chapter 2

Background and State of Research

2.1 Chemical composition of wood fibers

Softwood (*gymnosperms* or *conifers*) and hardwood trees (*angiosperms* or *dicotyledons*), are the main resources for the production of pulp and paper. Important representatives of softwoods are spruce and pine, and for hardwoods birch, beech, and eucalyptus. Wood contains various cell types, which fulfill different functions within the wood matrix, e.g. mechanical properties, conduction and storage functions (Fengel and Wenger 2003). In this thesis, the term *fiber* is used for either softwood tracheids or hardwood libriform fibers. Differences can be seen in their dimensions, as shown in Table 2.1.

Wood fibers are mainly built up of cellulose, hemicelluloses, and lignin. Moreover, they contain a certain amount of organic and inorganic extractives and minerals. Table 2.2 shows the average amount of wood components of some cellulose-containing species.

Table 2.1 Fiber dimensions of some wood species (extract of some data adopted from Fengel and Wenger (2003).

Species	Latin name	Length, mm	Width, µm
German spruce	*Abies alba*	3.4–4.6	25–65
Spruce	*Picea abies*	1.7–3.7	20–40
Pine	*Pinus sylvestris*	1.4–4.4	10–50
Beech	*Fagius sylvatica*	0.6–1.3	15–20
British oak	*Quercus robur*	0.3–1.6	10–30
Poplar	*Populus spec.*	0.7–1.6	20–40

Table 2.2 Main substances of some typical cellulose-containing materials (extract of some data adopted from Sixta (2006).

	Content, %		
Compound	Softwoods	Hardwoods	Cotton
Cellulose	40–44	43–47	95
Hemicelluloses	25–29	25–35	2
Lignin	25–31	16–24	1
Extract	1–5	2–8	0.4

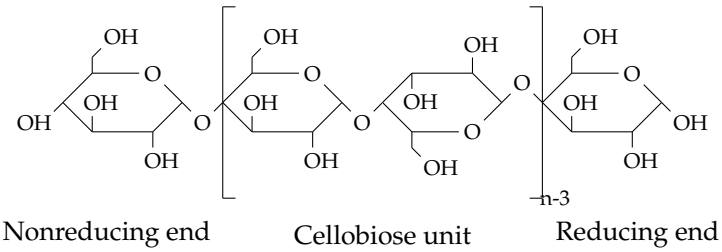

Figure 2.1 Part of the structure of the cellulose chain (replotted according to Sixta 2006).

2.1.1 Cellulose

Cellulose is present in all plants and forms the basic structure of the fiber cell wall. It is built up by glucose monomers, which are linked by β-(1,4)-glycosidic bonds. Due to the β-position, the following glucose unit needs a rotation of 180° at the axis between C1 and C4 forming cellobiose, the repeating unit of the molecular chain of cellulose with a length of 1.03 nm. The schematic structure of a cellulose molecule is shown in Figure 2.1. The rotation of each glucose base unit results in an elongated and unbranched chain of the cellulose molecule (Krässig 1993). An α-(1,4)-glycosidic bond would lead to a helical structure of the polymer, as it occurs with amylose in starch (Fengel and Wenger 2003).

There exist two possible conformations for the arrangement of the glucose unit. The chair conformation constitutes the lowest energy for bent hexagonal rings, e.g. pyranose. Compared to the boat conformation, the energy of the chair form is about 23.5 kJ/mol lower (Fengel and Wenger 2003). The hydroxyl groups may be positioned above and below the ring plane (axial conformation) or in the plane of the ring (equatorial conformation). The latter has the lower energy content hence it is most stable and predominant (Michell and Higgins 1965).

As presented in Figure 2.1, glucose is linked together to long chain molecules. The size of the chain molecule is commonly known as degree of polymerization (DP). Since the chain length varies between species and within the species, the cellulose chains exhibit a polydispersity. Cellulose in plants and woods has a DP of 7000–15000 (Fengel and Wenger 2003). However, chemical pulping or bleaching, where cellulose is exposed to an intensive chemical treatment, leads to a marked decrease of the DP-values (Sixta 2006).

2.1.1.1 Hydrogen bonds

The three hydroxyl groups in a glucose molecule are able to interact with each other or with other groups (e.g. *O*-, *N*-, and *S*-groups), forming hydrogen bonds. The interactions between the hydroxyl groups lead to stabilization and a certain stiffness

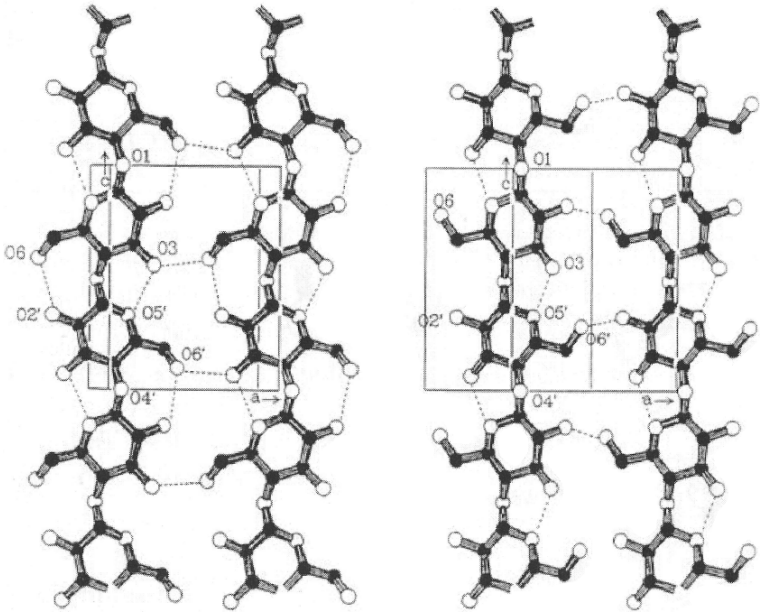

Figure 2.2 Inter- and intramolecular hydrogen bonds in cellulose I (left, according to Gardner and Blackwell 1974) and cellulose II (right, according to Kolpak and Blackwell 1976); adopted from Sixta (2006).

of the molecule. Moreover, these bonds are also responsible for the chemical and physical properties of cellulose (Fengel and Wenger 2003).

Two types of hydrogen bonds can be found in cellulose, *intermolecular* and *intramolecular* linkages (Gardner and Blackwell 1974; Kroon-Batenburg et al. 1986; Liang and Marchessault 1959; Nishiyama et al. 2002), as can be seen in Figure 2.2. Mainly two types of cellulose are present which is cellulose I and cellulose II. Cellulose I can be found in any plant and wood where cellulose II is regenerated or mercerized cellulose. Differences can be obtained in the orientation of the cellulose chains and in the free energy organization. In cellulose I the intramolecular bindings can takes place between the hydroxyl groups at C6 and C2′ of two adjacent glucose units with a bond length of 2.87 Å. A second hydrogen bond is formed between the hydroxyl group at C3 and the pyranose ring oxygen O5′ of the neighboring glucose molecule with a length of 2.75 Å. In cellulose II, the hydrogen bond between O3-H and O5′ has a length of 2.69 Å. These hydrongen bonds cause a relative stiffness and linear conformation of the cellulose chain. Intermolecular bonds on the other hand are linkages of hydroxyl groups between adjacent celluloses. These can be found between the hydroxyl groups at C6 and C3 forming supramolecular structures, such as *crystallites* or *fibrils*.

2.1.1.2 Supramolecular structure of cellulose

The hydrogen bonds between the cellulose chains provoke parallel and highly organized regions. These arrangements of crystallites and crystallite strands form the fundamental components of the supramolecular structure of cellulose, the so-called *micelles*. These regions are not accessible to water and resist the attack of diluted acid for a certain amount of time. The degree of crystallinity, measured by X-ray diffraction, was found for pulp fibers to be 60–70% (Thygesen et al. 2005), 68–79% for cotton (Wakelin et al. 1959), and 45% for viscose rayon (Hindeleh and Johnson 1974).

Disordered or *amorphous* domains can also be found within cellulose polymers, which are referred to as fringes. In these regions free hydroxyl groups are available, where water can be adsorbed leading to swelling of the cellulose. Due to the length of the cellulose chains, the molecules are involved in several crystallites by passing through intermediate amorphous regions.

2.1.1.3 Fibrillar structure of cellulose

The arrangement of the molecules results in the formation of fibrillar elements. Fibrils are highly organized associations of cellulose molecules, due to longitudinal oriented chains (parallel or antiparallel), but also consisting of disordered regions. Three basic principles are discussed in the literature, differing primarily in the formation of the amorphous regions within the fibrillar units (Fengel and Wenger 2003):

1) the longitudinal arranged molecules change from one ordered region to the subsequent one, the transition areas being the less ordered regions (fringed micelle system);
2) the fibrillar units are individual cords consisting of longitudinally arranged molecules and sequences of ordered and disordered regions;
3) the ordered regions are packages of chains folded in a longitudinal direction, the areas containing the turns between adjacent chain packages being the less ordered regions.

The fibrillar structure of cellulose can be characterized on basis of hierarchical levels of the fibrils. The high tendency of the cellulose chains to arrange themselves leading to a *paracrystalline* state results in the formation of elementary crystals with lengths of 10–20 nm for regenerate fibers and somewhat larger for cotton (Krässig 1968). These aggregates assemble to *elementary fibrils*, having lengths of 100 nm and cross-sections of 2 nm to 4 nm (Heyn 1966, 1969; Krässig 1993). Jayme and Koburg (1959) obtained differences in the fibrillar diameters in various pulp samples (10–

20 nm). Sullivan (1968) detected different sizes of the thickness (1.8–3.8 nm) of the fibrils in several pulps and holocellulose. In sulfate pulp a uniform distribution of the width of the fibrils was determined by Heyn (1977). The elementary fibils form *microfibrils* with diameters of about 10 to 25 nm (Frey-Wyssling 1954). The so-called *macrofibrils* are built up of microfibrils. The microfibrils are covered with lignin and hemicelluloses.

2.1.2 Hemicelluloses

Besides cellulose, hemicelluloses or polyoses, e.g. xylans, mannans, glucans, galactans, or pectins, are one of the most common native biopolymers in higher plants and wood. Xylans are the most frequent polyoses in wood and compose between 25% and 35% of the total mass (Ebringerová and Heinze 2000). Compared to cellulose, hemicelluloses are heteropolysaccharides and consist of various anhydrosugar units with a much lower DP, between 50 and 200 (Sixta 2006). The main chain (backbone) of the polymer can be made up of only one sugar unit (homopolymer), e.g. xylan, or two or more units (heteropolymer), such as glucomannans (Fengel and Wenger 2003). Different side groups are linked to the backbone at irregular distances, giving the polymer a branched structure. The sugar components of hemicelluloses can be classified into:

1) pentoses (β-D-xylose, α-L-arabinopyranose, and α-L-arabinofuranose);
2) hexoses (β-D-glucose, β-D-mannose, and α-D-galactose);
3) hexuronic acids (β-D-glucuronic acid, α-D-4-*O*-methylglucuronic acid and α-D-galacturonic acid);
4) deoxy-hexoses (α-L-rhamnose, and α-L-fucose).

2.1.2.1 Hardwood xylans

Hardwoods contain 10 to 35% of xylan (Sixta 2006). The DP of hardwood xylans vary from 100 to 200 (Fengel and Wenger 2003). In xylan the backbone is built up by xylose (Xyl) units, which are covalently linked by β-(1,4)-glycosidic bonds. Further, 4-*O*-methylglucuronic acid residues (MeGlcA) are irregularly attached to the backbone by α-(1,2)-glycosidic bonds forming the main hemicellulose component in hardwoods, 4-*O*-methyl-α-D-glucorono-D-xylan. The ratio of Xyl:MeGlcA of most of the extracted hardwood xylans is about 10:1. Native xylans also contain *O*-acetyl groups with a ratio of Xyl:acetyl of 1:0.5 to 1:0.6 and exhibit small amounts of rhamnose and galacturonic acid. Rhamnose and galacturonic acid are responsible for the alkali resistance of xylan molecules after splitting off the reducing end. Part of the chemical structure of an *O*-acetyl-4-*O*-methylglucuronoxylan is shown in Figure 2.3.

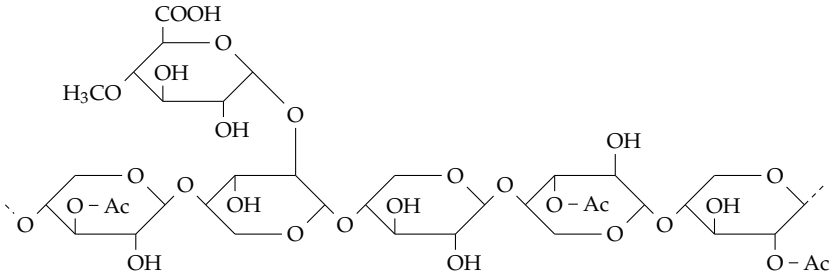

Figure 2.3 Part of the chemical structure of a hardwood *O*-acetyl-4-*O*-methylglucuronoxylan (replotted according to Fengel and Wenger 2003).

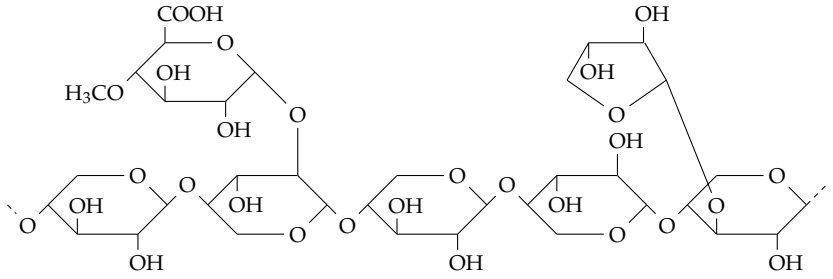

Figure 2.4 Part of the chemical structure of a softwood arabino-4-*O*-methylglucuronoxylan (replotted according to Fengel and Wenger 2003).

2.1.2.2 Hardwood mannans

Besides xylan, hardwoods also contain 3 to 5% of glucomannan. In contrast to xylan, hardwood mannans have a heteropolymer backbone consisting of mannose (Man) and glucose (Glu) monomers, linked by β-(1,4)-glycosidic bonds. The ratio of Man:Glu ranges from 1:1 to 2.3:1, depending on the type of wood. Further, the DP is about 60–70 (Fengel and Wenger 2003). Teleman et al. (2003) found, that aspen and birch glucomannans are slightly *O*-acetylated at C2 and C3 with a degree of approximately 0.3.

2.1.2.3 Softwood xylans

Softwood xylans constitute 7 to 10% of the wood dry matter. Compared to hardwoods, softwoods have a considerable quantity of (arabino)glucuronoxylan. The backbone is branched by α-L-arabinofuranose residues, which might also have a slight amount of *O*-acetyl groups. In addition, they are more heavily substituted by MeGlcA with a ratio of Xyl:MeGlcA of 5:1 to 6:1. The determination of the degree of polymerization of various softwood xylans resulted in a DP from 70 to 130 (Fengel and Wenger 2003). A segment of a softwood xylan is shown in Figure 2.4.

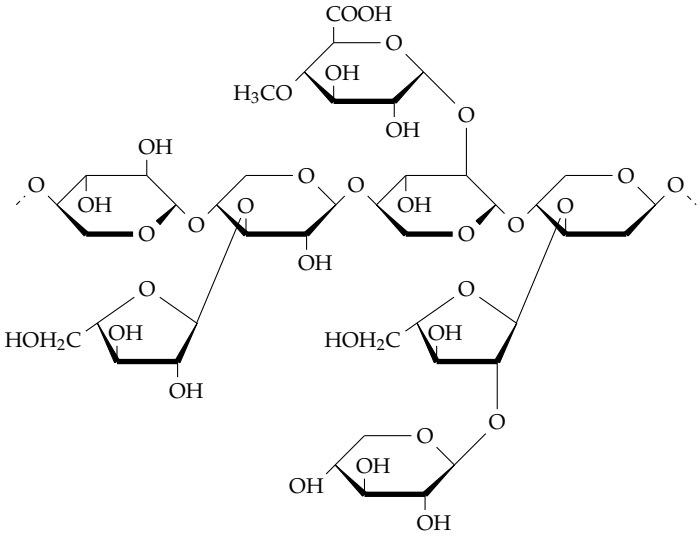

Figure 2.5 Schematic structure of barley husk xylan (4-*O*-methylglucuronoarabinoxylan) (replotted according to Höije et al. 2006).

2.1.2.4 Softwood mannans

Mannans are the main hemicellulose in softwoods with a content of 20 to 25%. The heterogeneous backbone has a randomly distributed ratio of Man:Glu of about 3:1 within the molecule. Moreover, it is branched by acetyl groups and galactose (Gal) units. Galactose is connected with the backbone by α-(1,6)-linkages. The amount of galactose varies in mannans from a ratio of Man:Glu:Gal of 3:1:1 in water-soluble and 3:1:0.2 in alkali-soluble galactoglucomannan (Ebringerová et al. 2005; Fengel and Wenger 2003; Sixta 2006).

2.1.2.5 Xylans in other plants

Xylan from annual plants, e.g. wheat, corn fiber, straw, or sugarcane bagasse, are more heterogeneous, than from wood. They are more heavily substituted by side groups. The schematic structure of barley husk xylan is shown in Figure 2.5. Birch wood xylan consists of 89.3% xylose, 1% arabinose, 1.4% glucose, and 8.3% anhydro-uronic acid (Kormelink and Voragen 1993). Wheat arabinoxylan on the other hand contains 65.8% xylose, 33.5% arabinose, 0.1% mannose, 0.1% galactose, and 0.3% glucose (Gruppen et al. 1992). Corn fiber xylan features one of the most complex structures containing β-(1,4)-linked xylose residues and contains 48–54% xylose, 33–35% arabinose, 5–11% galactose, and 3–6% glucuronic acid (Doner and Hicks 1997; Saha and Bothast 1999).

2.1.3 Lignin

Lignin is the third major and most abundant polymer in the cell wall of higher plants (e.g. *pteridophytes* and *spermatophytes*), where it occurs in the vascular tissue to provide liquid transport and mechanical strength properties. Lignin acts as a glue between the fibers and holds them together. Moreover, it has a fungicidal character, due to its hydrophobic nature. Lignin is a highly branched polymer with a random structure resulting from polymerization reactions of *p*-coumaryl (4-hydroxy-cinnamyl), coniferyl (3-methoxy-4-hydroxy-cinnamyl), and sinapyl (3,5-dimethoxy-4-hydroxy-cinnamyl) alcohol (Fengel and Wenger 2003).

During the polymerization of lignin in wood, it is also getting bonded on a network of fibrils consisting mainly of hemicelluloses present in the cell wall layers (Košiková et al. 1978). The lignin is covalently linked to carbohydrates forming network structures (Lawoko et al. 2004), also known as lignin-carbohydrate complexes (LCCs). Barakat et al. (2007) proposed that the formation of supramolecular structures of LCCs is influenced and controlled by local noncovalent interactions between lignin and carbohydrates. The inter-lignin bonds can be of benzyl ester type (Lundquist et al. 1980; Takahashi and Koshijima 1988a), benzyl ether type (Leary et al. 1983; Takahashi and Koshijima 1988b), and phenyl glycosidic linkages (Košiková et al. 1972). The β-*O*-4 bond is the predominant inter-lignin linkage (Lawoko et al. 2005), but the etherification can also take place at any hydroxy group to form e.g. 5-*O*- or 6-*O*-benzyl ethers (Leary et al. 1983). Lawoko et al. (2006) isolated four major LCC fractions from spruce wood: (1) galactoglucomannan LCC ($\approx 8\%$ of the wood lignin); (2) glucane LCC ($\approx 4\%$ of the wood lignin); (3) xylan-lignin-glucomannan network LCC (xylan $>$ glucomannan; $\approx 40\%$ of the wood lignin); and (4) glucomannan-lignin-xylan network LCC (glucomannan $>$ xylan; $\approx 48\%$ of the wood lignin). Lignin can also be linked to pectin or cellulose and further cross-links various polysaccharides to each other, e.g. xylan fractions with a high lignin content can induce self-assembly of xylan (Westbye et al. 2007). However, all these findings are based on extraction methods, which may affect the chemical and supramolecular structure of LCCs.

Chemical pulping (see section 2.3.1) also affects the network of LCCs resulting in major structural changes. Precipitated compounds from cooking liquor showed that neither lignin-free hemicellulose nor carbohydrate-free lignin was available (Simonson 1971a,b). At an early stage of the cook lignin is predominantly linked with xylan (birch wood) as well as xylan and glucomannan (beech wood). At the end of the cook, but also in more delignified kraft pulps, xylan is degraded and lignin is more linked with glucomannan (Lawoko et al. 2004). Futher, these LCCs undergo a partial condensation to form more high molecular mass material (Lawoko et al. 2005).

2.2 Anatomy of the cell wall structure

The three main compounds in wood are cellulose, hemicelluloses, and lignin. The distribution and arrangement of these polymers vary within the cell wall and give the fiber a layer construction. Regarding the chemical composition and the alignment of the cellulose fibrils to the longitudinal direction to the fiber, the cell wall consists of a texture of different layers (Meier and Wilkie 1959). The variations in the angle of microfibril orientation in the different cell wall layers provide a mechanical locking effect, resulting in a high stiffness of the fiber. The layers are called, *middle lamella* (ML), *primary wall* (P), *secondary wall*, which can be classified into three different regions (S1, S2, and S3), and *tertiary wall* (T) (Fengel and Wenger 2003). The tertiary wall layer separates the cell wall from the lumen and can be covered with a wart layer (W). A model of the cell wall structure is shown in Figure 2.6 (p. 17).

The middle lamella is a thin layer between neighboring fibers and not an integral part of the cell wall. It consists predominantly of lignin which glues the fibers together and prevents them of swelling as well as fungal decay. The term compound middle lamella can be also found in the literature, since single fibrils may cross the ML.

The primary wall is the first formed cell wall layer and has a thickness of about 0.1 µm. The amount of cellulose is limited, which is embedded in a matrix of hemicelluloses and pectin. The outer surface consists of loose aggregation of microfibrils, which are oriented more or less transverse to the longitudinal direction of the fiber. The arrangement of the fibrils is in thin crossing layers to allow the growth of a cell.

The narrow S1 wall is the first formed layer of the stiff secondary wall with a thickness from 0.12 to 0.35 µm and a crossed fibrillar texture which provides compression resistance. The microfibrils are helically arranged with an orientation from 50° to 70° relative to the cell axis. The S2 is the thickest layer (2–5 µm) and has a lamellar structure. The microfibrils are oriented with a high degree of parallelism and the angle varies from 10° to 30°. Up to 90% of the bulk of cell wall material is embedded in this layer. Thus, it contributes predominantly to the physical and mechanical properties of a fiber. The S3 wall is only present in parenchyma cells.

The tertiary wall is the last fibrillar layer of a fiber (0.1–0.14 µm) and separates the cell wall from the lumen. The fibrils are arranged in spiral patterns along the cell axis with an angle between 60° and 90°. This layer consists of a higher concentration of nonstructural substances. Sometimes, the luminal surface is covered with warts.

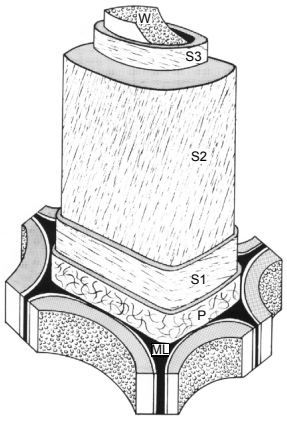

Figure 2.6 Model of the cell wall structure of wood fibers. ML = middle lamella, P = primary wall, S1 = secondary wall 1, S2 = secondary wall 2, S3 = secondary wall 3, W = wart layer (adopted from Smook 1982 labels are replotted).

The amount of the main components varies between the different cell wall layers (Luce 1964; Meier and Wilkie 1959). The ML and P wall consist mainly of lignin, due to its function as a glue between single fibers. Nevertheless, the highest amount of each chemical compound is located in the secondary wall, since it is the thickest cell wall layer. Figure 2.7 shows the chemical composition in the cell wall layers of a softwood fiber.

2.2.1 Molecular models of the cell wall ultrastructure

Looking at the internal cell wall structure of wood fibers, polyoses are connected with cellulose (Åkerholm and Salmén 2001; Atalla et al. 1993; Uhlin et al. 1995) but also with lignin forming LCCs. Studies via polarized infrared spectroscopy or electron microscopy observed longitudinal orientation of xylan molecules to the cellulose fibrils (Liang et al. 1960; Meier and Welck 1965; Ruel et al. 1976) with a lammellar arrangement (Kerr and Goring 1975). Therefore, polyoses are considered to act as a link between celulose and lignin in the supramolecular structure (Fengel et al. 1978). Several models are proposed in the literature to describe the molecular structure and association of the components within the cell wall. Figure 2.8 represents the model proposed by Fengel (1970), which shows the fibrillar units of cellulose enclosed by polyoses and lignin. The model from Kerr and Goring (1975) considers, that matrices of cellulose and hemicelluloses are partly surrounded in the radial and tangential direction by blocks of lignin and polyoses. However, both models take a close contact of polyoses with celluloses and lignin into consideration. The model proposed by Lawoko et al. (2005) depicts the association of the cell wall components, especially lignin, glucomannan, and xylan between two cellulose fibrils, as shown in Figure 2.9.

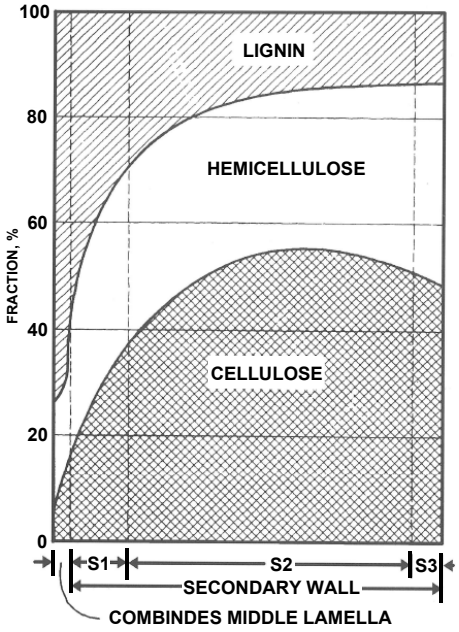

Figure 2.7 Distribution of the main chemicals in the cell wall layers of a softwood sample (adopted from Gullichsen and Paulapuro 2000.

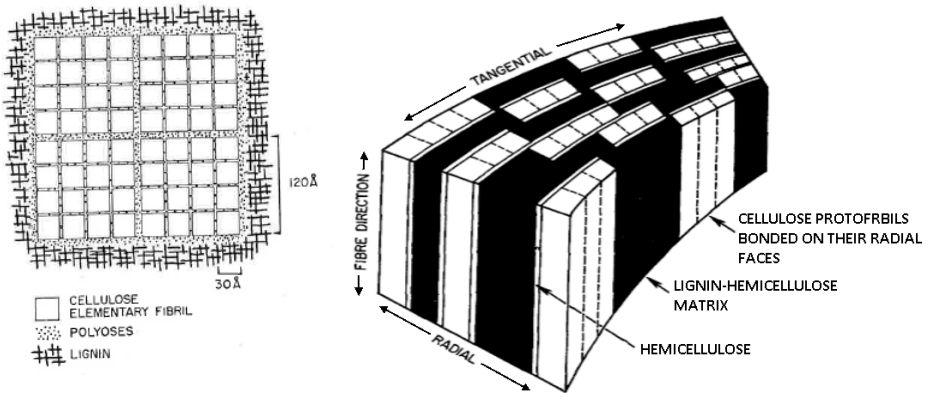

Figure 2.8 Models of the association of the cell wall components by: Fengel 1970 (left); Kerr and Goring 1975 (right).

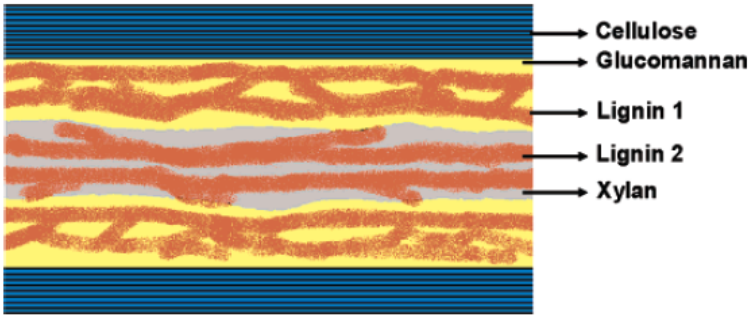

Figure 2.9 Model of the association of the cell wall components by Lawoko et al. (2005).

2.3 Xylan

As mentioned in section 2.1.2, xylan is the second most abundant polysaccharide in higher plants and wood. Chemical pulping is the predominant procedure to provide fibers for the production of paper. During the chemical attack, xylan undergoes several reactions, resulting in dissolution, degradation, and changes in the chemical structure. This affects the solubility of the molecule but also its behavior for redeposition and precipitation/adsorption on the fiber surface.

2.3.1 Reactions of xylan during chemical pulping

The main purpose of chemical pulping is the removal of the lignin-rich middle lamella and lignin from the different cell wall layers of the fiber. The decomposition of the middle lamella results in separation of the fibers from the composite without the need of mechanical disintegration (Sixta 2006). Due to the existence of LCCs and the nonselective removal of lignin during chemical pulping, carbohydrates, such as glucan, xylan, or mannan, are getting dissolved and degraded in the cooking liquor. Chemical pulping mainly differs in the chemical environment and the pH, alkaline or acid (Gullichsen and Paulapuro 2000; Sixta 2006).

2.3.1.1 Alkaline environment

Sulfate or *kraft pulping* is the most common procedure, taking place in a strong alkaline environment. The decomposition and removal of lignin starts from the lumen in direction to the fiber surface, resulting in a complete and intact primary layer of the fiber (Bachner et al. 1993; Gullichsen and Paulapuro 2000). However, considerable reactions of hemicelluloses occur, resulting in a large loss in yield.

The dissolution rate of carbohydrates, i.e. mostly xylose, increases at elevated temperature (above 140°C) during the heating-up period and reaches a maximum concentration at the end of this period, usually around 160–170°C (Axelsson et al. 1962; Simonson 1963, 1965). Further carbohydrates, such as mannose as well as small amounts of galactose and arabinose residues can be found in the warm-up phase (Simonson 1965). Compared to xylose, the dissolution of mannose takes place faster (Sjöström 1977) and the rapid removal even starts at temperatures below 100°C (Wigell et al. 2007). Moreover, Sjöström (1977) detected a ratio of the removal of lignin : nonlignin material of 1 : 3 for pine in this stage. In addition, a reduction in crystallinity of cellulose as well as a loss of disordered cellulose can be detected in the early stage of pulping (Newman et al. 1993). During the bulk phase, where cooking proceeds at constant temperature, alkaline degradation predominates, than dissolution, resulting in a decrease in the degree of polymerization

and chemical changes due to hydrolysis and peeling reactions (Simonson 1971a). This can be forced by higher alkali concentration (Berggren et al. 2003; Simão et al. 2005b). Different values for the decrease in the DP of xylan can be found in literature, depending on the source and the conditions during cooking: e.g. 160 to 40 (Axelsson et al. 1962), 130 to 80–90 (Croon and Enström 1962), or 119 to 70 (Meier 1962). Saarnio and Gustafsson (1953) recognized a stronger resistance of dissolved pentosans (xylan) against the chemical attack in a kraft cook, than hexosans (mannan) which is in conformity with the findings of Simonson (1963) and McIntosh (1963).

Besides dissolution and lowering the DP, splitting off and converting of side groups occur as well, changing the chemical structure of the molecule. Most of MeGlcA side groups are removed and transformed to hexuronic acid (HexA) residues by β-elimination (Buchert et al. 1995; Casebier and Hamilton 1967; Croon and Enström 1961; Hansson and Hartler 1968; Johansson and Samuelson 1977; Lisboa et al. 2005; Meier 1962; Simonson 1971a). The incomplete removal of MeGlcA groups is caused by the consumption of alkali, as cooking proceeds (Clayton 1963; Croon and Enström 1961). Simão et al. (2005a) found that around 87% of the dissolved MeGlcA was converted to HexA for *Eucalyptus globulus*, whereas for Scott pine, the loss of uronic acid groups was 60–70% (Croon and Enström 1962). The formation of HexA is stronger activated at higher temperatures and alkali charge (Buchert et al. 1995; Simão et al. 2005b). However, the amount of MeGlcA and HexA are higher for dissolved xylans than in pulp (Danielsson et al. 2006).

On the other hand, arabinose substitutes in the C3 position exhibit a resistance to peeling reactions and make the molecule stable in an alkaline environment (Aurell and Hartler 1965; Buchert et al. 1995). Galactose residues in cooking liquor possess a comparatively greater resistance to peeling (Bhaskaran and von Koeppen 1970). As hardwood xylans consist of a small portion of rhamnose and galacturonic acid, it was found that especially the (1,2)-linkage between these substitutes show a retarding effect against degradation after isomerization of the reducing xylose group (Johansson and Samuelson 1977). At the end of cook, mostly dissolved xylan can be detected in the liquor, due to its stability (Gellerstedt and Lindfors 1984).

Extensive modifications of dissolved xylan in the cooking liquor, changes of the chemical composition of the fibers, and a reduction of the alkali concentration of the cooking liquor result in resorption (or "retake") of part of the xylan on the fibers increasing the yield (Hansson and Hartler 1968; Jansson and Brännvall 2011; Kleinert 1966; Meller 1965; Wikström 1967). The amount of resorbed xylan in birch kraft pulps is estimated to represent 5–10% of the total xylan in pulp (Axelsson et al. 1962) or about 3% of the pulp (Clayton and Stone 1963). For pine kraft pulps, the amount has been claimed to be much higher and half of the xylan featured in pine

kraft pulp has been relocated (Yllner and Enström 1957). However, this value for pine kraft pulps is estimated to be too high (Meller 1965).

2.3.1.2 *Acidic environment*

Sulfite pulping is carried out in an acidic environment. Under acidic conditions, lignin becomes sulfonated making it hydrophilic and able to dissolve in the cooking liquor (Gullichsen and Paulapuro 2000). However, the higher removal of hemicelluloses in an acidic environment, except for galactoglucomannan, is the main disadvantage for this process, resulting in lower strength properties of paper as well (Sixta 2006).

The dissolution of hemicelluloses and other organic components from spruce starts in the early stage at temperatures around 100 °C (Eriksson and Samuelson 1962). The heterogeneous acid hydrolysis leads to a cleavage of glycosidic linkages, with the result that hemicelluloses and their DP are degraded more rapidly than cellulose. Arabinofuranosidic bonds are cleaved at the beginning of the sulfite cook, whereas glucuronic acid side groups retard hydrolysis (Meier 1962). He also observed that uronic acid remains nearly constant in spruce pulp, but will decrease when raising the pH, as it is the case for *bisulfite pulping* (Sjöström and Enström 1967). The removal of birch xylan was found to be more selective at yields below 50% (Pettersson and Rydholm 1961).

2.3.2 Xylan adsorption

During delignification, lignin and a part of the xylan is simultaneously dissolved in the cooking liquor. It is of great interest to decrease the dissolution of xylan and other carbohydrates in order to increase the yield after pulping but also to improve the properties of the fibers, e.g. strength characteristics (see section 2.3.5.2). Yllner and Enström (1956) for example showed, that cotton fibers, exposed to cooking liquor from birch sulfate, can take up part of the dissolved xylan. Under similar conditions, compared to cooking, cotton linters take up more xylan than CTMP[1] from spruce (Henriksson and Gatenholm 2002). In the following sections, the influence of several parameters on the adsorption/precipitation of xylan on the surface of cellulose fibers will be discussed in more detail.

2.3.2.1 *Influence of temperature and time*

The temperature has a strong influence on adsorption which is generally enhanced with increasing temperature (Ban and van Heiningen 2011; Clayton and Phelps

[1] Chemithermomechanical pulp

1965; Eriksson et al. 1963; Hansson 1970b; Hartler and Lund 1962; Henriksson and Gatenholm 2001; Köhnke and Gatenholm 2007; Linder et al. 2003; Mitikka-Eklund 1996; Ribe 2010; Silva et al. 2011; Yllner and Enström 1957). The adsorption of xylan onto cellulosic surfaces at room temperature was found to be very slow (Ström et al. 1982) and an euqilibrium was not even reached after 25 hours (Eriksson et al. 1963). At temperatures between 110–170°C, the sorption rate was highest at the beginning (after 10 min) and slowed down after 20 min (Hansson 1970b). At those temperatures, adsorption occurred more rapidly. Nevertheless, the highest amount of xylan was reached at the highest temperature and longest time (Hansson 1970b; Silva et al. 2011). The energy of activation was calculated to be 4.4 kcal/mol, meaning that it is more a physical process than chemisorption (Hansson 1970b). Moreover, Hansson and Hartler (1969) observed that approximately 70% of xylan adsorbed irreversible at 170°C onto cotton fibers, when treating with 10% of sodium hydroxide solution at room temperature. Surewicz (1962) and Yllner and Enström (1956) obtained a lower amount of irreversible adsorption of xylan.

Many of the adsorption experiments described in the literature were performed under alkaline conditions, which can result in degradation and chemical changes of the xylan reducing the solubility and favoring precipitation (Hartler and Lund 1962; Mitikka-Eklund 1996) but also aggregation of xylan molecules resulting in xylan assembly on cellulose surfaces (Linder et al. 2003). A higher temperature can also lead to degradation (Mitikka-Eklund 1996). The most likely reason is proposed, that with increasing temperature the water molecules surrounding the number of xylan molecules is decreasing (dehydration of the xylan), forcing an increase in sorption. Hydrogen bonds between water molecules and xylan molecules could retard a close contact between xylan and cellulose (Hartler and Lund 1962; Mitikka-Eklund 1996), which is supported by experiments using birch xylan in dimethylsulfoxide (DMSO) containing various amounts of water (Hansson and Hartler 1969).

2.3.2.2 Influence of the xylan composition

The interaction between xylan and cellulose and therefore the aggregation of xylan on cellulosic surfaces also depends on the molecular weight, side groups of the xylan molecule, and consequently the origin and extraction method (Hansson and Hartler 1969; Kabel et al. 2007; Meller 1965). Side groups, especially uronic acid residues and arabinose have an impact on sorption. A lower amount of substituents on the xylan backbone is favorable for adsorption (Axelsson et al. 1962; Hansson and Hartler 1969; Henriksson and Gatenholm 2001; Mitikka-Eklund 1996; Muguet et al. 2011; Silva et al. 2011; Walker 1965). This has been explained by a lower solubility (Axelsson et al. 1962; Mitikka-Eklund 1996; Walker 1965), a reduced steric repulsion between xylan and cellulose (Mitikka-Eklund 1996), dehydration of xy-

lan (Hansson and Hartler 1969; Hartler and Lund 1962), and a higher interaction between xylan molecules (Kabel et al. 2007; Linder et al. 2003).

Köhnke et al. (2011) observed, that not only the amount of side groups is important, but also the substitution pattern is influencing the solubility and consequently the hydrodynamic properties of xylan. The amount of nontilted orientations of adsorbed short-chained xylans increased significantly with decreasing substituent pattern (Mazeau and Charlier 2012) possibly allowing crystallization of xylan on the surface and in the fiber (Marchessault et al. 1967; Marchessault and Sarko 1967; Meller 1965; Yundt 1951). Moreover, a lower degree of polymerization or molecular mass has a positive influence on adsorption of xylan (Hansson and Hartler 1969; Kabel et al. 2007; Mitikka-Eklund 1996; Silva et al. 2011). This could be also due to a lower amount of substituents of xylan with a low molecular weight. It is shown that an unsubstituted backbone length of at least 15 xylose residues is needed for adsorption (Kabel et al. 2007). Water soluble xylan had a higher tendency of sorption onto cellulose with a lower molecular mass (Winter et al. 2006). However, longer polymers feature a stronger driving force for aggregation, due to a lower reduction in entropy per unit mass relating to adsorption (Fleer et al. 1993). The accessibility of the surface is also of great importance for aggregation. It is also suggested, that lignin residues linked to xylan can both, either promote (Linder et al. 2003; Winter et al. 2006) or inhibit (Simonson 1971b) adsorption.

2.3.2.3 Influence of cellulosic surfaces

The adsorption of xylan onto cellulose fibers and surfaces greatly depends on the morphology and nature of the substrate, i.e. surface area, porous structure, swelling behavior, crystallinity, and chemical composition (Clayton and Stone 1963; Hansson 1970b; Hansson and Hartler 1969; Mitikka-Eklund 1996; Yllner and Enström 1956).

It was obtained, that raw cotton and purified cotton linters adsorbed twice as much xylan as bleached and cold alkaline purified sulfite pulp from spruce (Yllner and Enström 1956). An increased surface area of cotton fibers by beating leads to a larger adsorption, which correlates with the swelling behavior of the fibers (Hansson and Hartler 1969). Moreover, lowering the degree of polymerization by acid hydrolysis, which is supposed to attack in the amorphous regions and consequently increase the crystallinity of the cotton fibers had a positive impact on adsorption. This could be also a result of a more open fiber structure due to acid hydrolysis. The effect that a higher surface area supports xylan adsorption was also observed by Linder and Gatenholm (2004). According to Newman et al. (1993), an increased degree of crystallinity should have a higher possibility of resorption, since part of disordered cellulose is removed in the early stage of the cook.

Mitikka-Eklund (1996) obtained, that aggregation of xylan occurs more extensively on kraft pulp than on cotton fibers which was explained by the different accessible surfaces as well as the degree of crystallinity. Furthermore, xylan seemed to adsorb in a lager quantity on bleached pulp than unbleached pulp, which is in accordance with Clayton (1963). This was partly discussed by the the lower lignin content and a lower amount of negative charges of the bleached fibers. The lignin content but also the amount of hemicelluloses of the fibers have an influence on adsorption. The affinity between cellulose and hemicelluloses is indicated to be larger than between hemicelluloses and lignin. Mora et al. (1986) observed a higher affinity to retake solubilized xylan on cellulose microfibrils which contain a certain amount of unextracted xylan, while Hansson and Hartler (1969) noticed a lower adsorption of xylan, when cotton fibers already contain glucomannan.

2.3.2.4 Influence of the pH and the ionic strength

A decrease of the pH from a strong alkaline level to a neutral environment promotes precipitation of dissolved xylan to a certain extent (Surewicz 1962; Wikström 1967). During kraft cooking, the alkali is consumed to a large extent, leading to a lowered pH at the end of the cook. This favors xylan adsorption on cellulose fibers (Aurell 1963; Hansson and Hartler 1969; Yllner and Enström 1957). However, Aurell (1963) observed an undesirable redeposition of dissolved lignin onto the pulp fibers by a reduction of the pH from 13.1 to lower than 12.5. Depending on the effective alkali at the end of the cook a yield increase of 1–2% by xylan can be achieved after kraft cooking (Aurell 1963, 1965). Adsorption treatments taking place already in these conditions (pH between 2–11) resulted in the attachment of hemicellulose/xylan only to a small extent (Eriksson et al. 1963; Henriksson and Gatenholm 2001). Nevertheless, the adsorption behavior was stronger at lower pH values (Eriksson et al. 1963).

The adsorption of xylan by reducing the pH is discussed as the decrease in solubility (Hansson and Hartler 1969; Mitikka-Eklund 1996; Yllner and Enström 1957) and a decrease in electrostatic repulsion between the hydroxyl and carboxyl groups (Köhnke and Gatenholm 2007; Mitikka-Eklund 1996). The pKa value of hexuronic acid (3.03) and 4-*O*-methylglucuronic acid (3.14) (Teleman et al. 1995) is in general lower than of hydroxyl groups (14 at 25°C) (Sjöström 1989). This means that carboxyl groups are stronger acidic groups and only protonated in a strong acidic environment.

To compensate or diminish electrostatic repulsion between hydroxyl and carboxyl groups of xylan and hydroxyl groups of cellulose, the ionic strength should be increased (Mitikka-Eklund 1996; Ström et al. 1982) resulting in a reduction in the surrounding water layer and shielding of the charges. Thus, an intimate contact be-

tween cellulose and xylan is possible. Moreover, a higher ionic strength results in the formation of clusters which can adsorb on cellulose forming patches (Tammelin et al. 2009). A higher ionic strength leads to more a coiled conformation polymer chains, thus resulting in a higher packing of polymers. On the other hand, the adsorption of highly cationized barley husk xylan decreased with increasing salt concentration possessing also a nonelectrostatic cellulose surface affinity (Köhnke et al. 2009).

2.3.2.5 Influence of the xylan concentration

Adsorption of xylan is also driven by its concentration in the liquid phase. Surewicz (1962) noticed a stronger retake of organic substances from the cooking liquor onto cotton at a higher concentration of these substances in the liquor. Similar observations were made by Eriksson et al. (1963) and Hansson and Hartler (1969). The lower take up of pine xylan than birch xylan onto cotton fibers was explained by the higher degree of substitution (Hansson and Hartler 1969). Ström et al. (1982) recognized an increased amount of adsorbed xylan by a larger dosage of pine xylan on sulfite pulp as well. Besides the xylan concentration, the ratio between the cellulose substrate and xylan is also of great importance for a sufficient attachment of xylan (Ban and van Heiningen 2011).

2.3.3 Mechanism(s) of xylan deposition

Xylan adsorption has been distinguished as a very slow physical process involving Van der Waals forces and hydrogen bonds as driving forces between the hydroxyl groups of cellulose and xylan (Clayton and Phelps 1965; Danielsson and Lindström 2005; Hansson 1970a; Ribe 2010; Ström et al. 1982). Russo (1959) considered four steps, taking place during the assembly of hemicelluloses onto cellulose surfaces: 1) diffusion or transport of the polysaccharide through the solution to the fiber surface, 2) adsorption at the fiber surface, 3) diffusion of the sorbed molecules into the fibers, and 4) the reverse of steps 1 to 3.

The energy of activation for xylan adsorption was calculated to be 4.4 kcal/mol onto cotton (Hansson 1970a) and 6 kcal/mol onto α-cellulose (Clayton and Phelps 1965) suggesting that it is a physical process. A as possible reason for the slow adsorption it has been claimed that molecules are retarded from diffusion into the fiber wall (Clayton and Phelps 1965; Hansson 1970a; Ström et al. 1982). The slow adsorption behavior was also obtained onto smooth cellulosic surfaces (Claesson et al. 1995; Neuman et al. 1993; Österberg et al. 2001). This adsorption behavior behavior has been explained to be due to the polydispersity of xylan and the surface charges of cellulose and xylan which have the same sign. Thus, a depletion layer

could surround the surfaces reducing the rate of adsorption. Moreover, higher electrostatic repulsion could occur.

The role of strong hydrogen bonding as the driving force for the assembly of xylan onto cellulosic microfibrils has been demonstrated by Mora et al. (1986). However, the formation of hydrogen bonds between cellulose and xylan in aqueous solution as the main mechanism has been questioned. Paananen et al. (2004) suggested that the crucial factor of xylan adsorption is a combination of the inherent entropy increase and weak Van der Waals attraction. The entropy increase is associated with the release of solvent molecules when polymers are adsorbed. The reason for this behavior was considered from results by QCM-D[1]. If only hydrogen bonding is the driving force, the adsorbed layer would be flat and not swollen.

Based on the tendency of xylan to self-associate (Blake and Richards 1971; Saake et al. 2001) Linder et al. (2003) suggest xylan exists in aqueous solutions as dissolved single molecules and aggregated structures in the colloidal size range driven by interactions between unsubstituted regions of the backbone and by hydrophobic attraction due to residual lignin linked to xylan. This mechanism, including adsorption and precipitation, may be highly relevant in systems with low solubility of xylan.

Native cellulose is organized along a two-fold helical system, whereas the crystalline conformation of xylan possesses a three-fold helical system (Almond and Sheehan 2003; Nieduszynski and Marchessault 1971; Rees 1977; Teleman et al. 1995). CP/MAS ^{13}C NMR spectra confirmed that in the presence of cellulose xylan is able to adapt itself into a conformation different from the one present in its isolated state or in solution (Larsson et al. 1999; Liitiä et al. 2003; Mitikka-Eklund 1996; Teleman et al. 2001; Tenkanen et al. 2000). This has also been demonstrated by molecular dynamic modeling (Leeflang et al. 2006; Mazeau and Charlier 2012). Further, the intra- and inter-chain cooperative hydrogen bonding pattern is suppressed when the C5 is substituted with hydrogen instead of a hydroxymethyl group as in cellulose. Thus, the xylan molecule is becoming more flexible and capable of forming flat ribbon-like structures (Atkins 1992).

Xylan adsorption or precipitation on cellulose is considered to be an irreversible process, since only small amounts are removed by washing (Eriksson et al. 1963) or dilution (Paananen et al. 2004). Alkaline conditions on the other hand increase the extent and rate of desorption at high temperature (Hansson and Hartler 1969). The conditions during chemical pulping result in dissolution and degradation of xylan. This was explained as the reason for a higher resistance of adsorbed xylan than native xylan against acidic and alkaline environment due to a more physically well-ordered structure (Hartler and Lund 1962; Yllner and Enström 1957). Dahlman et al. (2003) obtained that adsorbed xylan from black liquor onto softwood kraft

[1] Quartz crystal microbalance with dissipation monitoring

pulp even remained after oxygen delignification and ECF[1] bleaching. A removal of adsorbed xylan can be performed by xylanases (Schönberg et al. 2001). Nevertheless, this is strongly limited by the porous structure of the fiber wall and the degree of crystallization of adsorbed xylan (Mitikka-Eklund 1996).

2.3.4 Location of adsorbed xylan

Adsorbed or resorbed xylan from cooking liquor is located predominantly on the cellulose surface, but small aggregates and molecules may be able to penetrate or diffuse into the pores of the fiber wall and absorb on the internal fiber wall. Mitikka-Eklund (1996) analyzed the chemical composition of bleached pine kraft fibers after adsorption of xylan by X-ray photoelectron spectroscopy (or electron spectroscopy for chemical analysis). The results indicate that the surface was enriched with additional xylan but adsorption could also occur throughout the fiber wall. This is in agreement with Linder and Gatenholm (2004) who visualized glucuronoxylan on dissolving pulp by immunolabeling in combination with confocal laser microscopy. These findings were explained by the fact that only part of the adsorbed xylan could be liberated by xylanases, which acts most probably only on the outer fiber surface. Suumäkki et al. (1995) studied the distribution of xylan on the outer surface by mechanical peeling. They obtained an increased adsorption (or resorption) of xylan on the outer surface during birch kraft pulping, whereas during pine kraft pulping the surface material exhibited a similar xylan content than the whole fiber which is in in accordance with Dahlman et al. (2003). They observed that xylan adsorbs primarily on the outer fiber surface.

Henriksson and Gatenholm (2001, 2002) observed an inhomogeneous and uneven distribution of bump-like particles with a size of about 0.1 µm on cotton linters and CTMP by scanning electron microscopy. By analyzing the contact angle of a water droplet on the fiber surface, they concluded that adsorbed xylan is nonuniformly distributed. Linder et al. (2003) noticed aggregates in the colloidal size range on bacterial cellulose after treatment with xylan, which grow with increasing time.

2.3.5 Influence of xylan and other hemicelluloses on pulp and paper properties

Hemicelluloses have an influence on the properties of pulp and paper. By changing the amount of xylan due to chemical pulping, bleaching, or enzymatic extraction, characteristic fiber properties, such as swelling, specific surface area, wet flexibility, and stiffness are affected. This also has consequences and influences on the mechanical strength performance of the paper.

[1] Elemental chlorine free

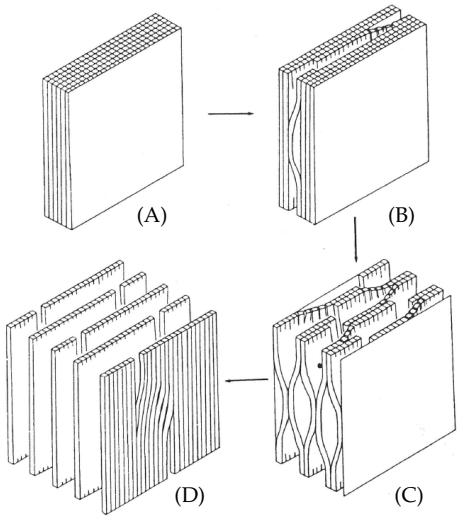

Figure 2.10 Model of the swelling process in direction A⟶D of the cell wall, according to Scallan (1974) (adopted from Lindström and Carlsson 1982a).

2.3.5.1 Fiber swelling and hornification

The cell walls of fibers consist of amorphous regions and gel layers of carbohydrates and lignin. These areas are able to take up water resulting in an increased cell wall thickness, also known as *swelling*. A model of the swelling process of the cell wall is illustrated in Figure 2.10. This behavior is influenced by the chemical composition of the fibers and by the pore volume and the pore size distribution in the cell wall. In addition, the way the fibers have been treated during pulping and bleaching, and in the process chain of papermaking, especially during wet pressing and drying, and further aging is affecting the swelling behavior. Fiber swelling is usually determined by the fiber saturation point, but most commonly by the water retention value (WRV). Rewetting of once-dried or multiple-dried fibers (recycled fibers) always show a lower capacity of re-taking water due to irreversible submorphological changes in the fiber wall, compared to the never-dried fibers (Back 1967; Lindström and Carlsson 1982a; Paavilainen 1993; Weise and Paulapuro 1999). This phenomenon is characterized as *hornification* and described as the loss in WRV.

Pulping has a strong influence on the porous structure of the fibers, which is increased due to the removal of lignin and LCCs. From that point, pores and the spaces between lamellae start to shrink and the ability of binding water in the cell wall layers is reduced (Stone and Scallan 1967). The pulping method itself also has an influence and by comparing pulps at similar yields the swelling behavior of sulfite and sulfate pulp was observed to be different (Stone and Scallan 1968). Oksanen et al. (1997) reported a loss in the total pore volume due to a selective enzymatic removal of accessible xylan, but also glucomannan. The pore volume correlates with the fiber saturation point (Wang et al. 2003). Pulping also leads to

irreversible bond formation or crosslinking as cooking proceeds (Klungness and Caulfield 1982). Since lignin and hemicelluloses are being removed during pulping and bleaching, the content of acidic groups (e.g. carboxylic acid) is decreasing (Lindström and Carlsson 1982b).

Moreover, the chemical environment (e.g. pH, electrolyte concentration, and valency of the counterion) has an impact on fiber swelling (Lindström and Carlsson 1982b). With increasing pH, acidic groups in the cell wall are ionized leading to electrostatic repulsion within the cell wall and the fiber can take up more water. In deionized water, sulfate pulp has a pronounced maximum in WRV between pH 9 and pH 10, whereas sulfite pulp shows a plateau between pH 5 and pH 9 at yields between 52% and 65% which is related to the dissociation of the sulfonate groups. In case of unbleached sulfate pulp, phenolic groups are also dissociated, due to the swelling maximum at higher pH-values. Lowering the pH, acidic groups will be protonated and the fiber shrinks by lowering repulsion effects within the cell wall. Upon increase in the electrolyte concentration, ionized groups in the fiber wall are shielded and the ability of taking up water is reduced. Also at higher pH-values, sodium hydroxide acts as an electrolyte and shields the charged groups. Adding ions with higher valency, this effect is more pronounced.

Drying is a major procedure in papermaking which also leads to irreversible bonding between the microfibrils in cellulose molecules forming macrofibrils (Wang et al. 2003). The result is a lower swelling behavior of the fiber affecting the sheet density and tensile strength of the paper. Wet fiber flexibility is important for paper properties to increase the area of fiber-to-fiber bonds. Häggkvist et al. (1998) recognized a reduction in pore size and pore size distribution by decreasing the moisture content, resulting in tighter molecular package of cellulose (Rebuzzi and Evtuguin 2006). Fernandes Diniz et al. (2004) concluded, that hornification is due to crosslinking of ester linkages (lacton bridges) between hydroxyl groups and carboxylic groups, since hornification can be reduced by alkaline solutions.

Since the (partial) removal of xylan will affect fiber swelling (Moss and Pere 2006), the addition of xylan before paper drying will influence the porosity and fibers exhibit an increased swelling, specific surface area, and wet fiber flexibility (Silva et al. 2011). Drying leads in fiber hornification, due to the aggregation of microfibrils which is measured as the swelling behavior. After drying fibers with additional xylan feature an improved re-swelling, compared to fibers without additional xylan (Köhnke et al. 2010; Östlund et al. 2010; Rebuzzi and Evtuguin 2006). On the other hand, glucomannan can prevent the aggregation between microfibrils during drying. This leads to the conclusion, that carboxylic groups in xylan do not have a major role in preventing hornification, these groups are not present in glucomannan (Oksanen et al. 1997).

2.3.5.2 *Mechanical strength properties of paper*

Paper is a complex network of individual fibers, which interact with each other. The mechanical properties of paper primarily depend on the strength of single fibers as well as the strength and the number of fiber-fiber joints (Page 1969). A large number of experimental studies have been performed in the past to take also the chemical composition of the fibers into account in the discussion of mechanical strength properties of the fibers, especially the content of hemicelluloses, since they are associated with the cellulose fibrils. Basically two different approaches can be found in the literature: (1) the influence of xylan on the mechanical properties of fibers by removal or extraction via pulping, bleaching, and further extracting methods; and (2) the impact of xylan on the strength properties by increasing the xylan content of the fibers due to adsorption.

Ratcliff (1949) bleached pine kraft pulps (*Pinus caribaea* Morolet) of varying pulp yields (43.0–66.4%) with acidified sodium chlorite to different yields (41.9–50.5%) to study the influence of the content of hemicelluloses on pulp properties. The burst factor and breaking length was higher for the pulps at higher yields, whereas the tear factor had a maximum at a yield of $\approx 46\%$ at a beating time of 40 min. However, comparing the pulp samples at the same beating degree, the pulp with the highest yield showed better strength properties. The tear factor vs. the beating degree was similar for all pulps. By considering the amount of xylan and mannan vs. the tensile strength, a correlation was not found. Nevertheless, the amount of hemicelluloses within the fiber has an impact on the strength properties. Since the pulps were bleached from and to different yields, structural changes within the fiber wall may have also an impact on the resulting tensile strength. Pettersson and Rydholm (1961) found similar correlations as the tensile strength properties of birch kraft pulp and birch sulfite pulp is reduced by continuing delignification to lower yields (from 70% down to 30%) and suggest, that the location of the hemicelluloses is also important. Alkaline extraction of loblolly pine holocellulose (springwood and summerwood) resulted in a linear correlation between strength properties of individual fibers and the amount of xylan (Leopold and McIntosh 1961). The amount of glucomannan and the DP, respectively, did not show any correlation. This might be due to the fact, that xylan is located between the fibrils, whereas glucomannan is embedded more in the internal structure of the fibrils. Therefore, adhesion between fibrils and further internal strength of a fiber is more affected by xylan. By treating chips of loblolly pine (springwood and summerwood) under kraft cooking conditions, no direct relationship between the chemical composition and bond strength of the fibers was found (McIntosh 1963). Nevertheless, the amount of xylan is also important for the wet flexibility of fibers and therefore it has a positive influence in preserving properties after recycling, due to a lower hornification tendency (Cao et al. 1998).

A removal of larger quantities of hemicelluloses by alkaline extraction, however, showed a significant reduction in breaking stress of individual summerwood fibers of longleaf pine holocellulose pulp dried under load and no load (Spiegelberg 1966). The modulus of elasticity[1] (E) was also reduced, especially by drying under no load. As the amount of hemicelluloses is reduced, cellulose fibrils are getting closer together forming more rigid linkages, which induce internal stress within the fiber and lowers the strength properties. Moreover, little alkaline degradation occurred, influencing the mechanical performance of the fibers. For cotton fibers on the other hand, an increase in breaking strength and E could be found under the same alkaline extraction conditions, probably due to alkaline swelling reducing stress in the internal fibrillar structure.

Selective enzymatic removal of hemicelluloses from never-dried bleached softwood kraft pulp suggested a minor reduction in the beatability, but the pulp properties (tear and tensile index) after refining did not change significantly (Oksanen et al. 1997). Schönberg et al. (2001) on the other hand have seen an influence of the xylan content on the z-strength (Scott bond) and the tensile strength. The removal of xylan from mainly softwood kraft pulp before oxygen delignification by enzymes resulted in higher fiber deformation and lower tensile strength (Rauvanto et al. 2006). Comparing different bleaching methods, a linear relationship between the hemicellulose content in the surface layer and the tensile index of unbeaten long-fibers was noticed, whereas no correlation was observed for the amount of hemicelluloses in the inner layers of the fiber wall (Sjöberg et al. 2004). However, after beating (6000 revolutions with a PFI mill) these effects disappeared.

As discussed above (section 2.3.5.1), hemicelluloses play an important role in the behavior of the swelling tendency of the fiber (Laine and Stenius 1997). Xylan consist of a portion of uronic acid groups. The introduction of charges within the fiber wall and on the fiber surface by such functional groups affects the swelling behavior of the fiber and increases the wet fiber flexibility during sheet formation. Therefore, a higher area in molecular contact during sheet formation is possible resulting in higher strength properties (Walker 1965). Torgnysdotter and Wågberg (2003) or Weber et al. (2013) found, that charges on the surface are important for the bonding strength of viscose fibers, probably due to the softening of the fiber surface. By increasing the surface charge of the fibers, stronger coulomb forces can be developed by adding cations between negatively charged fibers. In addition, the resistance against beating is reduced (e.g. Contela and Borruso 1967).

The addition of kraft and sulfite hemicelluloses, extracted from pulps, to the beater had an influence on the strength properties of the paper. However, the paper strength at comparable chemical composition could not be restored by adsorption of hemicelluloses and is the least efficient way to increase the amount of

[1] Young's modulus

hemicelluloses of pulp fibers (Pettersson and Rydholm 1961). Besides the role of improving fiber swelling and changing the hydrodynamics at the beater rolls (also Aurell 1965), they attributed a third function to hemicelluloses, which is a glueing effect. The addition of xylan and modified galactomannans, respectively, to various pulp samples resulted in improved strength properties of the paper, such as tensile index and z-strength (Hannuksela et al. 2004; Schönberg et al. 2001; Suurnäkki et al. 2003). Similar effects were found by adding hardwood hexenuronoxylan from black liquors to softwood kraft pulp fibers prior to and following oxygen delignification and ECF bleachnig (Dahlman et al. 2003), leading to higher tensile and tear strength as well as z-strength and sheet density at the same refining intensity (revolution). By comparing the strength properties vs. the beating degree, the oxygen bleached pulp had the highest values at a beating degree above 16 SR. The pulps with a higher amount of xylan showed slightly higher values. By comparing the tensile index vs. beating degree, the unbleached pulp had the best performance, but a similar tensile index was reached by the pulp with a higher and a lower amount of xylan. A likewise tendency was seen by Köhnke and Gatenholm (2007). When the tensile strength is represented at the same refining intensity, improved physical properties of the pulp could be noticed (Köhnke et al. 2008).

On the other hand, cationic xylan, as a retention additive was found to improve paper strength, but also increases the refining resistance to reach the same beating degree (Antal et al. 1997, 1991; Ren et al. 2009). The improvement is also dependent on the degree of substitution of those xylans and on the pulp itself, as the impact was larger for sulfate pulp, than sulfite (Schwikal et al. 2011). In addition, xyloglucans increased tensile strength after more than 20 hours of adsorption (Christiernin et al. 2003) or when added after refining as wet-end additive (Lima et al. 2003).

2.4 Bonding mechanisms within paper

As mentioned before (s. 2.3.5.2), the mechanical strength properties of paper primarily depends on the strength of single fibers as well as the strength and the number of fiber-fiber joints (McIntosh 1963; Page 1969; Torgnysdotter and Wågberg 2003). According to Lindström et al. (2005), five different bonding mechanisms occur within the area in molecular contact of single fibers, as shown in Figure 2.11.

Hydrogen bonding is the most known and over the last centuries most proposed boding mechanism within paper. The surfaces of cellulose and hemicelluloses exhibit hydroxyl groups, and hemicelluloses also have carboxylic acid groups. These functional groups are able to interact with each other, forming hydrogen bonds. The bonding energy of hydrogen bonds in carbohydrates is about 17–63 kJ/mol. *Van der Waals forces* are the results of attractive or repulsive interactions between molecules or parts of the same molecule, due to induced dipols (Askeland et al.

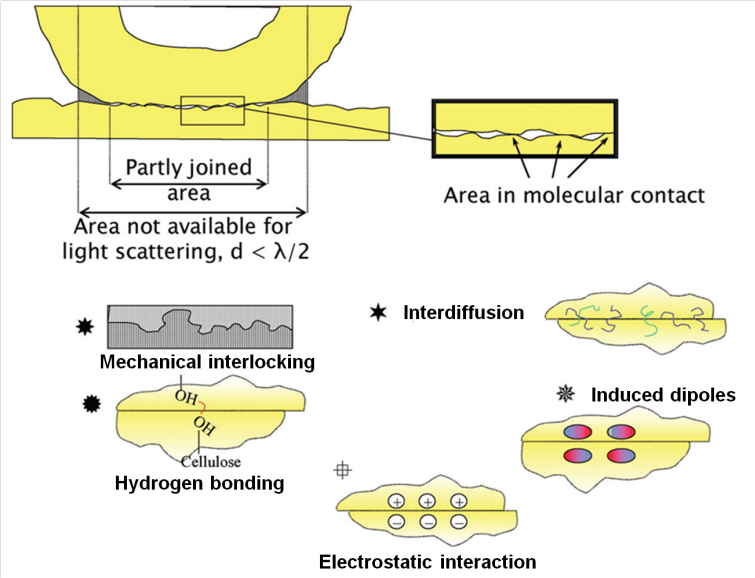

Figure 2.11 Bonding mechanisms between single fibers (according to Lindström et al. 2005).

2011). They can be found between two permanent dipoles (*Keesom force*), a permanent dipole and a corresponding induced dipole (*Debye force*), and two instantaneously induced dipoles (*London dispersion force*). The binding energy of a Van der Waals force is up to 5 kJ/mol and therefore relatively weak. However, Van der Waals interactions define a lot of properties of organic molecules, especially their solubility or the boiling point. *Mechanical interlocking* is generated due to the rough and rather soft fiber surface and the mechanical entanglement of the fibril on the surface of the fibers. *Coulomb force* is caused by permanent negative and positive charges on the fiber surface between two adjacent fibers, resulting in electrostatic interaction. Single molecules can also migrate from one surface to the opposite interface leading to the formation of linkages, which increase the adhesion between both surfaces and is referred to as *interdiffusion*. Persson et al. (2013) investigated the adhesion of cellulose fibers in paper and added a sixth bonding mechanism between single fibers, which are *capillary bridges*. This is illustrated in Figure 2.12. When producing paper, fibers are in a wet and swollen state. As the water is removed from the suspension a fiber mat is formed, but the fibers are still covered by a water film. The continuous removal of water during drying results in a continuously decreasing of the thickness of the water film and the formation of capillary bridges. The capillary adhesion can be determined by the Laplace pressure which is defined by the air-water surface tension and the two radii of curvature in the meniscus. When the distance between two surfaces is low and the area of a capillary bridge is large, strong forces can occur. Since paper has a water content of about 6%, this mechanism may also have an influence on the strength of paper.

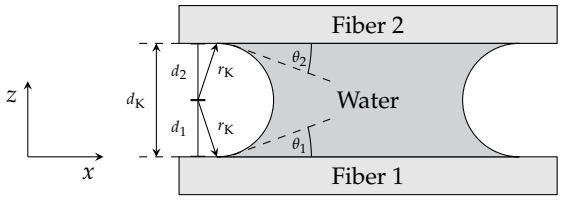

Figure 2.12 Schematic diagram of a capillary bridge between two adjacent fibers. The fluid surface in the (xz) plane is a segment of a circle (with a radius r_K) and the surface separation (*Kelvin length*), where $d_K = d_1 + d_2 = r_K(cos\theta_1 + cos\theta_2)$ and θ_1 and θ_2 are the water contact angles on the fibers 1 and 2, according to Persson et al. (2013).

Chapter 3

Materials and Methods

3.1 Characterization of the pulp samples

Different pulp samples have been used for the adsorption/precipitation of xylan to evaluate the impact of the xylan content on physical properties of the pulp and paper handsheets. The pulp samples were:

- bleached, once-dried, and unrefined sulfite pulp (SPB), a mixture of spruce and beech,
- bleached, once-dried, and unrefined softwood kraft pulp (SKPB), a mixture of spruce and pine,
- two unbleached, never-dried, and unrefined softwood kraft pulps (SKPUBs) with a Kappa number of 53 and 42, a mixture of spruce and pine, and
- viscose fibers (VFs) with a flat cross-section, a fiber length of 6 mm, and a titer of 9 dtex.

The standard pulp for the experiments was the bleached softwood kraft pulp. This pulp was used, to study the adsorption behavior of xylan, the distribution of aggregated xylan on the fiber, and the influence of xylan on strength properties of handsheets. The other pulp samples were used to compare the influence of additional xylan on their strength properties. The pulp samples were analyzed regarding the following characteristics:

- Chemical composition (polysaccharides) of the pulp samples
  - High-pressure liquid chromatography (HPLC)
  - ^{1}H nuclear magnetic resonance (NMR) spectroscopy
- Lignin content
  - Acid-insoluble lignin (Klason lignin), T 222 om-11
  - Acid-soluble lignin, Tappi Method UM 250, 1985
  - Kappa number, ISO 302:2004
- Solvent extractives, T 204 cm-07
- Macromolecular chain length by measuring the solution viscosity, T 230 om-82
- Metals
- Carbonyl content, Copper number, T 215 m-50

3.2 Composition of the xylan samples

The influence of two different xylans were investigated on their behavior to adsorb/precipitate on pulp fibers to investigate their impact on pulp and paper prop-

Table 3.1 Molecular weight and chemical composition of the used xylans. MeGlcA = methylglucuronic acid, Ara = arabinose, Gal = galactose, Glu = glucose, Man = mannose, Rha = rhamnose, and Xyl = xylose.

	Molecular weight, kg/mol		Chemical composition, %							
Sample	M_n[1]	M_w[2]	MeGlcA	Ara	Gal	Glu	Man	Rha	Xyl	total
X_1	4.6	5.6	4.8	0.1	0.0	0.8	0.4	0.0	90.6	96.7
X_2	9.0	17.6	3.7	0.0	0.4	0.2	0.0	0.0	89.4	93.9

[1] number average [2] weight average

erties. Both samples were provided in powder form and characterized at Lenzing AG. One xylan was extracted from a beech sulfite dissolving pulp and will be denoted by xylan 1 (X_1). The other xylan was extracted from eucalyptus kraft pulp and will be denoted by xylan 2 (X_2). The xylan samples differed in their molecular weight as well as their chemical composition, as presented in Table 3.1.

The molecular weight was determined by size exclusion chromatography. The molecular weight (weight average, M_w) of X_2 (17.9 kDa) was almost twice as high as that of X_1 (9.0 kDa). Differences were also found in their chemical composition which was analyzed by gas chromatography after depolimerization via acid methanolysis. The amount of xylose was 90.6% for X_1 and 89.4% for X_2. Further, X_1 had a small amount of arabinose (0.1%), glucose (0.8%), and mannose (0.4%), whereas X_2 consisted of slight amounts of galactose (0.4%) and glucose (0.2%). The small content of glucose of both xylans might be due to the alkaline treatment processing which most likely degraded and therefore short-chained cellulose in the liquor as well. In the following washing steps, where the pH is significantly lowered, these cellulose molecules are again able to precipitate and deposit with the xylan. A larger difference between both xylans can be seen in their content of uronic adic residued (MeGlcA) of about 4.8% (X_1), compared to 3.7% (X_2).

3.3 Adsorption experiments

For the investigation of the interaction between cellulose and xylan, six variables (temperature, pH, ionic strength, pulp consistency, xylan input (concentration), and time) were evaluated with regard to the adsorption/precipitation of the two xylans onto bleached softwood kraft pulp fibers (SKPB). The variables were set to the values, as shown in Table 3.2.

Table 3.2 Set values of the six variables investigated regarding their influence on adsorption.

Variable		Unit	Value
Ionic strength	I	mol/L	0.25, 1, 2
pH			7.0, 10.0, 12.6
Pulp consistency	C	%	1.0, 2.5, 5.0, 10.0
Temperature	θ	°C	40, 80, 140
Time	t	h	0.5, 1, 2, 3
Xylan input[1]	c_x	mg/g	80, 160, 320

[1] The amount of xylan in the pulp suspension during adsorption was calculated relating to the oven-dry pulp mass.

3.3.1 Overall process

The experimental work flow was divided into three parts:

1) preparation of the pulp and xylan samples,
2) performing the adsorption experiments at different conditions, and
3) analysis of the chemical composition before and after the treatment with xylan.

3.3.1.1 Pulp and xylan preparation

Dry SKPB (bale form) soaked in deionized water for at least 4 h and disintegrated for 25 min, according to ISO 5263-2:2004. Afterwards, the pulp was thickened to a dry content of about 20% and stored in a refrigerator until use.

Xylan was dissolved in 1 mol/L sodium hydroxide (NaOH) and stirred with a magnetic stirrer for 15 min (X_1) and 25 min (X_2) and heated to about 55°C for dissolution. Before use, the solution was cooled to room temperature. Due to the higher molecular weight of X_2, undissolved parts remained in the solvent which could have an effect on the adsorption of soluble xylan molecules. Higher temperatures (80°C and 140°C) resulted in a higher dissolution. The temperatures were chosen to minimize possible chemical changes of the xylan during dissolution.

3.3.1.2 Experimental design

A schematic overview of the experimental design is illustrated in Figure 3.1. After the pulp and xylans were prepared, the pulp was put into an Erlenmeyer flask (for temperatures at 40°C and 80°C) or into lab-scale steel autoclaves (for temperature at 140°C). The amount of sodium chloride (NaCl) was calculated to set the ionic

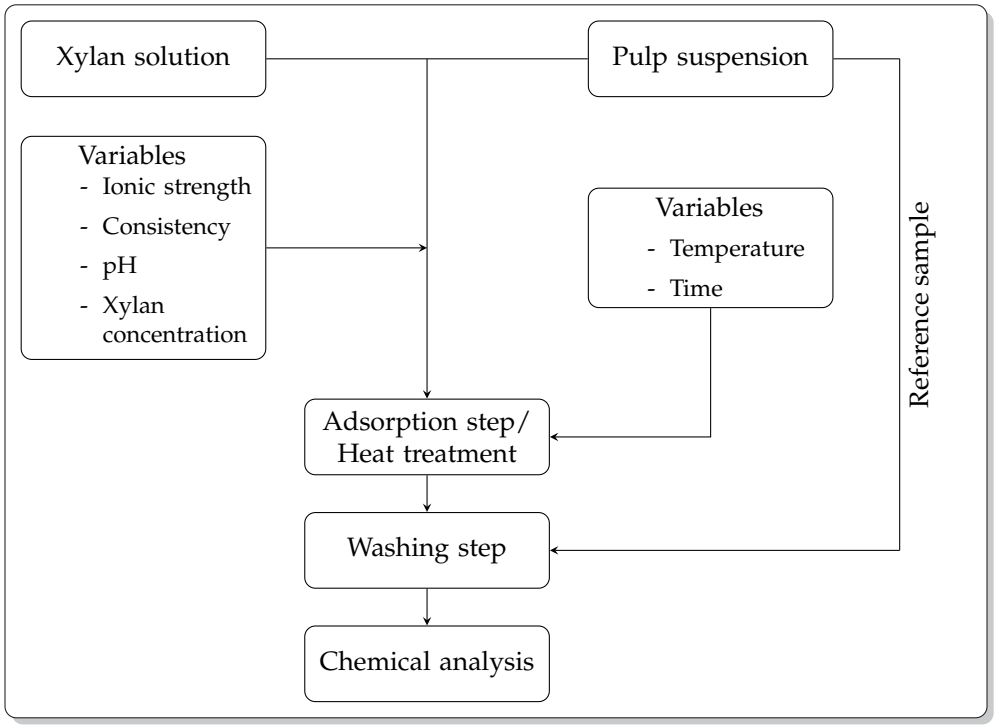

Figure 3.1 The overall work flow of the adsorption experiments of the pulp samples and the chemical analysis.

strength to the given value and was dissolved in deionized water. The amount of NaOH for the dissolution of xylan and diluted (4% and 1%) sulfuric acid (H_2SO_4) to adjust the final pH, were taken into account in the adjustment of the ionic strength. The water, including NaCl, was added to the pulp and the suspension was mixed, in order to separate the fibers. Then, the xylan solution was added to the suspension and the pH was adjusted by slowly adding H_2SO_4 to allow xylan precipitation preferably on the fiber surface. The final pulp consistency was reached after the adjustment of the pH. In case of the treatments without the addition of xylan the same amount of NaOH was added to the pulp suspension and the pH was carefully adjusted using H_2SO_4. The flask was sealed, heated to the desired temperature and placed in a heated water bath with respect to the heating-up period. For the trials at 140°C, the autoclaves were sealed and a heater band was placed around them. After the desired treatment time, the pulp was washed on a wire (100 µm) with deionized water. This washing step was repeated until the conductivity was below 10 µS/cm to remove free and unbound xylan, but also the ions from the suspension. Between each washing step, the pulp remained in deionized for about 10 min for a sufficient ion exchange between the liquid phase and the fiber. Finally, the samples were dried and the chemical composition was investigated.

3.4 Chemical analysis

The chemical composition of the pulp samples, before and after treatment with xylan solution, was analyzed by high pressure liquid chromatography and ^{1}H nuclear magnetic resonance spectroscopy.

3.4.1 Analysis via high pressure liquid chromatography

The technique of high pressure liquid chromatography (HPLC), also known as high performance liquid chromatography, is a powerful analytic method for separating components in a mixture, and afterwards identifying and quantifying each constituent part (Pryde and Gilbert 1979). The solvent (*mobile phase*) is filtered, pressurized, and pumped through a column which is packed with a solid adsorbent material (*stationary phase*), e.g. silica gel or aluminum, as depicted in Figure A.1. The components interact with the stationary phase causing different flow rates of each component and resulting in a separation of the components at the end of the column. Each solute is monitored by a detector and recorded as peaks. A detailed and mathematical description of this method is given in Appendix A.

3.4.1.1 Procedure for analysis

The pulp samples were milled and afterwards screened (40 mesh) at Lenzing AG. Afterwards, they were hydrolyzed to their sugar monomers in a two-stage hydrolysis by H_2SO_4, according to Sixta et al. (2001). A known pulp mass equivalent to approximately 40 mg was placed in a 10 mL centrifuge tube and 0.5 mL of 72.3% H_2SO_4 was added. The slurry was stirred for 3.5 h at around 25°C. Then, 8.5 mL of deionized water was added, the tubes were sealed and placed in a heatable rotator at 110 ± 1.0°C for 90 min. The tubes were removed and chilled in a water bath to room temperature.

Before the HPLC analysis, a certain amount of the hydrolyzed sample was diluted with 0.1% w/w of NaOH to a ratio of 1:50 w/v. This was done to set the pH in the neutral range in order to avoid deposits in the separation column. A further part of the hydrolyzed sample was diluted with deionized water to analyze the content of furfural and hydroxymethylfurfural, which is formed during the dissolution and degradation of xylan and glucan, respectively. Afterwards, the samples were transferred to a cuvette and analyzed. For the separation of the sugar monomers a Dionex CarboPac^{TM} Pa10 (4×250 mm) was used. The detection of the monomers was accomplished with pulsed amperometric detection (Dionex ED40).

3.4.2 Analysis via ^{1}H nuclear magnetic resonance spectroscopy

Nuclear magnetic resonance (NMR) spectroscopy is a method to study molecules with the help of a strong magnetic field. Therefore, interaction of material, especially the nuclei of molecules with radiofrequency (Rf) electromagnetic radiation at energies in the order of 10^6 Hz is recorded (Rahman and Choudhary 1996). The adsorption of Rf can occur, when a molecule exhibits an uniform periodic motion with a frequency that exactly matches the frequency of the adsorbed radiation. Therefore, the nuclei are first immersed in a magnetic field, and then the frequency at which they undergo precession with electromagnetic radiation of exactly the same frequency where energy adsorption can take place is matched. Thus, molecules can be differentiated due to differences in the frequencies. The principle set-up of a NRM spectrometer is illustrated in Figure B.1. A detailed and mathematical description of this method is given in Appendix B.

3.4.2.1 Procedure for analysis

The pulp samples were milled using a kitchen blender. Then, the samples were hydrolyzed in a two-stage hydrolysis by H_2SO_4 to their sugar monomers differing in the concentrations of H_2SO_4, reaction times, and temperatures compared to the method for the analysis by HPLC. This was done according to Bose et al. (2009). They tested different hydrolysis conditions on two softwoods and analyzed the hydrolyzed samples, until the results appeared to be representative of the expected carbohydrate composition. This preparation method was adapted also for time saving reasons.

A known pulp mass equivalent to approximately 0.5 g was placed in a 50 mL glass bottle and 16 mL of 70% H_2SO_4 was added. The slurry was stirred with a magnetic agitator for 2 h at around 25°C. Then, 21 mL of deionized water was added and the bottles were sealed and transferred to a water bath at 80°C for 1 h. Afterwards, the bottles were allowed to cool to room temperature.

The NMR measurements were performed at 10°C with a Varian 500 spectrometer (500 MHz ^{1}H frequency). The ^{1}H spectra were acquired with a spectral width of 16 ppm, 90° pulse angle, 2.048 s acquisition time and the relaxation delay was set to 2 s. The data were processed in TOPSPIN v3.1 from Bruker. 600 mol/L of the hydrolyzed sample was transferred to a NMR tube and 60 µL of a standardizing solution was added. This solution contained 1.82×10^5 mol/g of trimethylamine hydrochloride (TMA) and 0.05% of 3-(trimethylsilyl)propionic-2,2,3,3-d4 acid (TSP) in D_2O. The TMA conduced to calibrate the mass of each of the sugar monomers in the sample and the TSP was needed as a chemical shift reference (adjustment to

0.0 ppm). After the measurement, the C1-α and C1-β of the sugars were integrated, using the anomeric ratio (α/β), according to Robyt (1998).

3.5 Distribution of xylan on the fiber surface

Different spectroscopic and microscopic methods have been used to determine the distribution of adsorbed/precipitated xylan on the cellulosic surface. Attenuated total reflection and photoelectron spectroscopy as well as scanning electron and atomic force microscopy have been applied.

3.5.1 Infrared spectroscopy

Infrared (IR) spectroscopy is a useful technique to determine the surface chemistry of a substrate without destroying the sample. It is more often used in combination with Fourier transformation (FT), due to its high wavenumber (ν) accuracy as well as the possibility for detecting all frequencies that are emitted from the IR source. This is also called *multiplex* or *Fellget advantage* (Herres and Gronholz 1984). The circular apertures hold a larger area, the so-called *throughput* or *Jacquinot advantage* (Herres and Gronholz 1984). The most important and essential optical part in a FTIR spectrometer is the Michelson interferometer which can be seen in Figure C.1 in Appendix C as an idealized scheme.

3.5.1.1 Attenuated total reflection spectroscopy

Attenuated total reflection (ATR) spectroscopy features the possibility of investigating samples which contain strongly IR-adsorbing components using an optical near field effect taking place at total internal reflection (Fahrenfort 1961; Harrick 1960). Moreover, problems can occur when a sample exhibits different reflectivities which contribute to the transmission spectrum. This is the case for paper as the formation of the fibers is not uniform. Just using FTIR, it is not possible to obtain differences between changes in the reflectivity of paper or changes in the chemistry (growth of peaks). Due to the effective path length of ATR spectroscopy which is much smaller this problem can be eliminated (Conners and Banerjee 1995). A more detailed description about the measurement principle is given in Appendix C.

Preparation and analysis

IR measurements were performed on 2×2 cm sections of SKPB handsheets and on the pure xylan samples using a Bruker IFS 66 v/S FTIR spectrometer. ATR spectroscopy was performed, according to Gilli et al. (2009). A single reflection

unit from Specac (MKII Golden Gate) was equipped with a diamond as ATR crystal ($n_1 = 2.42$ for $\lambda = 589\,\text{nm}$ (Giancoli 2010). Figure C.3 illustrates a schematic view of the light path of the IR beam in the ATR unit. A sampling rate of 100 kHz and a recording time of 10 min was used. The incident angle was 45°. The spectra were processed in OPUS (Bruker).

Xylan features characteristic peaks at $1250\,\text{cm}^{-1}$ and $1460\,\text{cm}^{-1}$, but also between wavelengths of $1650\,\text{cm}^{-1}$ and $1750\,\text{cm}^{-1}$ resulting from C=O bond stretching vibration at the COOH group (Evans et al. 1995; Fengel 1992; Higgins et al. 1961; Kačuráková et al. 1999). The investigated SKPB handsheets consisted predominantly of cellulose. Therefore, a refractive index of $n_2 = 1.47$ for for $\lambda = 587.6\,\text{nm}$ (Kararova et al. 2007). The resulting penetration depth of the evanescent wave into a handsheet at wavelengths of $1750\,\text{cm}^{-1}$ and $1650\,\text{cm}^{-1}$ varies between 1.0 µm and 1.1 µm.

3.5.2 X-ray photoelectron spectroscopy

Another method for analyzing the surface chemistry of a substrate is X-ray photoelectron spectroscopy (XPS), also known as electron spectroscopy for chemical analysis (Siegbahn et al. 1967). Compared to ATR spectroscopy, XPS is more sensitive to the surface resulting in a much higher resolution. During the measurement, the sample is exposed to monochromatic X-radiation at a constant potential and current, superimposed on a *bremsstrahlung* background. When the energy of the incident photons $h\,\nu$ is greater than the energy of a bond, e.g. C−C, C−OH, or C=O, electrons within such a molecular bond can be disrupted. The X-ray photons are also able to ionize atoms, if the energy is high enough. A more detailed description of a XPS device and a mathematical background of this method is given in Appendix D

3.5.2.1 Preparation and analysis

XPS measurements were performed to verify the results done by ATR spectroscopy but also to investigate the chemical composition of the surface of the sample. The analysis depth of XPS varies between 0.5 nm and 10 nm for paper (Conners and Banerjee 1995), and therefore it is more sensitive regarding the surface, than ATR spectroscopy.

The XPS data were obtained by a SPECS Phoibus 150 electron energy analyzer and a nonmonochromated Mg K_α X-ray source with a corresponding photon energy of 1253.4 eV. The resolution of this setup was 0.8 eV. For the analysis a sample of ($10 \times 10\,\text{mm}$) from SKPB handsheets were fixed on carbon tape and placed in the vacuum chamber of the measurement device for 12 hours. The vacuum in

the chamber during the analysis was better than 3×10^{-9} mbar. The data were processed in CasaXPS from Casa Software Ltd (version 2.3.14dv38). Knowing the chemistry of the sample three peaks were created under the C1s peak with respect to the fit, where C1 corresponds to C−C bonding, C2 corresponds to C−OH bonding, and C3 corresponds C=O bonding. Since the chemical shift for a C−C bond is at 285 eV (Conners and Banerjee 1995) the peaks were calibrated regarding the C1 peak.

3.5.3 Scanning electron microscopy

Scanning electron microscopy (SEM) is a powerful technique to study topographical features of a sample by imaging the surface with a focused beam of electrons. Several variations of SEM have been developed, such as conventional SEM, low temperature SEM, environmental SEM, and Low voltage SEM (Conners and Banerjee 1995; Zankel et al. 2009). In this thesis SEM in the conventional and low voltage mode was used, and thus only these two methods will be described in more detail.

3.5.3.1 Conventional SEM

A schematic illustration of the interior of an SEM chamber is depicted in Figure 3.2. *Primary electrons* are sent from the electron gun to the specimen where different interactions take place leading to *elastic* or *inelastic* scattering. Elastic scattering is the result of the collision between primary electrons and the nuclei of the atoms of the sample. It is concluded that about 30% of the primary electrons re-emerge leading to the primary backscattered electron signal which increases with increasing number of atoms (Bishop 1966). Inelastic scattering is caused by transferring energy from the primary electrons to the atoms of the sample leading to the ejection of loosely bound electrons with a low energy (0...50 eV). These electrons are also known as *secondary electrons*. Moreover, inelastic scattering can generate X-rays, bremsstrahlung, or electrons from the conducting layer, in case for the conventional mode (Conners and Banerjee 1995). The secondary electrons are generated at low kinetic energies by a shallow depth of the sample close to the incident beam giving topographic information. The depth and shape of the interaction volume is dependent on the accelerating voltage, the atomic number of the elements in the specimen, and the angle of tilt between the incident beam and the specimen.

Since paper is a nonconductive material and will consequently build-up charges in a SEM, the surface needs to be coated with a conducting layer (e.g. C, Au, or Pt) for the conventional mode where an acceleration voltage of 5–60 keV is used. However, an additional coating layer can result in a loss in information about the surface morphology of the sample. Moreover, this layer is sputter coated under

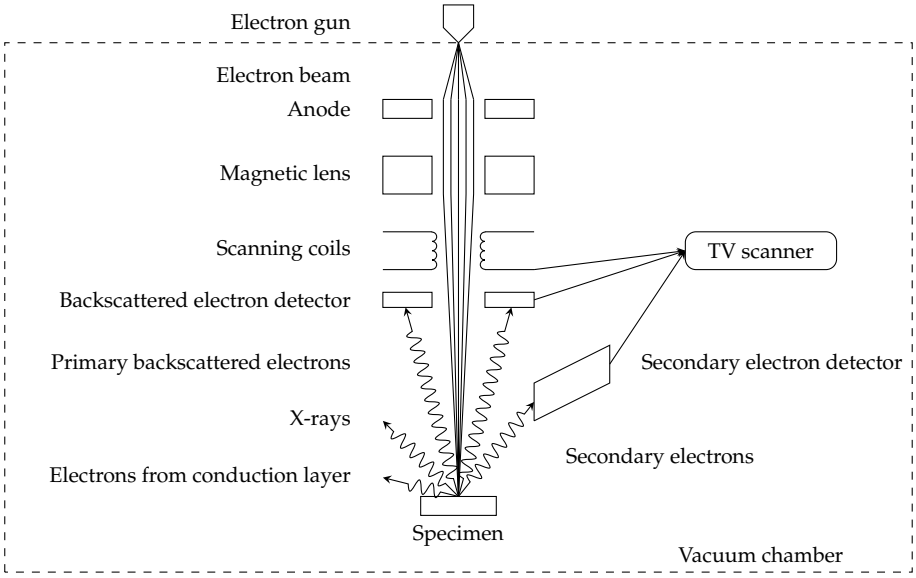

Figure 3.2 Schematic illustration of the interior of a SEM chamber, adopted from http://www.purdue.edu/ehps/rem/rs/sem.htm (seen on 08.08.2014).

vacuum resulting in an undefined layer thickness which can vary between 5–20 nm (Conners and Banerjee 1995).

3.5.3.2 Low voltage SEM

Low volage SEM has been performed, since it has several advantages compared with conventional SEM. Due to a good resolution, the intensity of the electron beam is much lower (below 5 kV). This results in a much higher surface sensitivity, since the interaction volume of the electrons in the sample is strongly limited (Joy and Joy 1996). When the energy (usually denoted as E_2 and a material constant (Goldstein et al. 2003; Joy and Joy 1996) reaches a certain value at which the incoming primary electrons are equal to the number of emitted electrons, no charges are built up on the surface of the sample. Therefore, nonconducting materials, such as paper, can be detected without coating the surface with a conducting layer. This reduces the risk of artifacts from the coating material, but also from heating during the sample preparation. For example, Fischer et al. (2014) observed a surface coating of several glues, which were used for the fixation of individual fiber-fiber joints on sample holders for testing the bond strength. This undesired surface coating by the glues could not be visualized by SEM in the conventional mode. However, the limitation of LVSEM is the magnification. At higher magnification the surface can be destroyed by the beam, also known as beam damage, and the possibility of drifting during scanning is increased causing fuzzy and warped pictures. Nevertheless, the risk of beam damage is lower for LVSEM, than for conventional SEM

and environmental scanning electron microscopy (Zankel et al. 2009), due to the lower intensities of the electron beam in LVSEM.

3.5.3.3 Preparation and analysis for conventional SEM

For the pretreatment, SKPB handsheets (with and without additional xylan) were placed in dionized water and mixed in order to separate the fibers from each other. Individual fibers were fixed on carbon tape and afterwards metallized for 90 s with gold. For the scanning of the surface a HITACHI S-4000 was used at an intensity of 8 kV.

3.5.3.4 Preparation and analysis for LVSEM

For the investigations via LVSEM pieces of SKPB handsheets (with and without additional xylan) were fixed on carbon tape. The same procedure was done with individual fibers, which were first rewetted in deionized water, separated from the handsheets, fixed and air-dried on the carbon tape. The measurements were performed in a Zeiss Ultra 55 at an intensity of 0.7 kV.

3.5.4 Atomic force microscopy

Atomic force microscopy (AFM) is a powerful tool to image the morphological features of conducting and nonconducting surfaces, such as the ultrastructure of the cell wall of fibers in the nanometer scale (Binnig et al. 1986; Niemi and Mahlberg 2002). The operating mode of AFM is depicted in Figure 3.3. An AFM tip is scanning the surface which is mounted on a cantilever. The cantilever is adjustable in x, y, and z direction, thus the topography can be scanned in three dimensions. Due to the small distance between the tip and the surface of the sample which is only a few Ångströms, attractive and repulsive forces start to have an impact on the deflection of the cantilever. A laser beam is focused on the cantilever and the deflection is recorded by a photodetector. The deflection of the cantilever $\triangle z$ is proportional to the force F given by Hooke's law (Demtröder 2013)

$$F = k \cdot \triangle z \tag{3.1}$$

where k is the spring constant (its stiffness). The operating mode of an AFM can be either in constant height (the height of the tip is fixed) or in constant force mode (the deflection of the tip is fixed). However, the sample surface should be rather smooth, as the maximum deflection in z direction is only of a few microns.

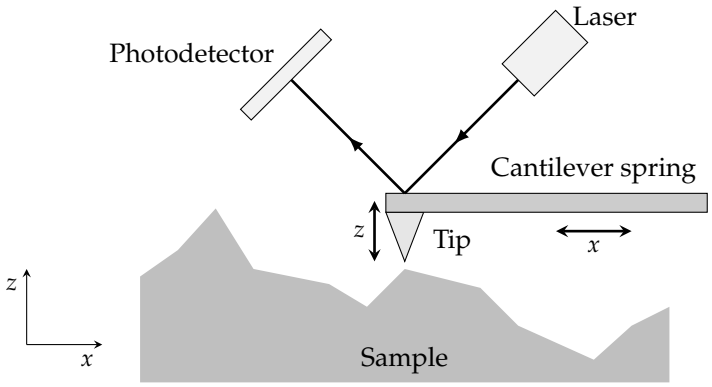

Figure 3.3 Operating mode of AFM in the (xz) plane.

3.5.4.1 Contact mode

In the contact mode, the tip is in contact with the surface of the sample. Due to the intimate contact, attractive as well as repulsive forces occur, generated by Van der Waals interaction (range of 1–2$\times 10^3$ Å) and capillary forces (Niemi and Mahlberg 2002). Therefore, the risk of causing damages on the tip as well as scratches on the surface by the tip can take place. This mode is usually performed on surfaces harder than the tip.

3.5.4.2 Tapping mode

The tapping mode is designed to investigate fragile or softer surfaces than the tip. Compared to the contact mode, the cantilever is oscillating near its resonance frequency and the tip touches the sample periodically. The topography of the sample is imaged by variations of the amplitude. The surface is slightly touched by the tip without sticking, the so-called *tapping*. This method is nondamaging.

3.5.4.3 Roughness analysis

Atomic force microscopy has been employed to obtain nanometer scale information on the topography of a reference SKPB sample and the samples treated with X1 and X2 to determine quantitative surface roughness data. $5 \times 5\,\mu m^2$ images containing 512×512 pixels have been recorded using an Asylum Research MFP-3D (Santa Barbara, CA), operated in tapping mode.

Olympus AC 240 TS silicon tips (resonance frequency $f_r \approx 60\,kHz$) and Olympus AC 160 TS silicon tips ($f_r \approx 280\,kHz$) were used. Both probe types feature a tetrahedral tip, located at the very end of a cantilever with a front angle of 0°, a back angle of 35° and a side opening angle of 15°. The radius at the tip apex is $<10\,nm$. Using the software package Gwyddion (Nečas and Klapetek 2012), the

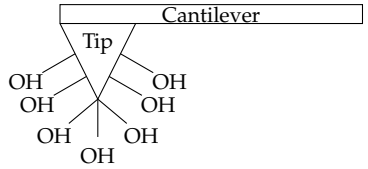

Figure 3.4 Schematic illustration of the set-up of a functionalized AFM tip by several OH groups.

1D height-height correlation function has been calculated from the topography images. This function is calculated from (Teichert 2002; Zhao et al. 2001)

$$C(x) =< [h(x_0 + x) - < h(x) >] \cdot [h(x_0) - < h(x) >] > \tag{3.2}$$

which is fitted with

$$C(x) = \sigma^2 \cdot \mathrm{e}^{-\left(\frac{|x|}{\xi}\right)2\alpha} \tag{3.3}$$

where σ is the root mean square (rms) roughness, ξ is the lateral correlation length, and α is the Hurst parameter (Sinha et al. 1988). Here σ describes the standard deviation of the height values and ξ the lateral roughness fluctuations. The Hurst parameter is a measure for the jaggedness of the surface, where a smooth surface corresponds to $\alpha = 1$ and a more jagged surface to $\alpha < 1$. Three independent fibers per sample were analyzed by recording three independent $5 \times 5\,\mu m^2$ topography images on each fiber.

3.5.4.4 Analysis with functionalized tips

Besides the surface roughness of the fibers, it was of interest to gain more information about the surface chemistry before and after adsorption/precipitation of xylan on the cellulosic surface. Therefore, a novel AFM technique was employed for the first time on a cellulosic surface using functionalized tips to study the adhesive forces between the surface and the functional groups. The functionalized AFM tips (Nanocraft) can be hydrophobic or hydrophilic by CH_3, CF_3, NH_2, COOH, or OH groups, and performed under atmosphere or in liquid. The set-up of a functionalized AFM tip is depicted in Figure 3.4.

Pretests were performed on cellulose thin films where parts of the films were coated with xylan and tips which had been functionalized with CH_3 and OH groups were analyzed regarding their hydrophobic and hydrophilic contrast to cellulose and xylan. This was also done on xylan modified fibers. However, the roughness of the fiber surface resulted in a fast brushing of the functionalized groups off the tip which is the reason for the use of cellulose thin films with the knowledge that the chemical composition of such a model film is different to pulp fibers.

Preparation of cellulose thin films

Thin cellulose model films were prepared, according to the method described by Rohm et al. (2014). Trimethylsilyl cellulose (TMSC) with a DS_{Si} of 2.8 was mixed in toluene over night, and then spin-coated onto the quartz crystals. Afterwards, the TMSC films were transformed into amorphous cellulose (Kontturi et al. 2003; Mohan et al. 2012) with the aid of a 10% HCl-solutions vapor for 10 min. A detailed description is given in Appendix F.

Xylan adsorption on cellulose model films studied by QCM-D

Adsorption experiments were done to investigate the adsorption behavior of X_1 on those cellulose model films and to study the quantity and shape of adsorbed xylan. The regenerated cellulose films on quartz crystals (AU-sensors) were mounted in a flow module of a Q-Sense E4 with quartz crystal microbalance and dissipation monitoring (QCM-D). Solutions of xylan (1.0 g/L) were prepared varying in pH (7, 8, and 9) and ionic strength (1 mmol/L and 100 mmol/L NaCl). Due to precipitation of xylan during the adjustment of the pH, part of the solution was filtered using a 5 µm polytetrafluoroethylene (PTFE) filter to remove the solids from the suspension. Both, solution and suspension have been used for the experiments. The sensors were first equilibrated to Milli-Q (MQ) water and then to NaCl solution at the appropriate pH and ionic strength for 60 min. Afterwards, the xylan solution/suspension was pumped over the sensors at a flow rate of 0.1 mL/min for 60 min and then rinsed again with NaCl solution (30 min) followed by MQ water (30 min). The frequency and dissipation were recorded to determine the adsorbed masses via the Voigt model (Höök et al. 2001; Voinova et al. 1999). A detailed description of the conditions during adsorption and some mathematical parameters are explained in more detail in Appendix F. The resulting films were investigated with functionalized AFM tips.

Imaging

An MFP-3D AFM (Asylum Research) was utilized which was equipped with a planar closed-loop scanner and operated in tapping mode. The tips were modified with OH and CH_3 groups and had an estimated tip radius of 20–40 nm. The spring constants of the cantilevers were 2–3 N/m. To obtain information on the adhesive interactions between tip and sample, the surfaces were scanned in the repulsive regime.

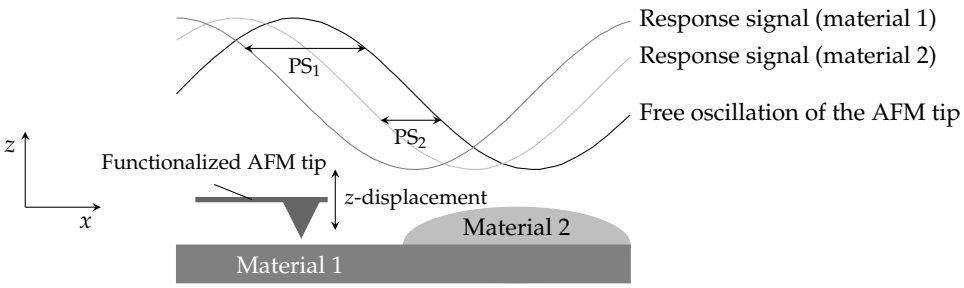

Figure 3.5 Principle of phase imaging. Energy of the oscillating functionalized AFM tip is dissipated into the substrate resulting in a phase shift of the response signal of the AFM probe. PS_1 is the phase shift by material 1 and PS_2 by material 2.

Phase imaging

Functionalized AFM tips were used to image the phase contrast of the cellulose model films and pulp fiber treated with xylan. The reason was due to very similar surface chemistry between xylan and cellulose, a simple phase imaging employing silicon cantilevers does not give useful results. In general, phase imaging in AFM refers to recording the phase shift signal in tapping mode. This phase shift ("delay") is the difference between the excitation oscillation and reference oscillation of the cantilever due to a difference in energy dissipation. This allows the determination of material contrast. The principle of phase imaging is depicted in Figure 3.5.

Force mapping

During force mapping, the surface is scanned in tapping mode. Due to the topography and geometry of the surface of the substrate, the contact area between the functionalized tip and the surface varies (see Figure 3.3). On top of a hill or peak on the substrate, there is less contact, whereas along the sides and the valleys the contact area is larger. Thus, the adhesion between the surface and the tip is proportional to the contact area.

The principle operating mode during force mapping is depicted in Figure 3.6. The tip is approaching the surface in z-direction and in contact with the substrate. By removing the tip from surface, attractive or repulsive interaction will affect the force that is need to separate the tip from the surface. Besides the contact area, this highly depends on the functionalization of the tip and the surface chemistry of the substrate. The adhesive force F_{ad} can be extracted from this method.

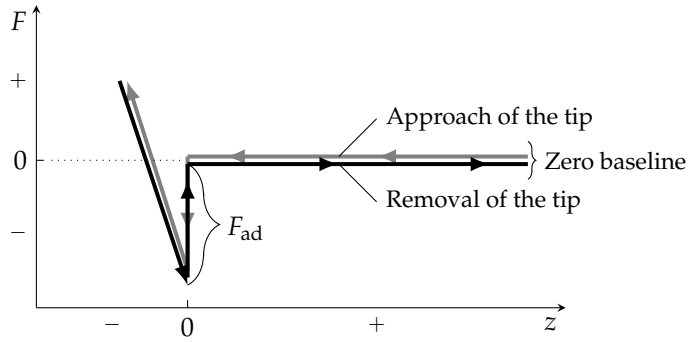

Figure 3.6 Principle of force mapping. F_{ad} is the adhesive force that is needed to separate a functionalized AFM tip from the surface of the substrate and z is the displacement of the tip in z-direction.

3.6 Pulp and paper properties

Another main aspect of this thesis was the analysis of the impact of additional xylan on pulp and paper properties, such as the swelling behavior, fiber charge, and strength characteristics.

3.6.1 Adsorption conditions

Before pulp and paper properties were determined, the pulp samples (see section 3.1) were modified by an adsorption step to increase the xylan content, as described in section 3.3.1.2. The SPB sample (sheet form) was soaked in deionized water and disintegrated for 10 min, according to ISO 5263-1:2004. Afterwards, the pulp was thickened to a dry content of about 20% and stored in a refrigerator until adsorption. The never-dried SKPUBs were already disintegrated and had a dry content of about 20%. The VFs were first washed in a laboratory dyeing apparatus (Labomat Mathis, Switzerland), with metal cuvettes in which the VFs were weighed and the standard soap solution with a concentration of 5 g/L (pre-heated to 60 °C were added at a bath ratio of 1:50. One washing cycle was carried out for 30 min at 60 °C and the frequency of rotation of the cuvettes was 40 min^{-1}. This was done in order to remove possible additives from the surface of the viscose fibers. Before adsorption, the VFs were soaked in deionized water for at least 4 h.

This adsorption step for all pulp samples was done at 80°C, pH 7, pulp consistency of 2.5%, xylan input of 80 mg/g, and ionic strength of 1 mol/L (NaCl) for 1 h. These conditions were chosen such that the amount of xylan of the fibers could be significantly increased. In case of the SKPB fibers a second adsorption condition was used with an increased xylan input of 320 mg/g.

3.6.2 Pulp properties

The impact of both xylans on the swelling behavior of the modified and unmodified SKWP pulp samples were analyzed by measuring the water retention value. Further, the fiber charge (surface and total charge) of these fibers was determined.

3.6.2.1 Fiber charge

The *total charge* was analyzed by conductometric titration, according to Katz et al. (1984). First, the pulp was transferred to its hydrogen from by using 1 mol/L of HCl until the pH was 2.00 ± 0.01 and kept constant for 30 min, as described by Horvath et al. (2007; 2006). Subsequently, the pulp sample was washed with deionized water until the conductivity was below 5 µS/cm. The polyelectrolyte adsorption was carried out similar to the method developed by Winter et al. (1986). Before the titration with NaOH (0.05 mol/L), 10 mL of NaCl and 5 mL of HCl, both 0.01 mol/L, were added to minimize the effect of a Donnan equilibrium. After the procedure, the pulp was removed from the suspension and dried, in order to determine the dry weight. The total charge can then be calculated from

$$\sigma_{\text{total}} = \frac{(V_{\text{EQ}_1} - V_{\text{EQ}_2}) \cdot c_{\text{NaOH}}}{m_{\text{DP}}} \cdot 1000 \tag{3.4}$$

where σ_{total} is the total charge (µeq/g), V_{EQ_1} is the volume of NaOH at the first inflection point, V_{EQ_2} is the volume of NaOH at the second inflection point, c_{NaOH} is the molar concentration of NaOH, and m_{DP} is the dry mass of the pulp sample. V_{EQ_1} and V_{EQ_2} are calculated from the plot of the sample via the tangent method as depicted in Figure E.1 (Appendix E).

For the analysis of the *surface charge*, the pulp was first transferred from its hydrogen form to its sodium form by using 1 mmol/L of $NaHCO_3$ and 1 mol/L of NaOH until the pH was 9.00 ± 0.01, kept constant for 30 min (Horvath et al. 2006) and washed with deionized water until the conductivity was below 5 µS/cm. A certain amount of polydiallyldimethylammonium chloride (pDADMAC) was added and stirred for 30 min. Afterwards, the fibers were separated from the suspension and dried, in order to analyze the dry weight. 200 µL of a 300 mg/L ortho-toluidine-blue solution was added to a certain amount of the filtrate and then diluted to ~ 75 mL with deionized water. A 0.001 N solution of potassium polyvinyl sulphate (KPVS) was titrated which interacts with the pDADMAC. When the pDADMAC has been consumed, KPVS changes its color and this is detected by a standard photometric probe (Mettler-Toledo), according to Terayama (1952). The surface charge is calculated by the following steps

$$m_{\text{total}} = m_{\text{poly}} + m_{\text{water}} + (m_{\text{WP}} - m_{\text{DP}}) \tag{3.5}$$

$$c_{\mathrm{EQ}} = \frac{V_{\mathrm{EQ}} \cdot \epsilon_{\mathrm{KPVS}}}{\epsilon_{\mathrm{poly}} \cdot V_{\mathrm{filtrate}}} \cdot 1000 \tag{3.6}$$

$$\Gamma = \frac{m_{\mathrm{poly}} \cdot c_{\mathrm{poly}} \cdot \epsilon_{\mathrm{poly}} - \frac{V_{\mathrm{total}}}{V_{\mathrm{filtrate}}} \cdot V_{\mathrm{EQ}} \cdot \epsilon_{\mathrm{KPVS}}}{m_{\mathrm{DP}} \cdot \epsilon_{\mathrm{poly}}} \tag{3.7}$$

where m_{total} is the total mass, m_{poly} is the mass of pDADMAC, m_{water} is the mass of water, m_{WD} is the mass of the wet pulp, c_{EQ} is the concentration at the equivalence point, V_{EQ} is the volume of KPVS at the EQ in the titration, ϵ_{KPVS} is the charge density of KPVS (meq/mL), ϵ_{poly} is the charge density of pDADMAC (meq/g), V_{filtrate} is the volume of the added filtrate, Γ is the adsorbed amount of electrolyte ($\mathrm{mg/g_{\,fiber}}$), c_{poly} is the concentration of pDADMAC solution, and V_{total} is the total volume. By constructing an adsorption isotherm by plotting Γ versus c_{EQ} and extrapolating the linear part of the curve back to $c_{\mathrm{EQ}} = 0$, as depicted in Figure E.2 (Appendix E). The surface charge ($\sigma_{\mathrm{surface}}$) is given by

$$\sigma_{\mathrm{surface}} = y - \mathrm{intercept} \cdot \epsilon_{\mathrm{poly}} \tag{3.8}$$

3.6.2.2 Water retention value

The water retention value (WRV) of the fiber samples was analyzed according to ISO 23714:2012 with a reduced time during the hydro-extraction of 15 min.

3.6.2.3 Beating degree

The beating degree of the pulp samples was determined according to DIN EN ISO 5263-1:2014.

3.6.3 Paper properties

The influence of xylan on physical strength properties of the fiber samples was also studied. First, part of the samples were modified during an adsorption step (see section 3.3.1.2 and 3.6.1). The samples were subsequently washed to remove free and unbound xylan from the suspension. Then, part of the pulps were refined in a PFI mill (ISO 5264-2:2011) at 1000 and 3000 revolutions. Handsheets with and without additional xylan were made with a Rapid-Köthen sheet former (DIN EN ISO 5269-2:2004) and conditioned (DIN EN 20187:1993) before the tensile index and stretch at break (ISO 1924-2:2008 and ISO 1924-3:2005), but also the tear index (DIN EN 21972:1998) were determined.

3.7 Fiber properties

Paper is a network of fibers and a network will always break down at its weakest point. To diminish this problem, bond strength measurements of individual fiber-fiber joints were performed.

3.7.1 Bond strength on individual fiber-fiber joints

The micro bond tester (Fischer et al. 2012) was employed to investigate the impact of the amount of xylan on the (specific) bond strength of individual fiber-fiber joints (FFJ). The main components of the micro bond tester are two linear tables, two load cells, which are placed under a microscope, and a film camera, as depicted in Figure 3.7. The resolution of the load cells is 0.5 mN and can be stressed with a maximum load of 1.5 N. The linear tables hold a displacement range of 20 µm at a speed range from 1–150 µm/s. One benefit is to simultaneously record and analyze the loading conditions as well as the stress deformation.

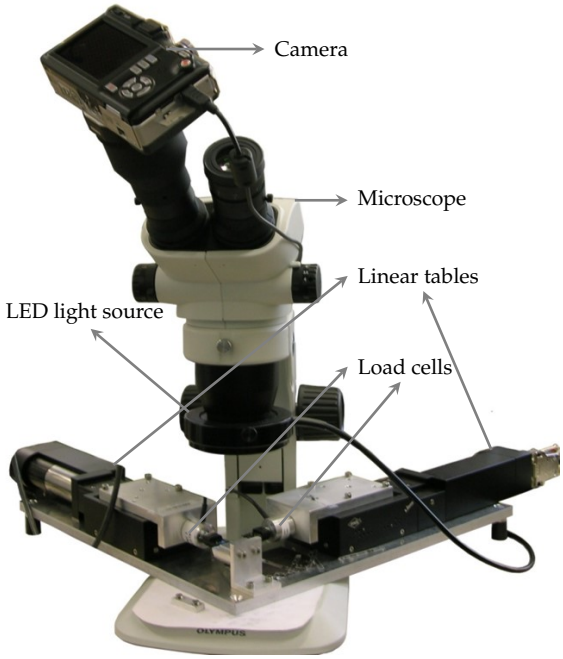

Figure 3.7 General view of the micro bond tester (Fischer et al. 2012).

3.7.1.1 Fiber modification

Individual FFJs of different samples have been tested, such as:

A: SKPB
B: SKPB treated with X_1 l (c_X = 80 mg/g)
C: SKPB treated with X_2 l (c_X = 80 mg/g)
D: SKPB treated with X_1 h (c_X = 320 mg/g)
E: SKPB treated with X_2 h (c_X = 320 mg/g)
F: SKPB treated with KOH for xylan extraction
G: SKPUB (κ42)
H: SKPUB (κ54)

The addition of xylan to the fiber sample C–E was done, as described in section 3.3.1.2 at 80°C, pH 7, pulp consistency of 2.5%, xylan input of 80 mg/g and 320 mg/g, and ionic strength of 1 mol/L (NaCl) for 1 h. The alkaline extraction was performed using 14% of potassium hydroxide (KOH) at a liquor to pulp ratio of 20:1 at 30°C for 1 hour, according to (Janzon et al. 2008). This was done in order to decrease the xylan content of the SKPB fibers. The chemical composition of the fiber samples (A–H) was analyzed by HPLC.

3.7.1.2 Sample preparation

For the testing of an individual FFJ, a fiber suspension of about 0.1% was produced of which a few droplets were given between two teflon strips and placed in a drier of a Rapid-Köthen sheet former at around 94°C for 1 hour. Afterwards, individual FFJs were glued on special designed acrylic sample holders (HESAGLAS® VOS, Topacryl AG) using nail polish, as illustrated in Figure 3.8. The reason for the use of nail polish was that cyanoacrylate glue (LOCTITE 454) forms a film on the fiber surface. This was shown by Fischer et al. (2012) by low voltage SEM. One advantage of these sample holders is the possibility of preloading the *cross fiber* (see Figure 3.8b) before testing by melting bridge iii (see Figure 3.8a). This allows the determination of the impact of biaxial load on the fiber joint strength.

3.7.1.3 Determination of the optical bonded area

The optical bonded area was imaged via polarized light microscopy, according to Gilli et al. (2009); Kappel et al. (2009, 2010) to calculate the specific bond strength of each tested FFJ. The bonded region appears darker than a single fiber or adjacent and unbonded fibers due to the absence of reflection. In this study, the use of a dye was omitted as the surface chemistry of the fibers will change, according

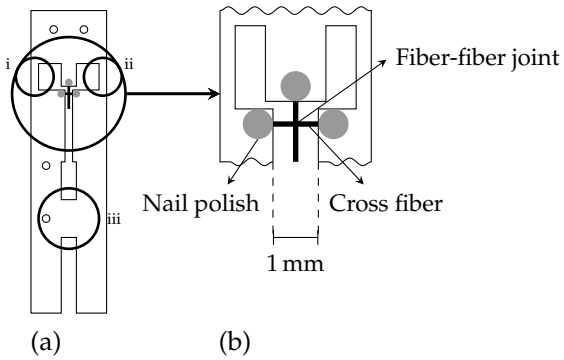

Figure 3.8 Schematic illustration of the fixation of an individual fiber-fiber joint with nail polish on a sample holder before testing with the micro bond tester: (a) overall illustration, the bridged i and ii will be melted before testing and (b) detailed illustration of a glued fiber-fiber joint.

Fischer (2013) and Weber (2014). After imaging, the bonded region was marked and converted into a binary image and the optical bonded area was calculated via Matlab.

3.7.1.4 Determination of the bond strength

The sample holder was mounted under the microscope on the linear tables in the micro bond tester (see Figure 3.9). The bridges i and ii (see Figure 3.8a) were melted and the sample holder was now divided into two parts (see Figure 3.10a). For the measurements, the cross fiber was not preloaded, therefore bridge iii was not melted before testing. Subsequently, part 1 of the sample holder was pulled away from part 2 (Figure 3.10b) at a speed of 1 µm/s and the force F and distance x were recorded until the joint broke (see Figure 3.10c). The generated values were also tested regarding possible outliers using a Dixon's Q test. An image of an individual FFJ during testing is presented in Figure H.1 (Appendix H). The tests were performed under standard atmosphere according to DIN EN 20187:1993.

3.7.2 Elastic modulus of single fibers

The tensile strength of individual fibers was measured to calculate their elastic modulus (E-modulus) or *Young's modulus*. This was done in order to investigate the influence of xylan on this fiber characteristic. The fibers exhibited the same modifications as described for the measurement of the joint strength of individual fiber crossings. The micro bond tester (see Figure 3.7) was used for this method.

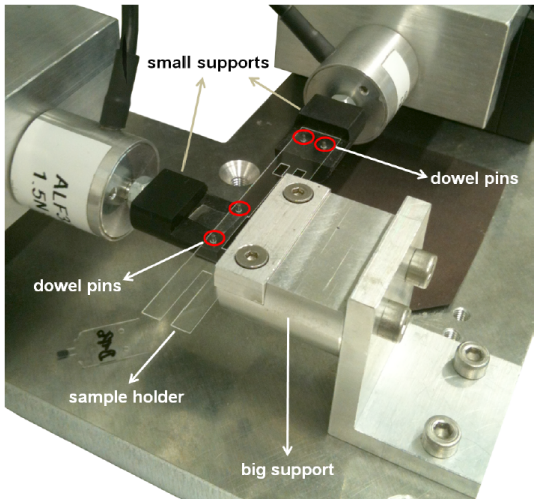

Figure 3.9 Mounting and positioning of a sample holder (Fischer 2013).

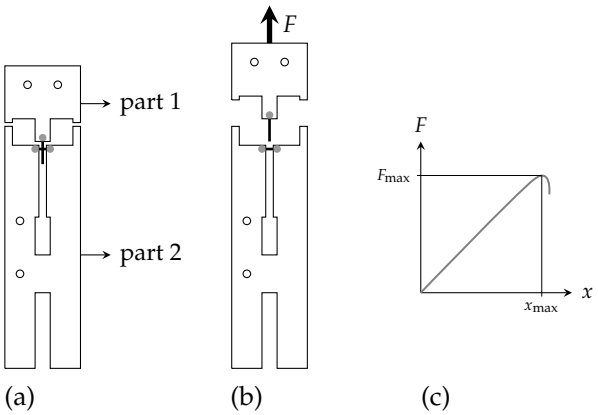

Figure 3.10 Sequence of preloading and breaking an individual fiber-fiber joint with the micro bond tester: (a) part 1 and 2 are only connected via the fiber-fiber joints after melting the bridges, (b) loading the fiber-fiber joint in x-direction until breakage by pulling part 1 at a speed of 1µm/s, and (c) recording of the force (F) and distance (x) during testing..

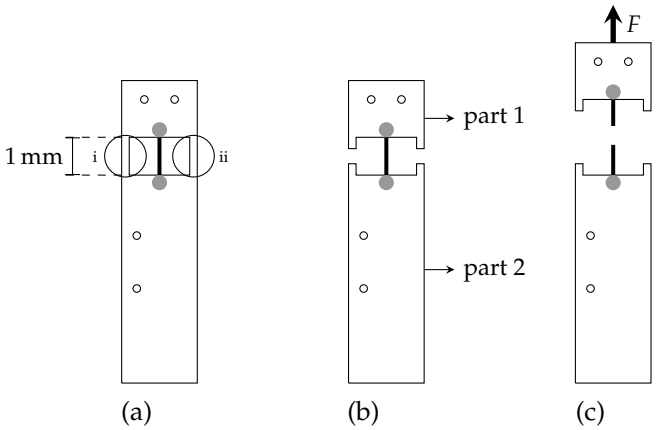

Figure 3.11 Schematic illustration of a fixed individual fiber before and after strength testing with the micro bond tester: (a) a single fiber is glued on the sample holder, (b) melting the bridges i and ii after mounting the sample holder in the micro bond tester, and (c) loading the in x-direction until the fiber breaks by pulling part 1 at a speed of 1 µm/min (force F and distance x are being recorded during testing.

3.7.2.1 Sample preparation

The same procedure was performed as before described in section 3.7.1. After drying, single fibers were glued on special designed acrylic sample holders using solvent free 2-component epoxy resin adhesive (UHU Plus endfest) as illustrated in Figure 3.11a. The reason for the use of an epoxy adhesive was that nail polish is too weak for single fiber tensile testing (Fischer 2013).

3.7.2.2 Determination of the E-modulus

After the epoxy resin was dried (12 hours), the sample holder was mounted in the micro bond tester and the two bridges i and ii were melted and the sample holder was now divided into two parts (see Figure 3.11b). Then, part 1 of the sample holder was pulled away (Figure 3.11b) at a speed of 1 µm/s and the force F and distance x were recorded until the fiber broke (see Figure 3.8c). The generated values were also tested regarding possible outliers using a Dixon's Q test. An image of a single fiber during tensile testing is presented in Figure 3.12. The tests were performed under standard atmosphere according to DIN EN 20187:1993.

After the fiber was broken into two parts, the length of the glued fiber before testing (l_0) and right before its failure (l_1) were determined from the images taken during the measurement (see Figure 3.12). Afterwards, the elastic modulus E was calculated by (Giancoli 2010)

$$E = \frac{\sigma}{\varepsilon} = \text{const.} \tag{3.9}$$

with

$$\varepsilon = \frac{\Delta l}{l_0} = \frac{l_1 - l_0}{l_0} \tag{3.10}$$

and

$$\sigma = \frac{F}{A} \tag{3.11}$$

where σ is the stress, ε is the strain of the fiber, and A is the area of the cross section of the fiber. The value for A was estimated to be 154 µm^2 at standard atmosphere (DIN EN 20187:1993). This value was determined by Lorbach et al. (2014). They calculated the area of 280 cross sections of unbleached softwood kraft pulp. The same pulp was used in this thesis (G–H). It was assumed that the bleached fiber samples (A–F) feature the same mean value. Moreover, the mean value of the fiber width of the fiber samples was 33.7 µm and the fiber thickness was 8.6 µm. The resulting aspect ratio is 3.92:1. This was also considered in a second step. The fiber width of the tested fibers was measured and the fiber thickness was calculated using this aspect ratio to determine the area of the cross section. For this it was assumed that the aspect ratio is the same for every fiber and the fibers are completely collapsed. The fiber cross sectional area was assumed to possess a shape of an ellipse and the areas was calculated by (Bartsch 2011)

$$A = \pi \cdot a \cdot b \tag{3.12}$$

where a is the half of the length of the fiber width and b is half of the length of the fiber thickness. On each tested fiber, the fiber width was measured on three individual place.

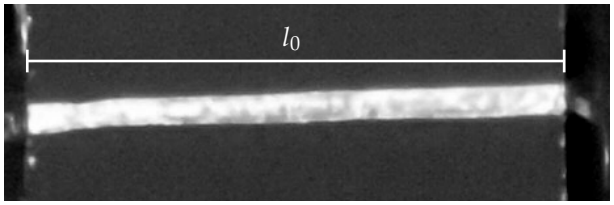

(a) Single fiber before tensile testing.

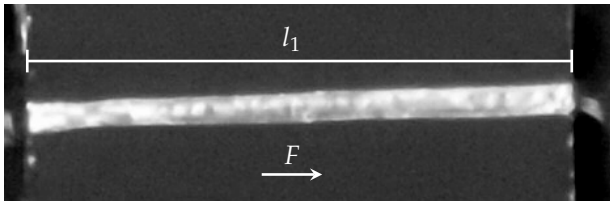

(b) Single fiber before failure.

Figure 3.12 Determination of the elongation $\Delta l = l_1 - l_0$ of a single fiber during tensile testing by (a) measuring the length l_0 before testing and (b) the length l_1 right before the failure of a fiber due to mechanical stress F.

Chapter 4

Results and Discussion

4.1 Characterization of the pulp samples

In a first step the pulp samples were analyzed regarding their chemical composition and structure. This was done in order to determine differences in the chemistry of the fiber samples. The results are represented in Table 4.1.

The xylan content of the bleached and unbleached softwood kraft pulps (SKPB and SKPUB) was similar between 7.8% and 7.9%. The mannose content was about 6.0–6.2% for the pulps. The SKPUB had a slightly higher amount of arabinose (+ 0.3%), galactose (+ 0.3%) and some rhamnose (0.1%). This is most probably due to the bleaching of SKPB. For the bleached sulfite pulp (SPB), the amount of both, xylose and mannose are lower. Further hemicelluloses could not be obtained for this pulp. During sulfite pulping, the fiber is attacked by the chemicals from the middle lamella in direction to the lumen. Thus the hemicellulose rich primary wall is completely dissolved (Bachner et al. 1993) as well as part of the first secondary wall resulting in a different morphology.

Further, the pulps varied in their amount of lignin. SKPUB_54 had the highest value for the Klason lignin (KL) with 8.04%. Due to the longer delignification of SKPUB_42 the KL content was reduced to 6.49%. After bleaching the amount of KL was further lowered to 0.22%. A similar trend was detected for the Kappa number from 53.8 (SKPUB_54) to 0.5 (SKPB). The acid-soluble lignin (SL) was slightly affected by bleaching. The SPB had the lowest amount of KL with 0.06% but a higher amount of SL with 1.02%. This means that the residual lignin is becoming more soluble due to the formation of polar groups (Lin 1992) which can lead to stronger repulsion between adjacent fibers as well as between the fibers surface and equally charged polymers dissolved in the cooking liquor.

The amount of extractives is higher for the unbleached pulps. Besides the removal of lignin, bleaching results in a decrease in extractives. This can be seen i.a. in the ash content as well. Moreover, during the washing steps after delignification and bleaching, a certain the amount of loosely bound extractives could be decreased. The viscosity is also reduced due to delignification and bleaching as can be seen for the softwood kraft pulps which is lowered from 1130 ± 14 (SKPUB_54) to 568 ± 4 (SKPB). The bleached sulfite pulp has a higher pulp viscosity, than the bleached sulfate pulp. This is due to the chemical attack during sulfite pulping which starts at the middle lamella in direction to the lumen. Thus the primary wall and part of the first secondary wall is removed which contains in general shorter cellulose chains.

All pulps exhibited a certain amount of different metals which is presented in Table 4.2. The amounts of different metals varied between the pulp samples and does not follow a clear trend.

Table 4.1 Chemical properties of the pulp samples.

Parameter	Unit	SPB	SKPB	SKPUB_42	SKPUB_54
Glucose	%	87.5 ± 0.5	80.5 ± 1.2	77.7 ± 0.4	75.2 ± 1.0
Xylose	%	5.3 ± 0.0	7.8 ± 0.1	7.8 ± 0.0	7.9 ± 0.1
Mannose	%	5.4 ± 0.1	6.2 ± 0.1	6.1 ± 0.0	6.0 ± 0.0
Arabinose	%	0.0 ± 0.0	0.5 ± 0.0	0.8 ± 0.0	0.8 ± 0.0
Rhamnose	%	0.0 ± 0.0	0.0 ± 0.0	0.1 ± 0.0	0.1 ± 0.0
Galactose	%	0.0 ± 0.0	0.2 ± 0.0	0.5 ± 0.0	0.6 ± 0.0
total	%	98.2 ± 0.6	95.6 ± 1.4	93.0 ± 0.4	90.6 ± 1.1
Klason lignin	%	0.06 ± 0.03	0.22 ± 0.01	6.49 ± 0.06	8.04 ± 0.21
Acid-soluble lignin	%	1.02 ± 0.01	0.22 ± 0.01	0.17 ± 0.01	0.18 ± 0.01
Kappa number		5.7 ± 0.2	0.5 ± 0.1	42.2 ± 0.8	53.8 ± 0.4
Extractives	%	0.049 ± 0.04	0.020 ± 0.04	0.119 ± 0.028	0.106 ± 0.025
Viscosity	mL/g	892 ± 5	568 ± 4	1137 ± 9	1130 ± 14
Copper number	g/100 g	1.23 ± 0.01	1.11 ± 0.12	1.18 ± 0.13	1.37 ± 0.04
Ash (850°C)	%	0.45	0.30	0.55	0.58

Table 4.2 Analysis of metals in the pulp samples.

Sample	Si $mg\,kg^{-1}$	Fe $mg\,kg^{-1}$	Ca $mg\,kg^{-1}$	Mg $mg\,kg^{-1}$	Ni $mg\,kg^{-1}$	Cu $mg\,kg^{-1}$	Mn $mg\,kg^{-1}$
SPB	592	32.9	310	1100	<0.42	<0.40	1.5
SKPB	544	48.5	100	520	<0.47	<0.43	1.3
SKPUB_42	170	18.2	2800	420	<1.2	12	37
SKPUB_54	115	13.4	3000	370	<1.2	8.2	38

4.2 Chemical analysis

The xylan content of the softwood kraft pulp fibers could be increased due to adsorption and precipitation. The amount of redeposited xylan onto the fibers depends on the adjustment of the investigated variables. The influence of the six variables on adsorption of the two xylans (X_1 and X_2) are presented in the following Figures 4.1–4.6. The xylan content was determined by HPLC. A comparison of the results determined via HPLC and NMR is shown in Figure 4.8.

4.2.1 Factors influencing xylan adsorption

The temperature (Figure 4.1) had a significant impact on adsorption. The lowest increase in the amount of xylan was obtained at the lowest temperature of 40°C. The amount of X_2 could be continuously enhanced by raising the temperature to 80°C and further 140°C. Moreover, an adsorption maximum is almost reached after

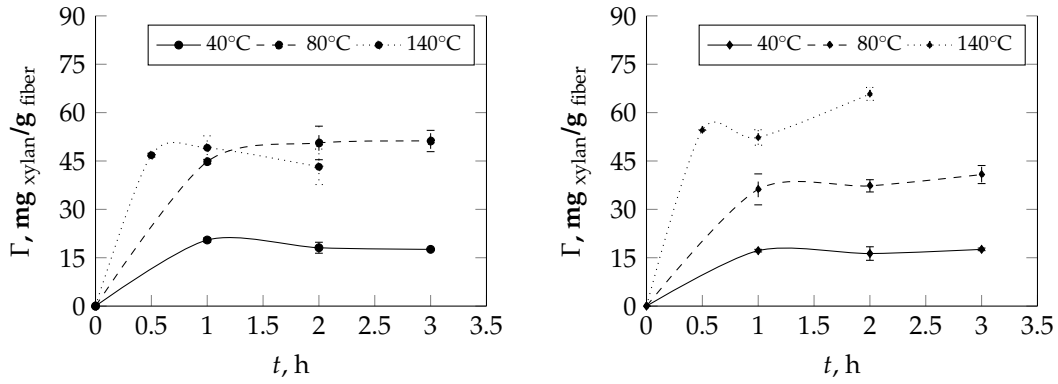

(a) Xylan 1. (b) Xylan 2.

Figure 4.1 Impact of the temperature on the amount of adsorbed X_1 and X_2 onto SKPB fibers at: pH = 7, I = 0.25 M (NaCl), C = 2.5%, and c_x = 160 mg/g.

1 hour for the temperature at 40°C and 80°C. At 140°C an adsorption maximum is not reached after 2 hours. A similar trend was obtained for X_1 at the lower temperature levels, but the adsorbed amount at 80°C was higher, compared to X_2. The reason for this is predominantly the lower molecular weight and better dissolution behavior of X_1 due to a higher content of MeGlcA. Longer and bigger aggregates/agglomerates of xylan could force higher steric repulsion towards cellulose. Further, stronger interactions could be induced between xylan and the fiber surface. However, higher temperatures, especially under alkaline conditions, will affect the chemical structure by splitting off MeGlcA. Thus, a reduction of the solubility of xylan follows. Consequently, precipitation of xylan onto the fiber surface is promoted (Mitikka-Eklund 1996). In case of X_1, more dissolved xylan can adsorb and precipitate on the surface. No difference was seen between 80°C and 140°C for X_1. This could be due to an equilibrium between adsorption and dissolution of xylan. On the other hand, raising the temperature to 140°C resulted in a higher amount of xylan for X_2. Due to the higher molecular weight and lower amount of MeGlcA, a higher temperature will increase dissolution of X_2. Nevertheless, the temperature dependence of adsorption could be due to the decrease in surrounding water forming hydrogen bonds by thermal vibration, allowing an intimate contact between the hydroxyl groups of xylan and cellulose (Hansson 1970a; Hartler and Lund 1962).

The pH (Figure 4.2) is important for an efficient xylan retention and it influences the solubility of the molecule. Lowering the pH from 12.6 to 10 resulted in an enhancement in deposition which is about twice as large. A further reduction in the pH level to a neutral range exhibited no further improvement. The amount of additional xylan on the SKPB fibers was higher for X_1 than for X_2, due to the lower molecular weight and higher amount of MeGlcA. Hydroxyl groups have a lower acid strength (pKa = 14 at 25°C), meaning these groups are ionized only in a strong alkaline environment. A decrease in the pH to a neutral level leads to a lower

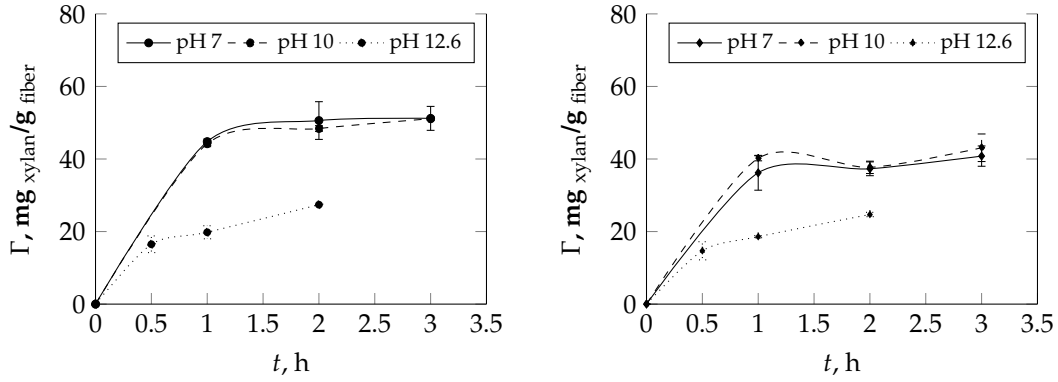

(a) Xylan 1. (b) Xylan 2.

Figure 4.2 Impact of the pH on the amount of adsorbed X_1 and X_2 onto SKPB fibers at: ϑ = 80°C, I = 0.25 M (NaCl), C = 2.5%, and c_x = 160 mg/g.

solubility of xylan and lower electrostatic repulsion between xylan molecules and cellulose and is favorable for precipitation onto the fiber surface (Sjöström 1989).

The way the pH is adjusted has an influence on the amount of precipitated xylan as well. This was confirmed for X_1 and X_2 at room temperature and a pH of 7, 10, and 12.6. The adsorption step lasted for 10 min after the pH was carefully adjusted. Xylan was dissolved in 1 mol/L NaOH. The pH was adjusted in two different ways: 1) the pH of the dissolved xylan was adjusted and the xylan suspension was added to the pulp suspension (X_1/X_2 before) and 2) the dissolved xylan was added to the pulp suspension and the pH of the xylan-pulp suspension was adjusted as done in the other experiments (X_1/X_2 after). Afterwards, the samples were washed, as described in section 3.3. The results are depicted in Figure 4.3. As can be seen, it is favorable to adjust the pH after the addition of dissolved xylan to the pulp suspension. This allows precipitation of xylan between single xylan molecules but also between xylan molecules and cellulose. This effect was more pronounced for X_1 due to its solubility behavior. The amount of xylan of the reference sample (SKPB) was not affected at a pH of 12.6. This is due to the short reaction time of only 10 min and the temperature level. However, at elevated temperature of 80°C, the xylan content decreased from $\approx$ 8.4% to around 7.5% due to dissolution but was not significantly influenced by different dwell times.

Besides the pH value, the ionic strength should be increased to enhance xylan deposition, as shown in Figure 4.4. Cellulose and xylan feature similar surface textures of hydroxyl groups, indicating likewise surface charges. Moreover, xylan contains carboxyl groups. Thus, the salt concentration should be high enough to diminish electrostatic and steric repulsion between xylan molecules, and between xylan and cellulose. In addition, it promotes interactions and associations between these interfaces (Linder et al. 2003; Mitikka-Eklund 1996; Ström et al. 1982). However, the solubility of xylan molecules is also dependent on the salt used to set the

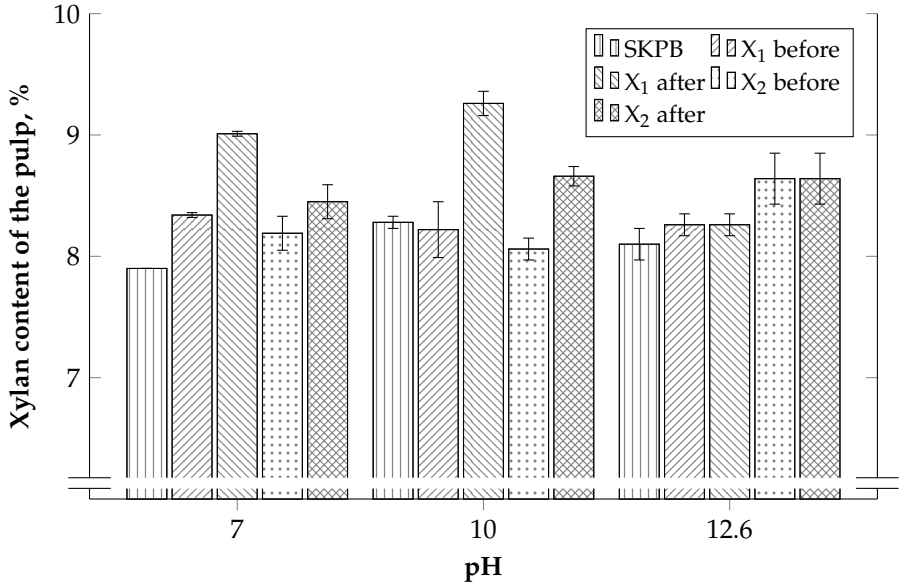

Figure 4.3 Influence of the adjustment of the pH for the adsorption of xylan at: room temperature, I = 0.25 M (NaCl), C = 2.5%, and c_x = 160 mg/g.

ionic strength. Ions can either promote or retard the solubility of xylan in aqueous solution (Hofmeister series), and thus affect precipitation of xylan.

The ratio between the amount of available xylan and the available surface area has an influence on the amount of deposited xylan. This ratio can be either influenced by the amount of xylan added to the suspension or by changing the pulp consistency. The latter showed a small impact on xylan adsorption/precipitation (Figure 4.5). At higher pulp consistencies a stronger effort is needed for a sufficient mixing. Thus, increasing the input of xylan seems to be an easier way to significantly increase the xylan content of the fibers, as illustrated in Figure 4.6. The difference between a xylan input of 80 mg/g and 160 mg/g was not significant but

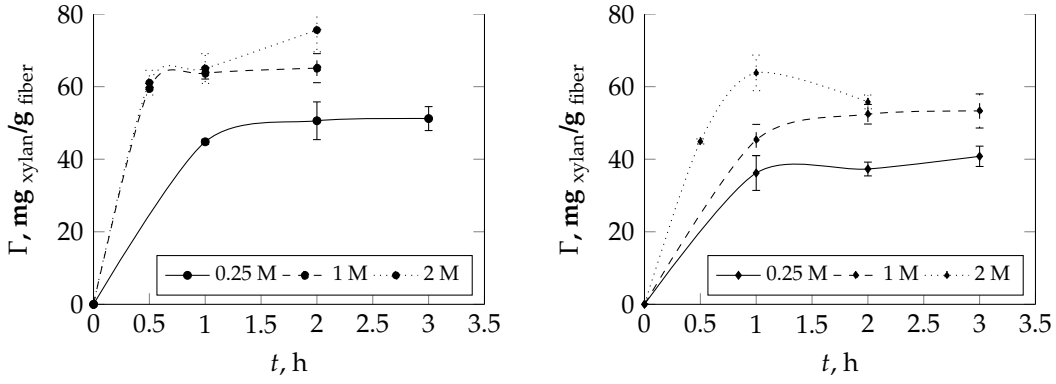

(a) Xylan 1. (b) Xylan 2.

Figure 4.4 Impact of the ionic strength on adsorption of X_1 and X_2 onto SKPB fibers at: ϑ = 80°C, pH = 7, C = 2.5%, and c_x = 160 mg/g.

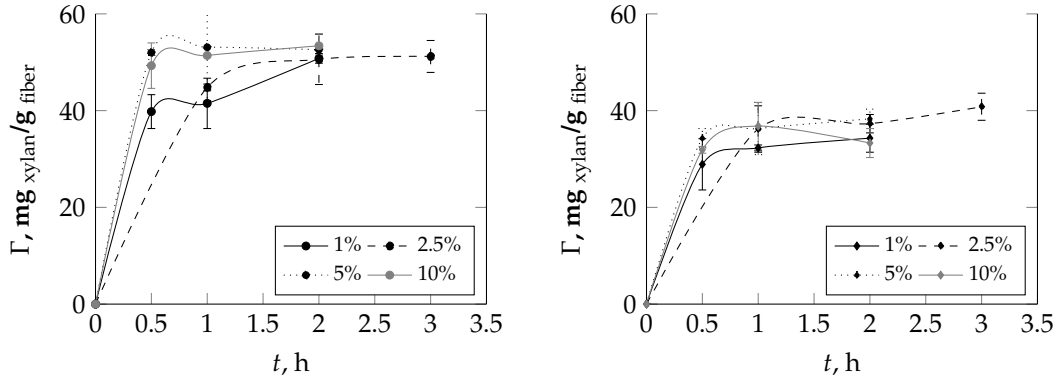

(a) Xylan 1. (b) Xylan 2.

Figure 4.5 Impact of the pulp consistency on adsorption of X_1 and X_2 onto SKPB fibers at: $\vartheta = 80°C$, $I = 0.25\,M$ (NaCl), $C = 2.5\%$, and $c_x = 160\,mg/g$.

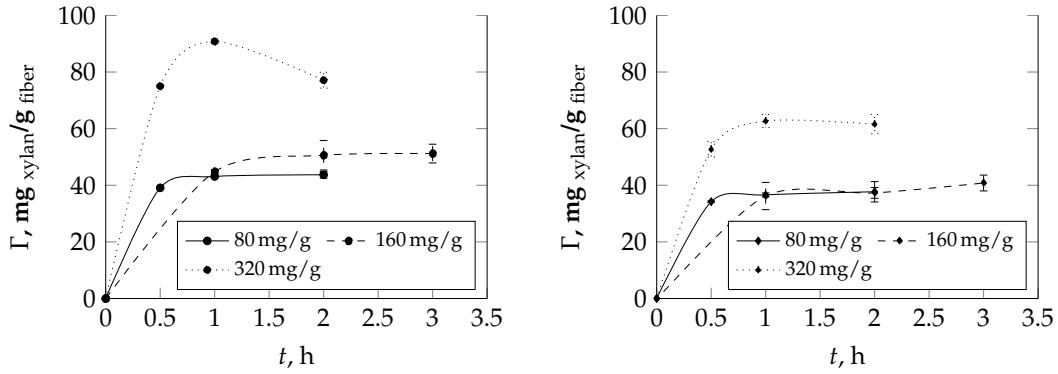

(a) Xylan 1. (b) Xylan 2.

Figure 4.6 Impact of the input of xylan on adsorption of X_1 and X_2 onto SKPB fibers at: $\vartheta = 80°C$, pH = 7, $I = 0.25\,M$ (NaCl), and $C = 2.5\%$.

a further increase to 320 mg/g resulted in a higher take up of xylan. The results again indicate, that an adsorption maximum is reached after almost 1 hour at elevated temperature and neutral environment.

When using additives for papermaking, the retention is also of huge importance. This has to be considered for the adsorption of xylan as well and is illustrated in Figure 4.7 for both xylans. As mentioned before, the take up of X_1 is stronger than of X_2. Thus, the retention for X_2 is in general lower. At the given values for the variables and an input of xylan of 80 mg/g the retention of X_1 was about 52%, whereas for X_2 the retention was around 37%. An increase in the amount of xylan added to the pulp suspension resulted in an increased xylan content of the fibers, but the retention of xylan decreased to about 28% (X_1) and 24% (X_2). Thus, it can be concluded that the retention of xylan is dependent on the input and the surface morphology and chemistry of the fibers. For a higher take up of xylan, the fiber could be treated with cationic polymers (Galván et al. 2012) to change the surface

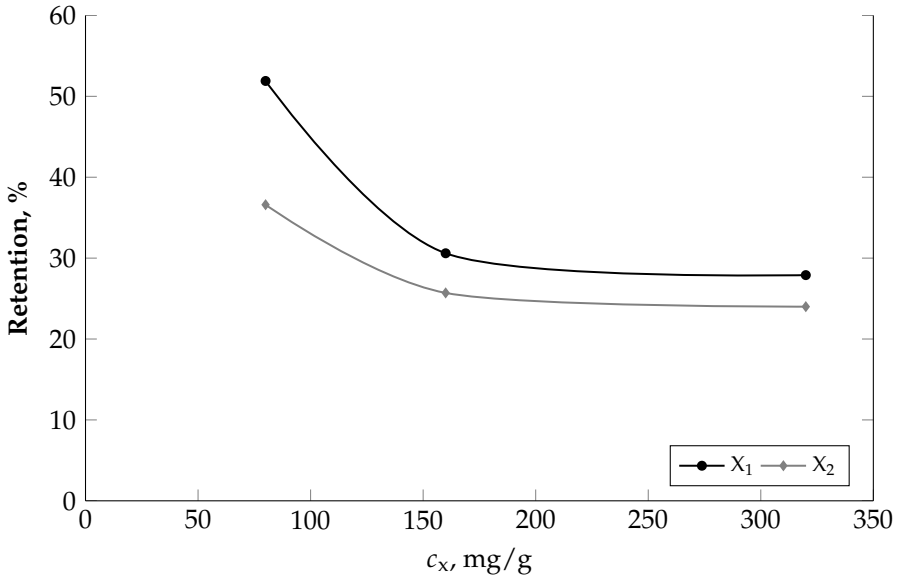

Figure 4.7 Retention of X_1 and X_2 at two different amouts of xylan input at: ϑ = 80°C, pH = 7, I = 0.25 M (NaCl), and C = 2.5%.

charge and reduce electrostatic repulsion between xylan and cellulose or using additional retention additives.

4.2.2 Comparison between HPLC and NMR

As mentioned before, HPLC and NMR measurements were performed to characterize the chemical composition of the SKPB samples before and after treatment with aqueous xylan solutions. Both measurement methods exhibited a similar development of the amount of xylan after adsorption, but the values show a slight offset. The differences in the values could be explained by two things. Firstly, the procedures to dissolve the pulp into their neutral sugar monomers are different regarding the concentrations of H_2SO_4 and the time during the two-step hydrolysis. This can have an effect on the amount of dissolved material. Moreover, the principle of the two measurements are different. Secondly, in HPLC the various dissolved sugar monomers are separated into fractions which are than counted, while during NMR the monomers are exposed to a magnetic field resulting in periodic motion. Each sugar component possesses a different frequency at which the periodic motion occurs. This could also lead to different values for each sugar fraction. The results by NMR are presented in Figure 4.8.

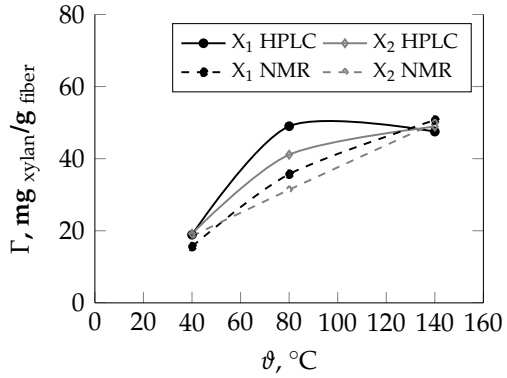

(a) Influence of the temperature: pH 7, I = 0.25 M (NaCl), C = 2.5%, c_x = 160 mg/g, and t = 1 h.

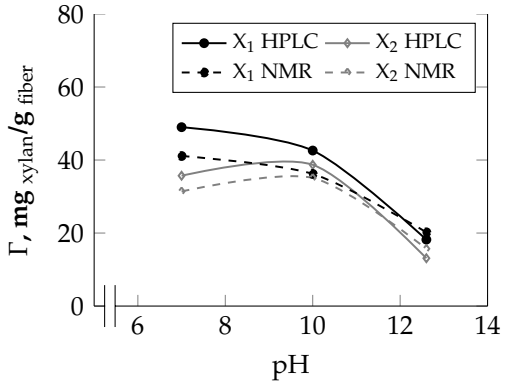

(b) Influence of the pH level: ϑ = 80°C, I = 0.25 M (NaCl), C = 2.5%, c_x = 160 mg/g, and t = 1 h.

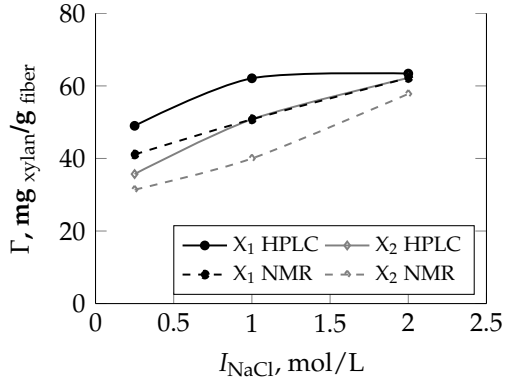

(c) Influence of the ionic strength: ϑ = 80°C, pH 7, C = 2.5%, c_x = 160 mg/g, and t = 1 h.

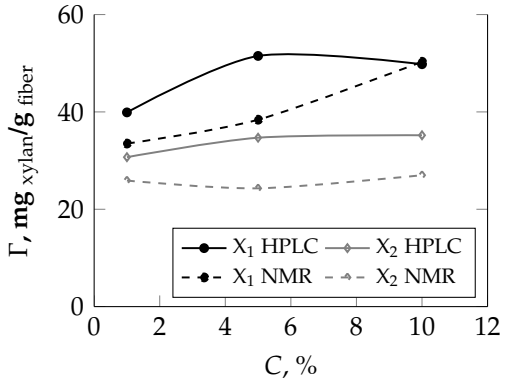

(d) Influence of the pulp consistency: ϑ = 80°C, pH 7, I = 0.25 M (NaCl), c_x = 160 mg/g, and t = 1 h.

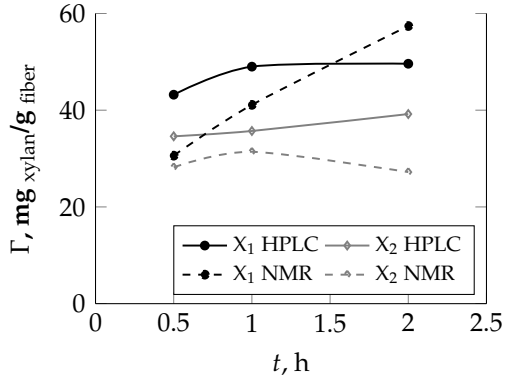

(e) Influence of the adsorption time: ϑ = 80°C, pH 7, I = 0.25 M (NaCl), C = 2.5%, and c_x = 160 mg/g.

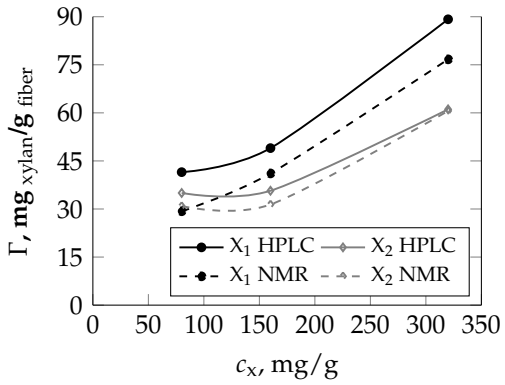

(f) Influence of the xylan input: ϑ = 80°C, pH 7, I = 0.25 M (NaCl), C = 2.5%, and t = 1 h.

Figure 4.8 Comparison between HPLC and NMR regarding the investigated influencing variables on adsorption of X_1 and X_2 onto bleached softwood kraft pulp: (a) influence of the temperature, (b) influence of the pH level, (c) influence of the ionic strength, (d) influence of the pulp consistency, (e) influence of the adsorption time, and (f) influence of the amount of added xylan with regard to the oven-dry pulp mass. .

4.3 Distribution of attached xylan

After studying the impact of the six variables on the adsorption of xylan onto softwood kraft pulp, the distribution of the attached xylan on the fiber was of interest. It was of interest whether xylan accumulates nonuniformly on the fiber surface or more homogeneously. Therefore, different methods have been applied such as attenuated total reflection (ATR) spectroscopy, X-ray photoelectron spectroscopy (XPS), scanning electron microscopy (SEM), and atomic force microscopy (AFM) in order to study the arrangement in more detail.

4.3.1 Attenuated total reflection spectroscopy

This method was used to investigate whether xylan is only adsorbed/precipitated on the surface of the SKPB fibers or also able to penetrate or diffuse into the pores of the fibers. During the mechanical treatment of refining some xylan from the pores might get accessible again on the surface for fiber-fiber interaction.

Handsheets of SKPB with and without precipitated xylan, unrefined (a) and refined at 1000 (b) and 3000 (c) revolutions (PFI mill) were analyzed by ATR spectroscopy in order to determine the intensity of the infrared (IR) peaks at the wavelengths of 1650 cm^{-1} and 1750 cm^{-1}. In this region COOH groups show characteristic stretching vibrations. Moreover, it was to prove whether the intensity of the IR peaks is higher for the refined samples.

Firstly, both xylans were analyzed in their powder form to determine the intensities of the characteristic IR peaks. X_1 shows a larger absorption of IR light between the wavelengths of interest than X_2 (see Figure 4.9). This behavior is due to a higher amount of uronic acid residues, containing carboxyl groups, in X_1.

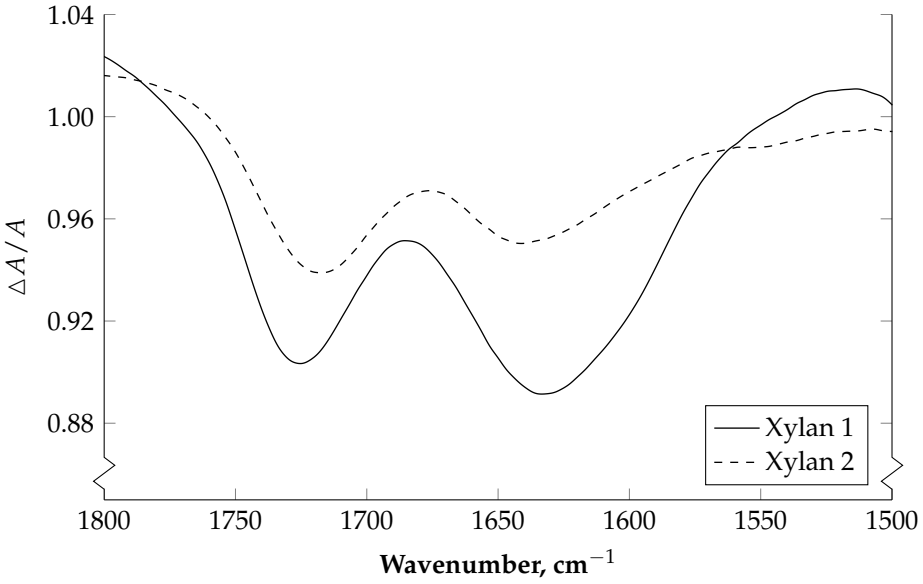

Figure 4.9 ATR spectra of pure xylan 1 and xylan 2.

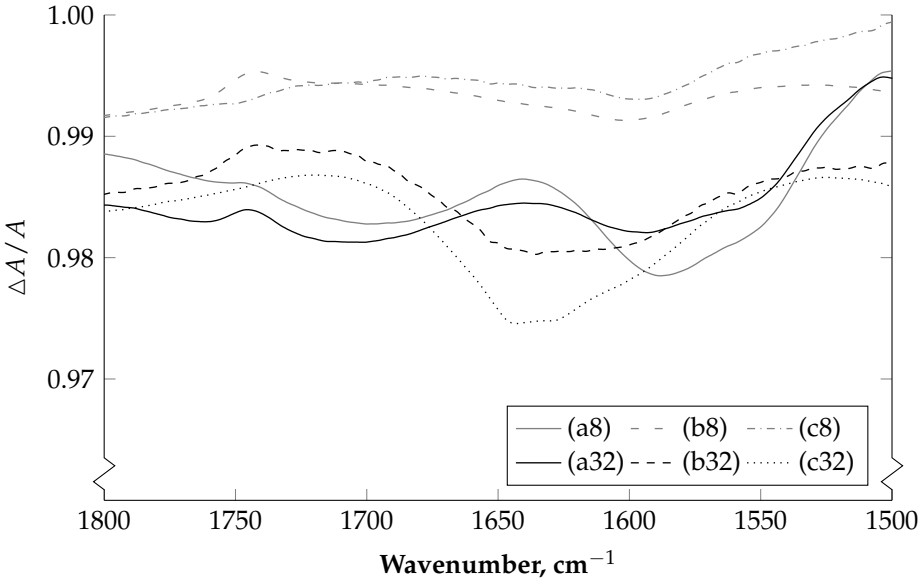

Figure 4.10 ATR spectra of SPKB handsheets with additional X_1 (xylan input during adsorption: 8 = 80 mg/g and 32 = 320 mg/g) at (a) 0, (b) 1000, and (c) 3000 revolutions.

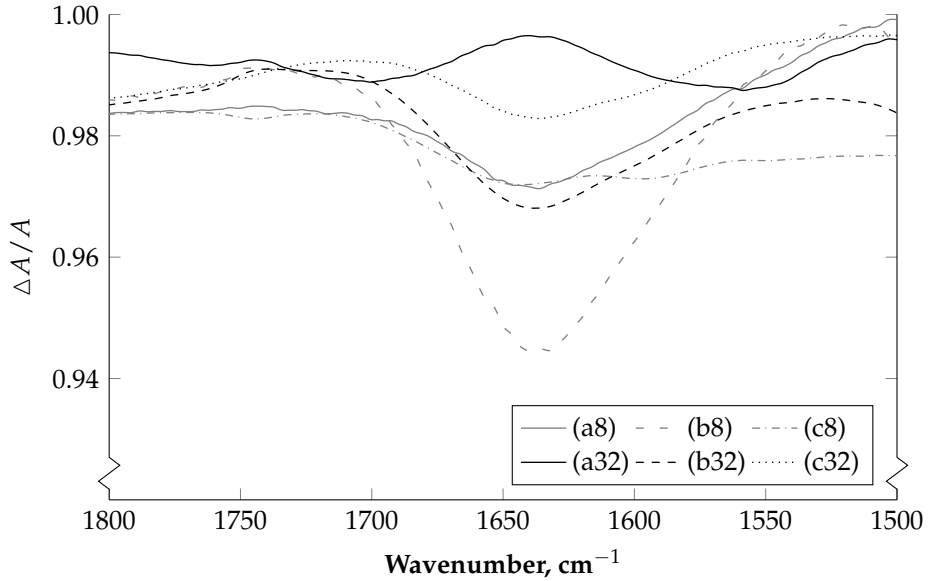

Figure 4.11 ATR spectra of SPKB handsheets with additional X_2 (xylan input during adsorption: 8 = 80 mg/g and 32 = 320 mg/g) at (a) 0, (b) 1000, and (c) 3000 revolutions.

The intensities of the IR peaks fluctuate between different refining intensities as well as different amounts of precipitated xylan (X_1 and X_2) on the samples of SKPB handsheets, as presented in Figure 4.10 and 4.11. In Figure 4.10, the intensities of the unrefined (a) and refined handsheets at 1000 revolutions (b) treated with 320 mg/g of X_1 are quite similar, whereas the peak at 1650 cm^{-1} of the handsheet beaten at 3000 revolutions (c32) is larger. In Figure 4.11, the intensity of (b8) is much larger than for (a8) and (c8) as well as at a higher input of xylan. Further measurements at other areas of the handsheets resulted in similar fluctuations. Sometimes the IR peaks at an input of xylan of 80 mg/g were larger than at 320 mg/g and reverse. The variations were also present between unrefined and refined samples. Therefore, no clear trend in the intensities of the IR peaks at an increased amount of adsorbed/precipitated xylan could be observed on the SKPB handsheets. This could indicate that xylan is nonuniformly and heterogeneously distributed on the fiber surface, even for additional xylan which is in accordance with Henriksson and Gatenholm (2002); Linder et al. (2003).

4.3.2 X-ray photoelectron spectroscopy

XPS was performed since it is more surface sensitive than ATR spectroscopy with an analysis depth of 0.5–10 nm (Conners and Banerjee 1995). Moreover, the atomic concentration can be calculated from the spectra allowing to quantify the chemical composition. Handsheets with the same modification as used for ATR spectroscopy were analyzed. Unfortunately, the resolution of the O1s peaks were too low to

Table 4.3 Binding energies and atomic concentration of the handsheets with and without additional xylan.

Sample	Peak	Binding energy, eV	Atomic concentration, %
SKPB	C1 [C−C]	285.00	30.52 ± 9.88
	C2 [C−OH]	286.55	42.76 ± 11.28
	C3 [C=O]	287.41	26.07 ± 7.87
SKPB with X_1	C1 [C−C]	285.00	28.77 ± 4.45
	C2 [C−OH]	286.54	44.65 ± 7.95
	C3 [C=O]	287.75	25.85 ± 9.17
SKPB with X_2	C1 [C−C]	285.00	29.43 ± 0.92
	C2 [C−OH]	286.55	44.98 ± 9.49
	C3 [C=O]	287.77	25.58 ± 8.84

distinguish differences between the samples. Thus, the C1s peaks were analyzed for all investigated samples. All C1s peaks were fitted by three carbon peaks (C1, C2, and C3). The position of a peak is equivalent to the binding energy of the emitted electron which is characteristic for each electron. Therefore, the peak area of each carbon peak corresponds to the atomic concentration. The most interesting peak is the C3 peak which corresponds to C=O bonds reflecting the amount of COOH groups. The results are presented in Table 4.3.

The atomic concentration for all three peaks are almost the same in the untreated and xylan-treated handsheets. The C1 peak is about 29% for all samples and the C2 peak, representing hydrogen bonds, varies from 42% to about 45%. Further, there is no difference in the samples for the C3 peak. The atomic percentage was observed to vary between 25% and 26%. It was expected, that the peak area of the C3 peak is higher for the handsheets with additional xylan, since this peak represents C=O bonds from carboxylic groups which are present at the backbone of xylan. The reason may be, that hemicelluloses but also other components, such as lignin ($\sim 0.44\%$), are present on the surface of the reference sample and within the fiber cell wall. Thus, areas with higher and lower amounts of COOH groups are present on the fiber surface. The increase in the amount of additional xylan may enhance the fluctuation of such areas. Moreover, the diameter of the investigated surface area was about 4–5 mm. This means, that the number of fibers investigated on each spot was different due to flocculations. Therefore, the atomic concentration would have to be standardized to the quantity of fibers in the investigated area. However, this is not feasible and the outcome of XPS is just an information about the chemical composition of the surface, but the amount of xylan cannot be quantitatively analyzed in an acceptable manner.

4.3.3 Scanning electron microscopy

The results of the analysis of the surface chemistry by ATR spectroscopy and XPS could indicate a nonuniform distribution of xylan on the fiber surface. Moreover, the investigated area during XPS and ATR spectroscopy is characterized by a few square millimeters. In literature the size of additional xylan on cellulosic fibers is reported to be in the nanometer and micrometer range. Therefore, scanning electron microscopy was employed to investigate the fiber surface in a much smaller area. If xylan can be detected in SEM a nonuniform distribution would be expected. The detection of the surface texture of individual SKPB fibers before and after the treatment with xylan were done in the conventional and low voltage mode.

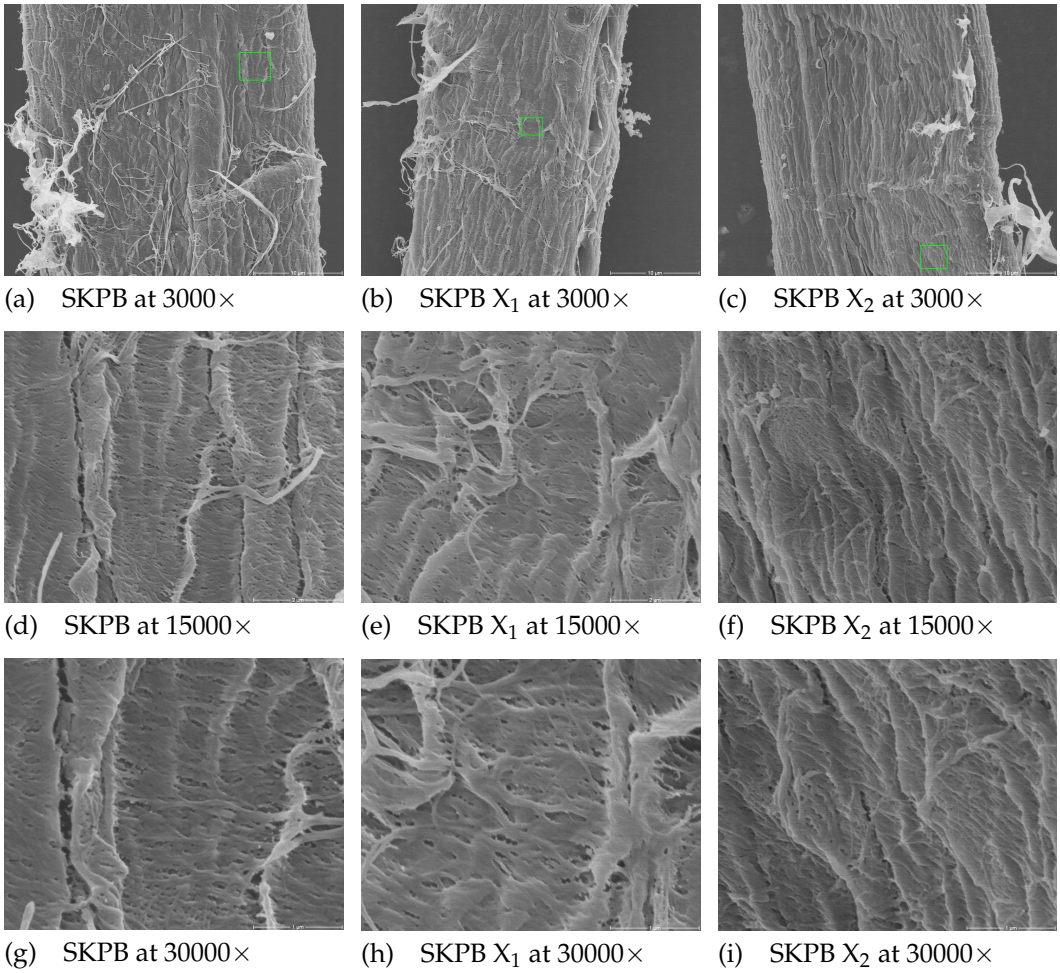

(a) SKPB at 3000× (b) SKPB X_1 at 3000× (c) SKPB X_2 at 3000×

(d) SKPB at 15000× (e) SKPB X_1 at 15000× (f) SKPB X_2 at 15000×

(g) SKPB at 30000× (h) SKPB X_1 at 30000× (i) SKPB X_2 at 30000×

Figure 4.12 Images of treated and untreated unrefined SKPB fibers generated in the conventional SEM: (a) reference sample at magnification of 3000×, (b) sample treated with X_1 at magnification of 3000×, (c) sample treated with X_2 at magnification of 3000×, (d) reference sample at 15000×, (e) sample treated with X_1 at magnification of 15000×, (f) sample treated with X_2 at magnification of 15000×, (g) reference sample at 30000×, (h) sample treated with X_1 at magnification of 30000×, and (i) sample treated with X_2 at magnification of 30000×. The size of the white bar is 10, 2, and 1 microm for 3000×, 15000×, and 30000× magnification..

In Figure 4.12 SEM images of individual unrefined SKPB fibers with and without additional xylan are shown which were generated in the conventional mode at various magnifications (3000...30000×). A few particles can be observed, especially on the reference sample. But it is not clear, whether they indicate adsorbed or precipitated xylan or deposits of other particles. By comparing the images no difference between the surface structure of the untreated fiber and the fibers treated with X_1 and X_2 were found. At higher magnification (15000...30000×) additional structures, such as aggregates or agglomerates could not be observed for the xylan-modified fibers. This was also obtained by evaluating different positions at various fibers and at magnifications up to 60000×. The results are in accordance with Köhnke and Gatenholm (2007).

On the other hand, Henriksson and Gatenholm (2001, 2002) adsorbed glucuronoxylan on pure cotton fibers and chemi-thermomechanical pulp fibers. Afterwards, the pulps were washed with hot water and sputter coated using gold for conventional SEM. They identified small particles on the treated fiber surfaces in a µm size range. Looking at the images depicted by Henriksson and Gatenholm (2002) in the literature similar particles are also visible on the reference sample, but a lower amount. Moreover, the indication of size of the samples in the images is not represented. Contrary to these observations, Muguet et al. (2011) and Silva et al. (2011) investigated the adsorption of xylan from brown and white liquor during oxygen delignification and xylan on eucalyptus kraft pulp. After sputter coating, they detected patterns and net-like structures between the fiber surfaces. Besides xylan adsorption, this could be a result of reprecipitated lignin during delignification (Schmied et al., 2012). Nevertheless, comparing the images presented in these papers, similar structures can be observed on the reference samples as well. The results published in the literature are difficult to compare with the results in this study, since the conditions during sample preparation (washing step and sputter coating) and the indication of size of the samples in the images are sometimes not clearly described. For example, it is not known if the hot water used for the washing step was deionized water or tap water. Thus, it could be possible that in case of tape water precipitated salt is visualized in the images. Further, the electron energy varied between 10 keV and 20 keV.

Linder et al. (2003) observed aggregates in the colloidal size range after adsorption of xylan on bacterial cellulose. This indicates, that the surface roughness of the fibers could be too high and small aggregates are not noticeable. Further, in the conventional mode the surface is sputter coated prior to analysis. This method is not well defined regarding the amount and distribution of the conduction layer on the surface. However, an additional layer on the surface results in general in a loss in information of the surface texture which could be more pronounced for rough surfaces, than for smoother surfaces.

Since SEM in the conventional mode was not successful to visualize differences between the xylan-modified and unmodified fibers, fibers were investigated in the low voltage (LV) mode. In this mode the surface does not need to be sputter coated with a conducting layer. Thus, a higher contrast of the surface texture can generally be achieved. In a first step, fibers in handsheets were investigated and images are presented in Figure 4.13. In case of the handsheets (Figure 4.13a–c), additional structures or deposits are visible on the reference sample and on the handsheets with additional xylan (here X_2). The circular hole in Figure 4.13c is related to a bordered pit. In Figure 4.13b these deposits can be seen more clearly at a magnification of 10000×. After rewetting of the handsheets in deionized water and fixing individual fibers on carbon tape, none of the samples carried these particles anymore. This concludes that these are loosely bound on the surface and/or water-soluble. However, adsorbed or precipitated xylan could not be visualized by both techniques, conventional and low voltage SEM. This could be due to the colloidal size range (Linder et al. 2003) of additional xylan on the fiber surfaces. Moreover, the surface roughness of the fiber may play an important role for this technique, if the size of adsorbed or precipitated xylan is much smaller than the roughness of the fiber surface, and therefore it might look just like the sample. The roughness of the fibers was determined by atomic force microscopy and will be presented in the next section (4.3.4). These methods may not be feasible to detect additional xylan aggregates on pulp fibers with a certain roughness. However, this also depends on the size of deposited xylan which can be influenced by the ionic strength of the aqueous solution during adsorption but also by the salt used to set the ionic strength (Hofmeister series). A lower salt concentration results in more elongated polymers, whereas a higher charge of polyelectrolyte forces polymers to a more coiled conformation (Dobrynin and Rubinstein 2005; Dobrynin et al. 2001). Further, ions can either promote or retard the solubility of xylan in aqueous solution and thus, affect precipitation of xylan.

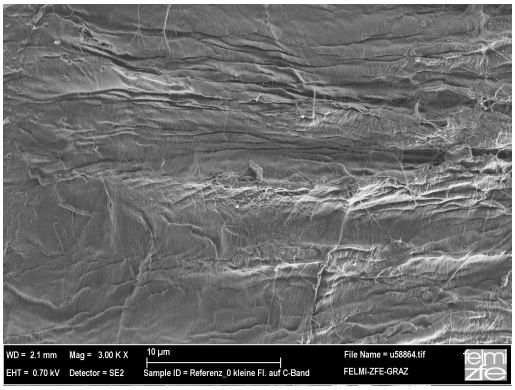

(a) SKPB handsheet at 3000×.

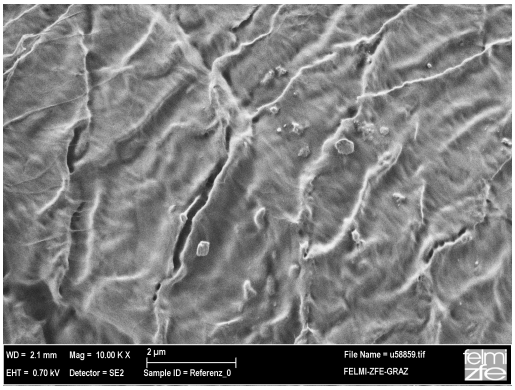

(b) SKPB handsheet at 10000×.

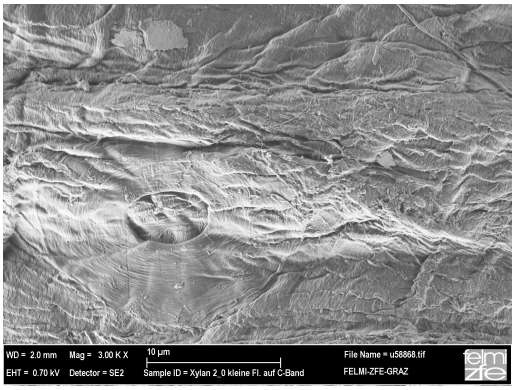

(c) SKPB handsheet with X_2 3000×.

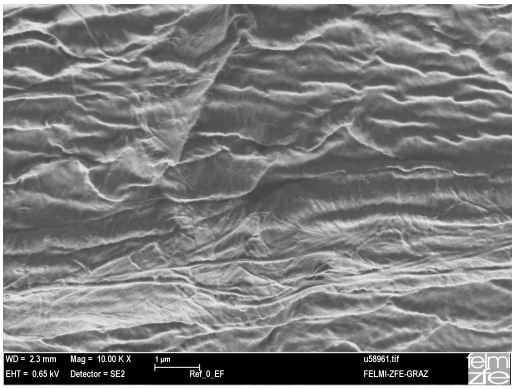

(d) SKPB fiber at 10000×.

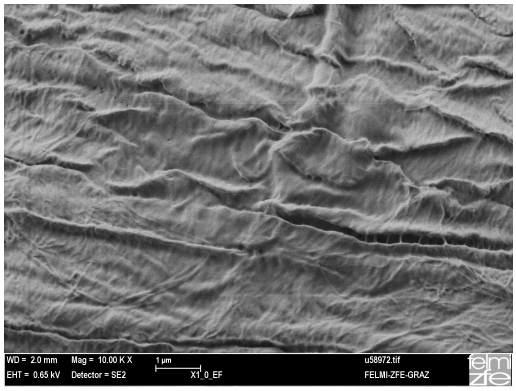

(e) SKPB fiber with X_1 at 10000×.

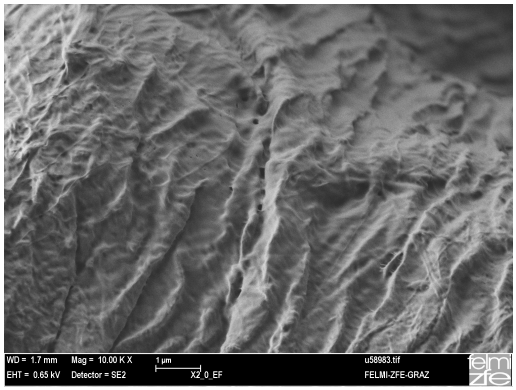

(f) SKPB fiber with X_2 at 10000×.

Figure 4.13 Images of treated and untreated SKPB handsheets and SKPB fibers generated in the low voltage SEM: (a) SKPB handsheet at magnification of 3000×, (b) SKPB handsheet at magnification of 10000×, (c) SKPB handsheet treated with X_2 at magnification of 3000×, (d) SKPB fiber at 10000×, (e) SKPB fiber treated with X_1 at 10000×, and (f) SKPB fiber treated with X_2 at 10000×.

4.3.4 Atomic force microscopy

Atomic force microscopy (AFM) was performed to investigate the fiber surfaces of the untreated and treated unrefined SKPB fibers and cellulose model films in the nanoscale range. Three methods have been employed, topographical imaging, phase imaging, and force mapping. For the analysis of the topography standard commercially available silicon AFM cantilevers have been used, while for phase imaging and force mapping functionalized AFM tips were utilized. These techniques are novel especially to study the surface chemistry of cellulose surfaces and have not yet been used for xylan. Due to the rough surface of pulp fibers, phase imaging and force mapping was first employed on cellulose model films after the adsorption of xylan under controlled conditions using a QCM-D technique. First results of pulp fibers, before and after adsorption of xylan are also presented, but still several questions have to be answered when using functionalized AFM tips on pulp fibers. This investigation was carried out in collaboration with the Institute of Physics (Montanuniversität Leoben), Institute for the Engineering and Design of Materials (University of Maribor), and the Institute for Chemistry and Technology of Materials (Graz University of Technology).

4.3.4.1 Topography of cellulose model films

In pretests OH- and CH_3-functionalized AFM tips were employed on pulp fibers, but the functional groups were easily brushed off during scanning. For this reason, cellulose model films were used to study the spatial distribution of xylan after adsorption with such tips. Knowing that the chemical composition of a cellulose thin film is different, than of pulp fibers one still has a model system. In the next sections the surface analysis of these thin films after adsorption of xylan is presented.

In Figure 4.14 the topography of xylan-treated cellulose model films at different pH-values (7, 8, and 9) and electrolyte concentrations (1 and 100 mmol NaCl) are shown. The topography was analyzed using AFM silicon probes. For each adsorption condition two images are shown which will be important in the following section for comparison reasons with the images generated with functionalized AFM tips. For all samples, hills can be recognized corresponding to aggregated cellulose on the surface of the QCM-sensors. The mean size of these structures ranged between 170 ± 30 nm and 245 ± 80 nm. In addition, for the samples with xylan spherical shaped or dot-like structures and elongated rod-like patterns are visible on these hills. While the dot-like features preferably adsorbed on the hill structures, the elongated structures were located along the slope of the hills and were only visible at pH 8 and 1 mmol salt concentration. The size of these patterns ranged from 1.6 to 4.9 nm and did not follow a clear trend in terms of adsorption conditions. Further, the additional patterns are nonuniformly distributed on the

cellulose films. These adsorbed structures could not be obtained on the cellulose model films treated in the same way as for the adsorption trials of xylan, except no xylan was pumped over the model films. This leads to the conclusion, that these features correspond to adsorbed xylan.

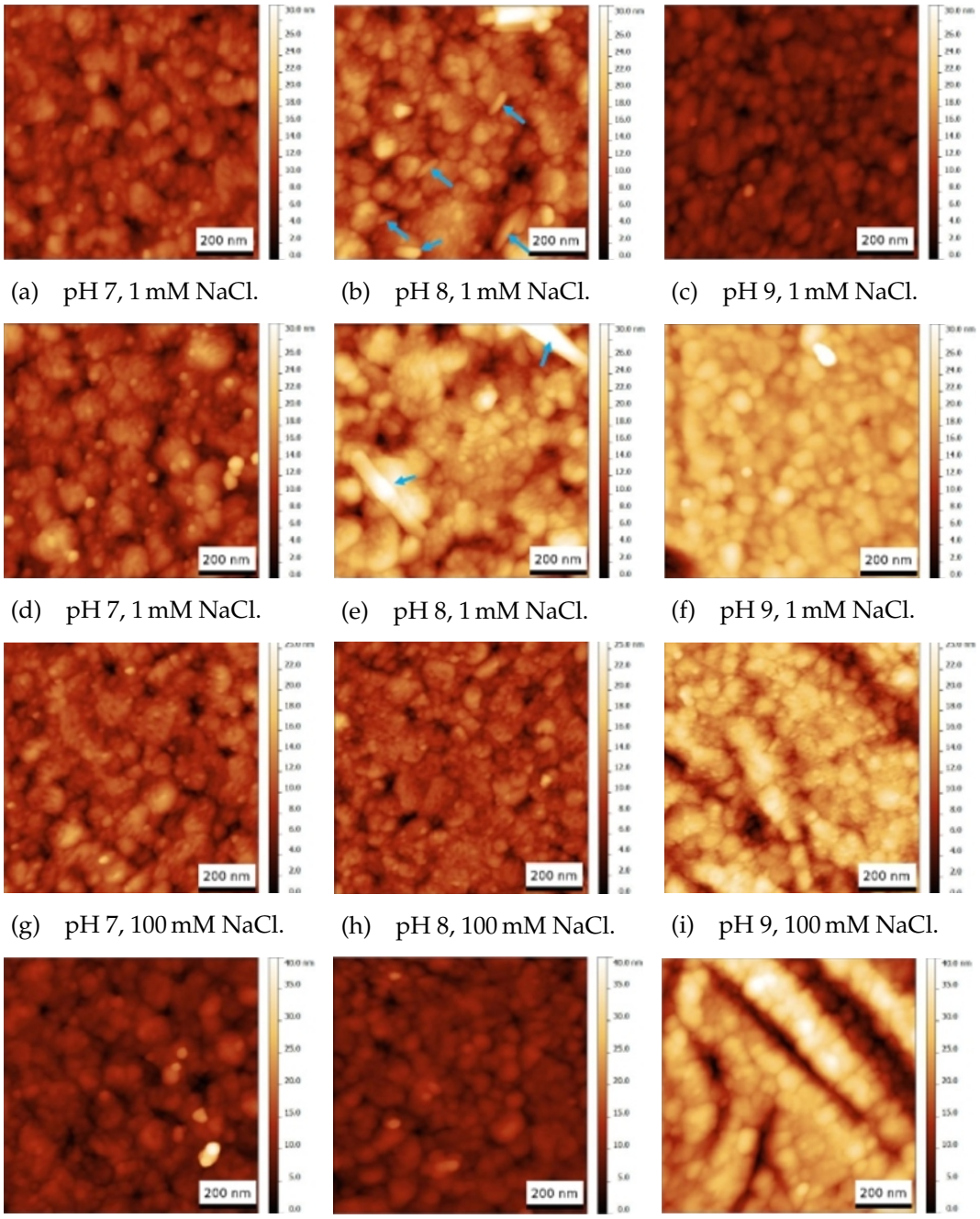

(a) pH 7, 1 mM NaCl. (b) pH 8, 1 mM NaCl. (c) pH 9, 1 mM NaCl.

(d) pH 7, 1 mM NaCl. (e) pH 8, 1 mM NaCl. (f) pH 9, 1 mM NaCl.

(g) pH 7, 100 mM NaCl. (h) pH 8, 100 mM NaCl. (i) pH 9, 100 mM NaCl.

(j) pH 7, 100 mM NaCl. (k) pH 8, 100 mM NaCl. (l) pH 9, 100 mM NaCl.

Figure 4.14 Images of the topography of the cellulose model films at: (a,d) pH 7 and 1 mM NaCl, (b,e) pH 8 and 1 mM NaCl, (c,f) pH 9 and 1 mM NaCl, (g,j) pH 7 and 100 mM NaCl, (h,k) pH 8 and 100 mM NaCl, and (i,l) pH 9 and 100 mM NaCl. The surfaces were scanned using a silicon AFM tip. The image size is $1 \times 1\,\mu m^2$.

4.3.4.2 *Phase imaging and force mapping on cellulose model films*

To get a better image of adsorbed xylan as well as to study the surface chemistry of such films, functionalized AFM tips were employed to scan the surface of cellulose thin films before and after adsorption of xylan. Compared to cellulose, xylan features a branched structure including attached carboxylic groups to the backbone at irregular distances. Thus, different attractive or repulsive interactions between cellulose and xylan towards the functionalized tips were expected. Phase imaging and force mapping was performed on these films (see section 3.5.4.4). The use of functionalized AFM probes was also done, due to the fact that phase imaging of cellulosic surfaces utilizing silicon cantilevers does not give useful results.

In Figure 4.15 and 4.16 images of the phase contrast of xylan-modified cellulose thin films at different pH-values and salt concentrations are presented. The phase images in Figure 4.15 were recorded using OH-functionalized tips and in Figure 4.16 CH_3-tips were employed. By comparing these images with the images in Figure 4.14 the surface is reproduced in more detail and higher resolution. It can be seen that the dot-like and rod-like structures in the topography images appear as black structures in the phase contrast images. The reason for this is a lower phase shift between the tip and xylan, than between the tip and cellulose. Xylan features carboxylic groups on the backbone leading to a higher negative charge density. Thus, xylan tends to show a higher repulsion, than attraction towards functionalized tips. A large amount of these features is visible on all surfaces differing slightly in size and diameter. Moreover, the elongated structures can be observed for the samples at pH 8 and 1 mmol NaCl. From the measurements it was observed, that the interaction of the surface is higher for the OH-functionalization leading to images with a higher resolution than with CH_3-functionalized AFM tips.

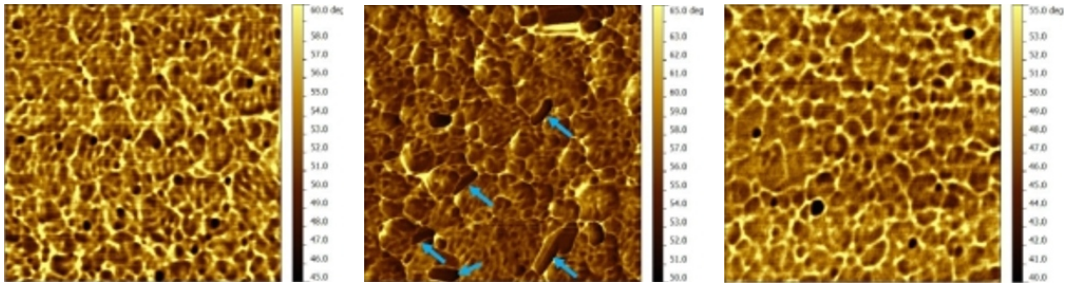

(a) pH 7, 1 mM NaCl. (b) pH 8, 1 mM NaCl. (c) pH 9, 1 mM NaCl.

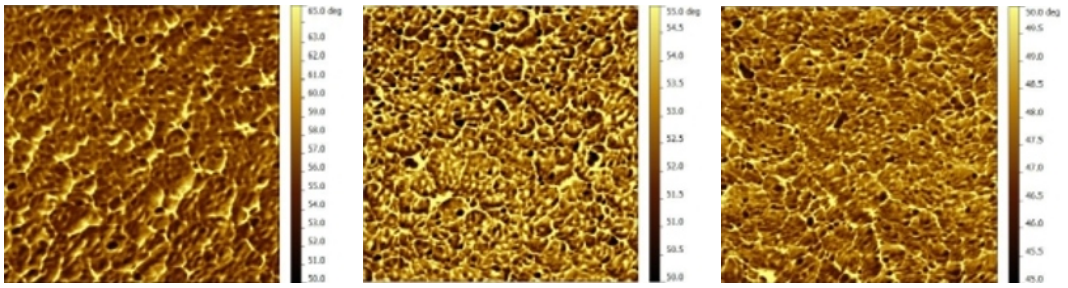

(d) pH 7, 100 mM NaCl. (e) pH 8, 100 mM NaCl. (f) pH 9, 100 mM NaCl.

Figure 4.15 Images of the phase contrast of cellulose model films treated with X_1 at: (a) pH 7 and 1 mM NaCl, (b) pH 8 and 1 mM NaCl, (c) pH 9 and 1 mM NaCl, (d) pH 7 and 100 mM NaCl, (e) pH 8 and 100 mM NaCl, and (f) pH 9 and 100 mM NaCl. The phase images were recorded using OH-functionalized tips and can be compared with the topography images in Figure 4.14: (a⟶a), (b⟶b), (c⟶c), (d⟶g), (e⟶h), and (f⟶i). The image size is $1 \times 1\,\mu m^2$.

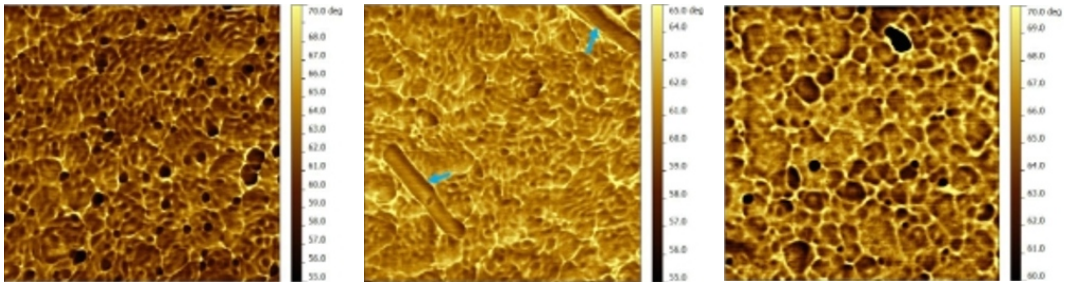

(a) pH 7, 1 mM NaCl. (b) pH 8, 1 mM NaCl. (c) pH 9, 1 mM NaCl.

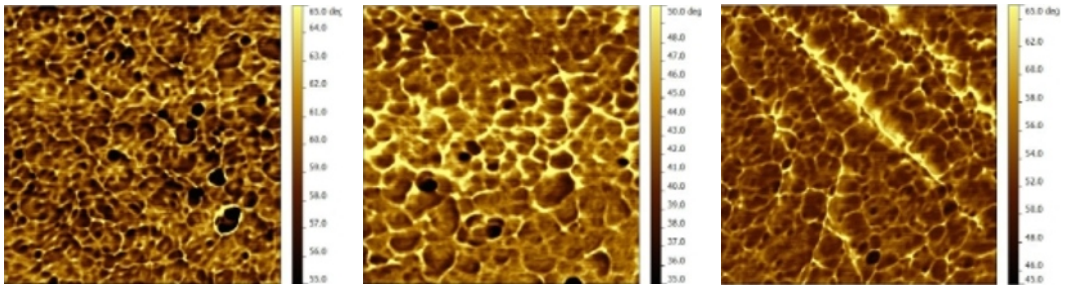

(d) pH 7, 100 mM NaCl. (e) pH 8, 100 mM NaCl. (f) pH 9, 100 mM NaCl.

Figure 4.16 Images of the phase contrast of cellulose model films treated with X_1 at: (a) pH 7 and 1 mM NaCl, (b) pH 8 and 1 mM NaCl, (c) pH 9 and 1 mM NaCl, (d) pH 7 and 100 mM NaCl, (e) pH 8 and 100 mM NaCl, and (f) pH 9 and 100 mM NaCl. The phase images were recorded using CH_3-functionalized tips and can be compared with the topography images in Figure 4.14: (a⟶d), (b⟶e), (c⟶f), (d⟶j), (e⟶k), and (f⟶l). The image size is $1 \times 1\,\mu m^2$.

The adhesive force between the tip and the surface was extracted from force mapping measurements. In a first step, the phase contrast was imaged at an image size of $500 \times 500\,\mathrm{nm}^2$, and afterwards force mapping was performed in the same area. Images from experiments at pH 8 and an electrolyte concentration of 1 and 100 mM NaCl are presented in Figure 4.17 for both functionalized tips. The blue marked areas in the phase contrast images correspond to areas with lower phase shift. The same areas can be found in the force mapping images which are marked in green. They also exhibit the same size as in the phase contrast images.

The adhesive force between pure cellulose and the OH-functionalized AFM probes was around 19 nN and for the CH_3 probes about 12.9 nN. The additional dot-like and rod-like patterns exhibited much lower adhesive forces of around 8 nN. These values were detected for all surfaces treated at different conditions. The lower adhesive force for xylan was expected as it possesses carboxylic groups on the backbone resulting in stronger repulsive interaction towards the functionalized tips. The results suggest that the adsorbed structures on the cellulose model films correspond to xylan.

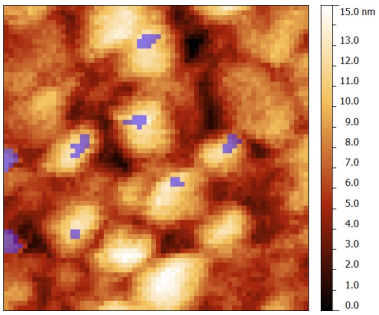

(a) pH 8, 1 mM, OH-tip.

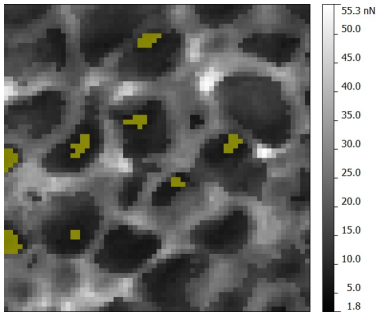

(b) pH 8, 1 mM, OH-tip.

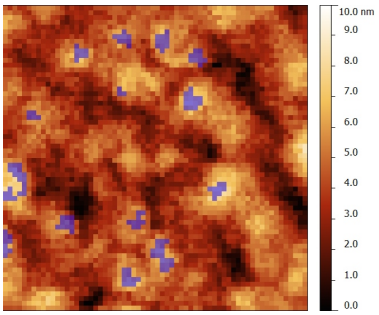

(c) pH 8, 1 mM, CH_3-tip.

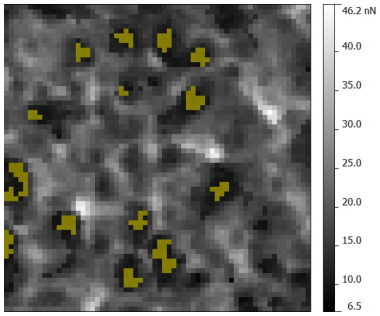

(d) pH 8, 1 mM, CH_3-tip.

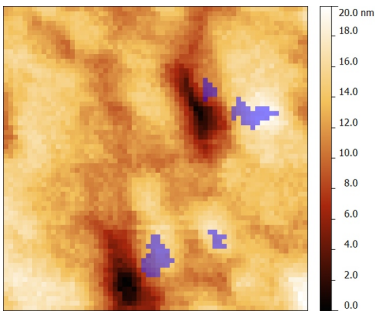

(e) pH 8, 100 mM, OH-tip.

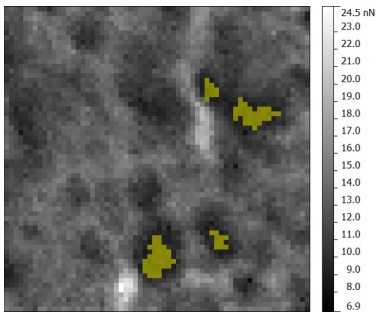

(f) pH 8, 100 mM, OH-tip.

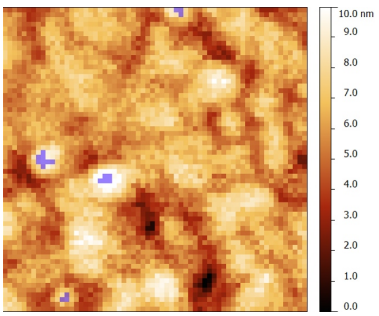

(g) pH 8, 100 mM , CH_3-tip.

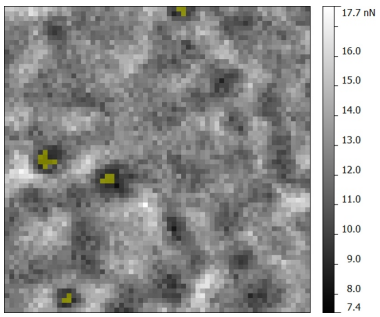

(h) pH 8, 100 mM, CH_3-tip.

Figure 4.17 Images of the phase contrast (left) and the corresponding force map (right) of cellulose model films treated with X_1 at: (a,b,e,f) pH 8 and 1 mM NaCl and (c,d,g,h) pH 8 and 100 mM NaCl. The images (a,b,c,d) were employed with OH-functionalized tips and (e,f,g,h) with CH_3-functionalized tips. The image size is $500 \times 500\,nm^2$.

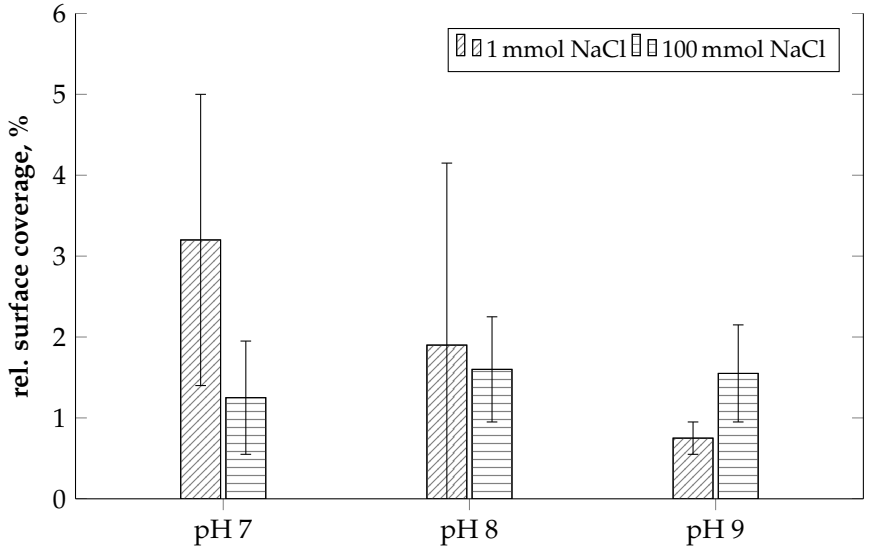

Figure 4.18 Relative surface coverage of xylan on cellulose model films determined by AFM phase imaging in dependence on the adsorption conditions. The values are averaged over four different measurements.

When comparing the mean size of the aggregates on the surfaces between the topography images (Figure 4.14 and the images from phase imaging (Figures 4.15, the functionalized tips yield larger sizes of the aggregates which seem to be influenced by the electrolyte concentration. At a salt concentration of 1 mmol the mean size of xylan was about 20 nm, whereas at a higher salt concentration of 100 mmol yields smaller particles of around 15 nm. However, the differences are rather small but significant. From phase imaging and force mapping the relative surface coverage can be calculated as well. The relative surface coverage of xylan on the surfaces is shown in Figure 4.18. The surface coverage varied between 0.75% and 3.2%. Despite the variations, a trend in the series at an electrolyte concentration of 1 mmol can be seen, whereas at 100 mmol the surface coverage at the different pH levels are within the standard deviation.

4.3.4.3 Roughness analysis of fiber samples

After the cellulose model films have been analyzed, OH- and CH_3-functionalized AFM probes were employed to pulp fibers. This work is yet not fully completed, but first results will be presented in this section. In a first step, the topography and surface roughness of the fiber samples was analyzed using silicon AFM probes. The xylan concentration during the adsorption step varied between 80 mg/g (l) and 320 mg/g (h) to investigate possible changes in the roughness values due to adsorption. However, no difference could be analyzed between the surface roughness of the unmodified and modified SKPB fibers. The values for the rms roughness (σ), the lateral correlation length (ξ), and the Hurst parameter (α) are presented in

Table 4.4 Roughness analysis of the reference sample (SKPB) and SKPB treated with X_1 and X_2 at two different xylan concentrations (l = 80 mg/g and h = 320 mg/g).

$5 \times 5\,\mu m^2$	σ, nm	ξ, nm	α
SKPB	120 ± 35	535 ± 200	0.60 ± 0.05
SKPB X_1 l	150 ± 80	545 ± 225	0.70 ± 0.10
SKPB X_2 l	130 ± 45	500 ± 240	0.65 ± 0.10
SKPB X_1 h	180 ± 140	500 ± 225	0.75 ± 0.10
SKPB X_2 h	150 ± 75	590 ± 200	0.60 ± 0.10

Table 4.4. The mean values are within the range of the variations. The reason could be a heterogeneous and nonuniform distribution of adsorbed/precipitated xylan on the fiber surface (Henriksson and Gatenholm 2001, 2002; Linder et al. 2003). Moreover, the size of xylan aggregates on cellulosic surfaces is observed to be more in the colloidal size range and grows from 95 nm to 155 nm at high temperatures (Linder et al. 2003). The size of adsorbed xylan aggregates on cellulose model films under room temperature was noticed to be in the range between 15 nm and 20 nm. Therefore, small xylan particles may not be detectable by rms measurements as the surface roughness of the pulp fibers is much larger.

4.3.4.4 Topography of the pulp fibers

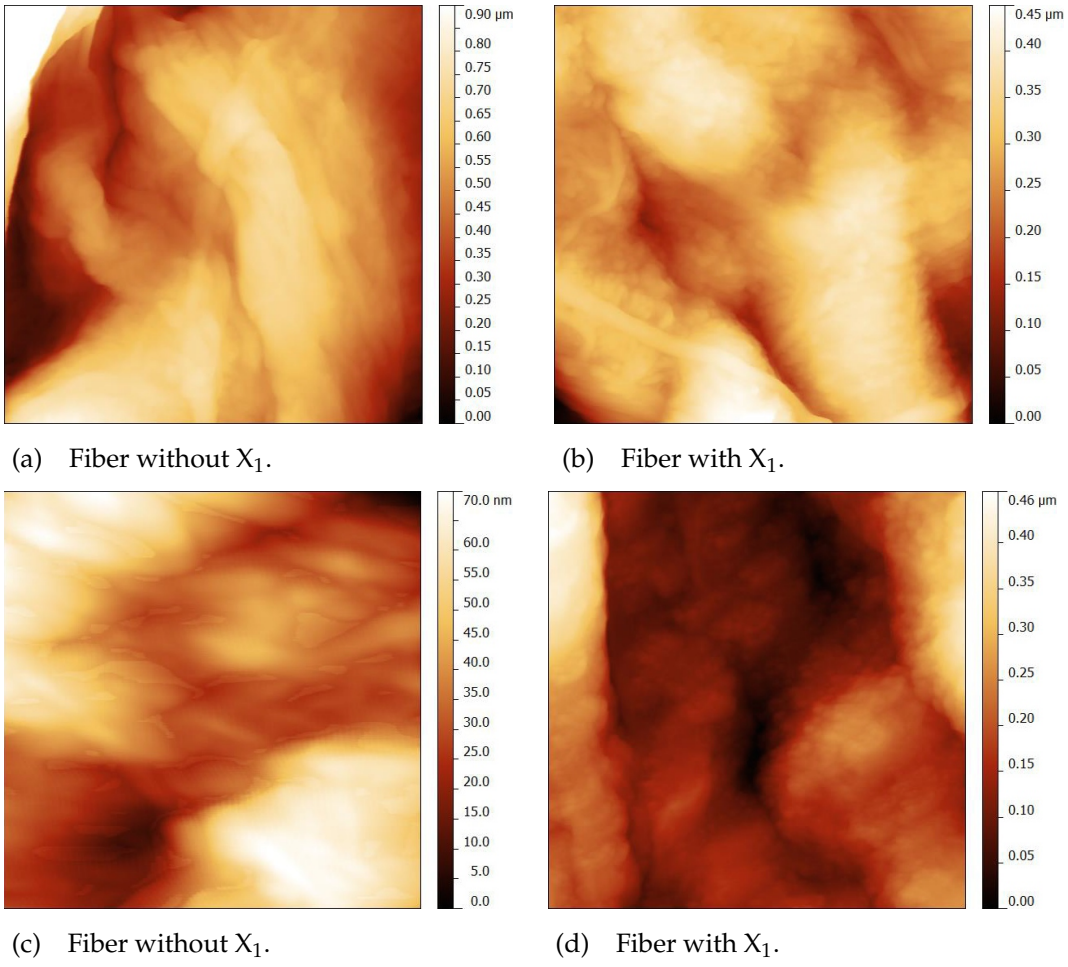

(a) Fiber without X_1.

(b) Fiber with X_1.

(c) Fiber without X_1.

(d) Fiber with X_1.

Figure 4.19 Images of the topography of: (a,c) SKPB without additional xylan and employed by a silicon probe and (b,d) SKPB with additional X_1 and employed by a silicon probe. The image size is $2 \times 2\,\mu m^2$.

Softwood kraft pulp fibers, treated with X_1 at a concentration of 80 mg/g and untreated fibers were analyzed so far. In Figure 4.19 the topography images of the fibers are presented. The images do not give a sufficient resolution regarding additional structures on the fibers surface and no clear difference between the fiber with and without additional xylan can be obtained.

4.3.4.5 Phase imaging and force mapping on pulp fibers

Phase imaging and force mapping was performed on the same fiber samples as for the topography measurements. The images analyzed by AFM phase imaging are yielding a higher resolution and the surfaces appear in more detail as depicted in Figure 4.20. The blue marked areas correspond to areas with a significant lower phase shift, thus higher repulsion occurs between the functionalized tips and the

surface. These areas were larger for the fibers with additional xylan for both, the OH- and the CH_3-functionalization. Due to the higher interaction between the fiber surface and the OH groups at the AFM tip, these tips yield larger areas with a lower phase shift.

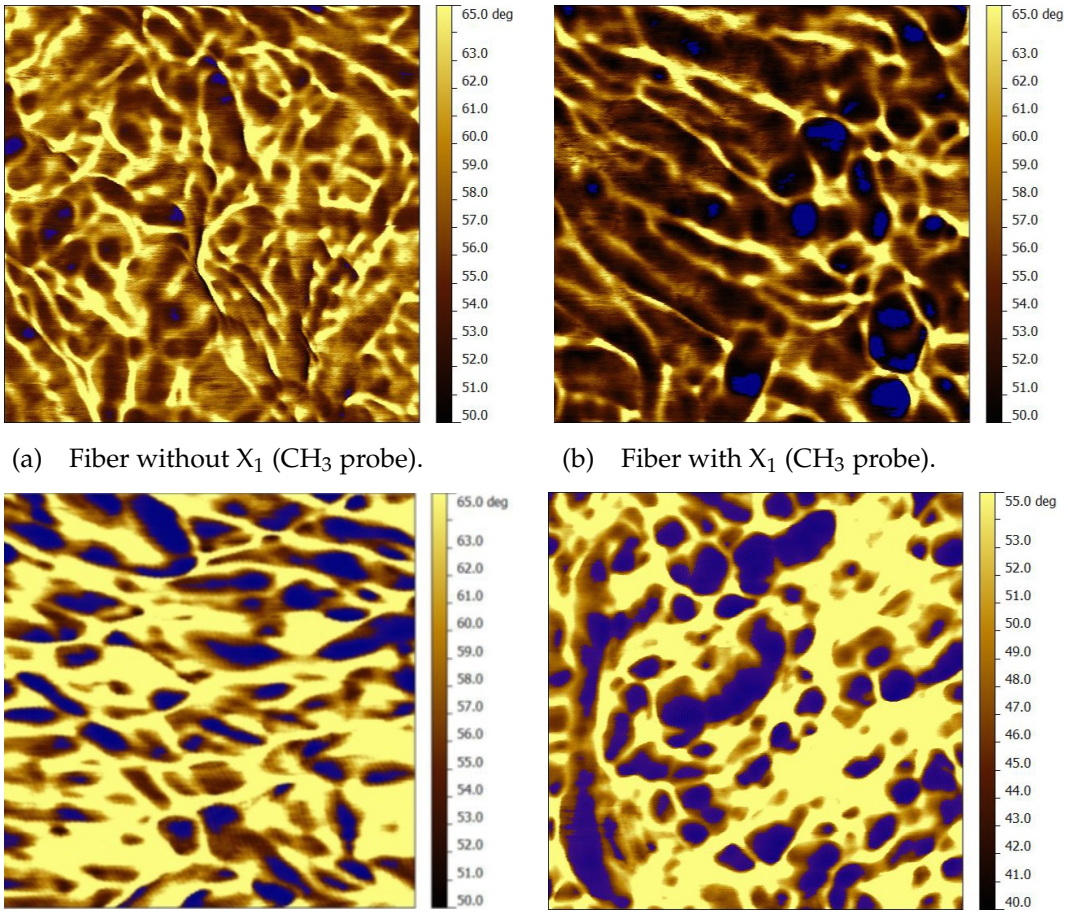

(a) Fiber without X_1 (CH_3 probe). (b) Fiber with X_1 (CH_3 probe).

(c) Fiber without X_1 (OH probe). (d) Fiber with X_1 (OH probe).

Figure 4.20 Phase imaging: (a) SKPB without additional xylan and employed by a CH_3 probe, (b) SKPB with additional X_1 and employed by a CH_3 probe, (c) SKPB without additional X_1 and employed by a OH probe, and (d) SKPB with additional X_1 and employed by a OH probe. The blue marked areas correspond to areas with a lower phase shift. The image size is $500 \times 500\,nm^2$.

Force mapping yielded different adhesive forces regarding the used functionalization and different areas on the substrate. The adhesive force was around 11.3 ± 6.0 nN between the OH-functionalization and cellulose, whereas for the CH_3-functionalization it was obtained to be lower at 5.2 ± 1.1 nN. In the areas with a lower phase shift lower adhesive forces were found between 4.2 ± 0.6 nN (OH tip) and 2.5 ± 0.3 nN (CH_3 tip). The values indicate, that the attraction of bleached softwood fibers is higher towards OH groups, than CH_3 groups. By comparing the surface coverage of the samples, the marked areas in Figure 4.20 (phase imaging) and 4.21 (force mapping)are different. Phase imaging yielded higher values for the

surface coverage of the fibers, than force mapping which is presented in Figure 4.22. Moreover, it can be seen that in phase imaging the surface coverage is enhancing with increasing the amount of xylan for both functionalizations. In case of force mapping, the surface coverage is increasing for the OH-functionalized tips and decreasing using AFM tips with CH_3 groups.

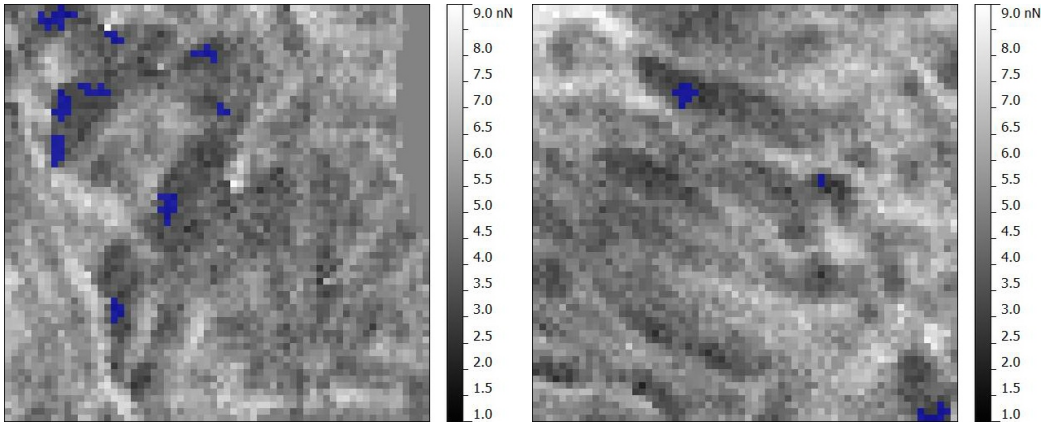

(a) Fiber without X_1 (CH_3 probe). (b) Fiber with X_1 (CH_3 probe).

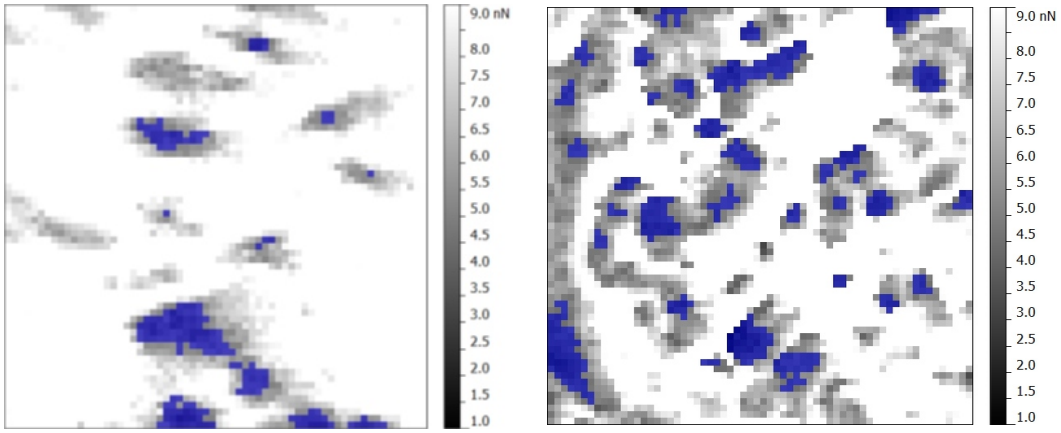

(c) Fiber without X_1 (OH probe). (d) Fiber with X_1 (OH probe).

Figure 4.21 Images of force mapping of: (a) SKPB without additional xylan and employed by a CH_3 probe, (b) SKPB with additional X_1 and employed by a CH_3 probe, (c) SKPB without additional X_1 and employed by a OH probe, and (d) SKPB with additional X_1 and employed by a OH probe. The blue marked areas correspond to areas with a lower adhesive force. The image size is $500 \times 500\,nm^2$.

Moreover, the areas with a lower adhesive force and phase shift are nonuniformly and heterogeneously distributed on the fibers surface. However, since these areas are present on the untreated fibers and the xylan-treated fibers it is not clear, if these areas correspond to additional xylan on the fiber surface. The chemical composition of pulp fibers is more complex, than that of a cellulose model film which consists of cellulose only. Thus, it could be possible that the detected areas with a lower phase shift and adhesive force correspond to other hemicelluloses, lignin, or remaining metals, as presented in Table 4.2. Therefore, more investigation on

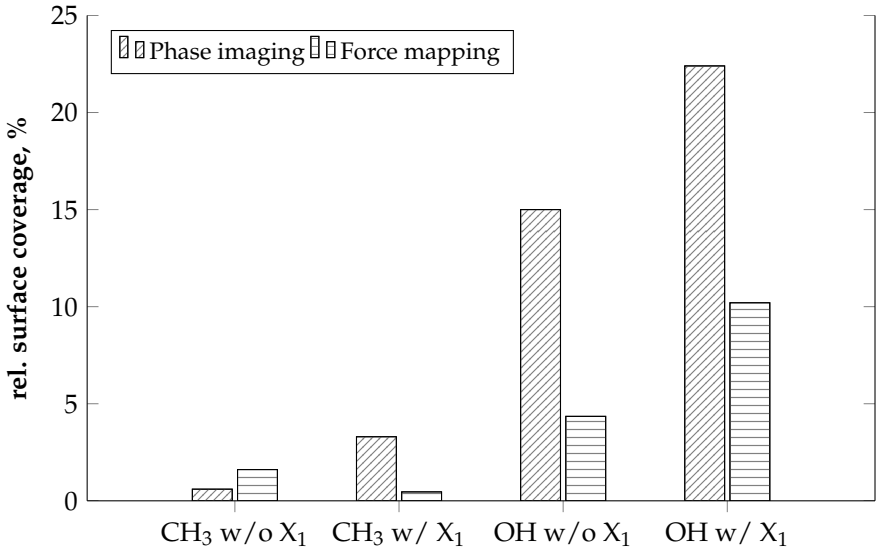

Figure 4.22 Relative surface coverage on pulp fibers determined by AFM phase imaging and force mapping. The values are averaged over three different measurements.

pulp fibers and other chemical constituents of pulp fibers need to be analyzed with this method. Further questions have to be answered like the stability of functionalized AFM tips. However, with this novel technique it is possible to investigate not only the distribution of xylan on cellulosic surfaces, but also to study the adhesion forces of cellulose and xylan of various resources and other chemical components (e.g. lignin and further hemicelluloses) on cellulosic surfaces. A more practical application would be the investigation of swollen fibers in water with such tips. This would allow to use COOH-functionalized tips, which would be protonated under papermaking conditions, to study the distribution of charges on pulp fibers in aqueous solutions.

4.3.5 Summary

The detection and localization of adsorbed or precipitated xylan on cellulosic surfaces is of great interest also with respect to the bonding mechanism of paper which will be discussed in the next section. The results determined by attenuated total reflectance spectroscopy, X-ray photoelectron spectroscopy, and scanning electron microscopy are in accordance with results presented in literature (Henriksson and Gatenholm 2001, 2002; Köhnke and Gatenholm 2007; Linder et al. 2003). Additional xylan on cellulosic surfaces seems to be nonuniformly and heterogeneously attached. This was observed by ATR spectroscopy and XPS which yields information about the chemical composition of a surface. However, no quantitative analysis was possible. Thus, SEM was used to visualize the fiber surface. No additional patterns or structures on the fibers with adsorbed or precipitated xylan could be ob-

tained which may be due to the small sizes of aggregated xylan (Köhnke and Gatenholm 2007; Linder et al. 2003) and the surface roughness of pulp fibers. Atomic force microscopy concluded a nonuniform and heterogeneous distribution as well and yielded mean sizes of xylan aggregates between 15 nm and 20 nm on cellulose model films. Further investigations are required to clearly identify additional xylan on pulp fibers by functionalized AFM tips. This novel technique presented in this work could be a useful method and could play a key role to localize xylan on cellulosic surfaces. Another advantage is the determination of adhesive forces between the surface and the different functionalized tips. Using different tips the hydrophobic and hydrophilic character of cellulosic surfaces can be obtained and the charge distribution can be analyzed. This also may be helpful to get a better understanding and gain a closer insight into the different bonding mechanisms within a paper network (Figure 2.11).

4.4 Influence of xylan on pulp and paper properties

After the distribution and location of adsorbed and/or precipitated xylan onto cellulosic surfaces was characterized, the influence of xylan on pulp and paper properties was investigated.

4.4.1 Fiber charge

Pulp fibers feature weak acid groups which dissociate under neutral and weakly acidic conditions. This introduces anionic charges to the fibers. Under alkaline delignification conditions, kraft lignin is oxidized, introducing carboxyl groups in the cell wall (Eklund and Lindström 1991). Further groups, such as phenolic and catecholic groups are generated in the cell during delginification (Sjöström 1993). However, hemicelluloses, i.e. arabinoglucuronoxylan (softwood) and glucuronoxylan (hardwood) (Buchert et al. 1995) feature the main contribution to the anionic charge of pulp fibers. Due to the simultaneous removal of large quantities of hemicelluloses and lignin during delignification, the anionic charge, or ion exchange capacity, of a pulp fiber decreases (Lindström 1989).

The addition of xylan to the fiber by adsorption or precipitation ($\sim 50\,\mathrm{mg/g}$ fiber) introduces further acidic groups (i.e. MeGluA), thus increasing the anionic charge, both total and surface charge. The impact of additional xylan is illustrated in Figure 4.23. Both, X_1 and X_2 increased the total charge of the pulp by $\sim 20\%$ from $37.6\,\mu\mathrm{eq/g}$ to $45.8\,\mu\mathrm{eq/g}$ (X_1) and $44.7\,\mu\mathrm{eq/g}$ (X_2). The slightly higher mean value for the fibers with additional X_1 could be due to a higher content in uronic acid residues. However, there is no significant difference between both samples. The heat-treatment in deionized water and the treatment under the same condi-

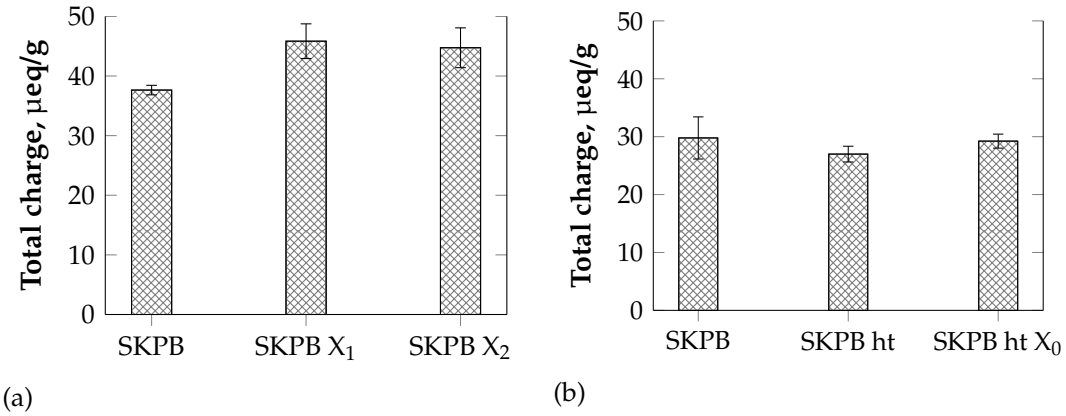

Figure 4.23 Trend of the total charge of the unrefined samples: (a) SKPB = untreated reference sample, SKPB X_1 = softwood kraft pulp treated with X_1, SKPB X_2 = softwood kraft pulp treated with X_2, (b) SKPB = untreated reference sample, SKPB ht = heat-treatment of softwood kraft pulp in deionized water, and SKPB ht X_0 = softwood kraft pulp treated under the same conditions for adsorption without additional xylan.

tions for the adsorption step without the addition of xylan to NaOH did not have an influence on the anionic charge of the SKPB fibers. This may not be surprising due to the fact that no additional weak acid groups were introduced. These tests were done to prove, whether the conditions during the adsorption step could also have an influence on the fiber charge, since the temperature was elevated and constituents could be removed by the addition of NaOH. The values obtained for these samples are a little lower. Between these measurements was a certain lapse of time. Thus, the chemical needed for these measurements were freshly prepared. This is most probably the reason for the lower values.

The surface charge of the SKPB fibers in its hydrogen form were determined by the adsorption of cationic pDADMAC. In theory, the polyelectrolyte will completely adsorb until the fiber reaches saturation. However, the adsorbed amount of polyelectrolyte increases with the amount dosed, due to a kinetic blocking that prevents the polyelectrolyte from reconforming to an equilibrium state. Thus, the amount of polyelectrolyte needed to saturate the fiber surface was determined by extrapolating the adsorbed amount Γ of pDADMAC at different equilibrium concentrations which gives a charge ratio (Horvath 2003). The adsorption isotherms of pDADMAC are illustrated in Figure 4.24.

The surface charge of the treated and untreated SKPB fiber samples is represented in Figure 4.25. The modification with xylans also resulted in an approximately 60% higher surface charge from 2.72 µeq/g to 4.38 µeq/g (X_1) and 4.59 µeq/g (X_2). The surface charge was not affected by the heat-treatment in deionized water and the treatment under the same conditions for the adsorption step without the addition of xylan to NaOH as well.

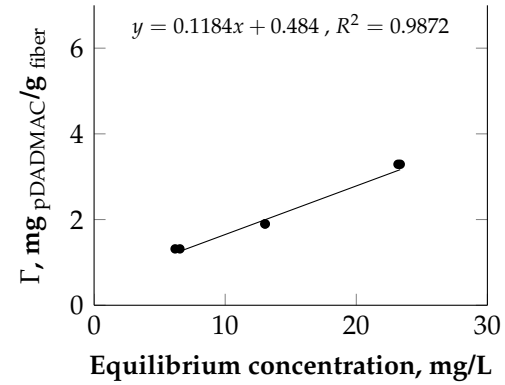

(a) untreated SKPB.

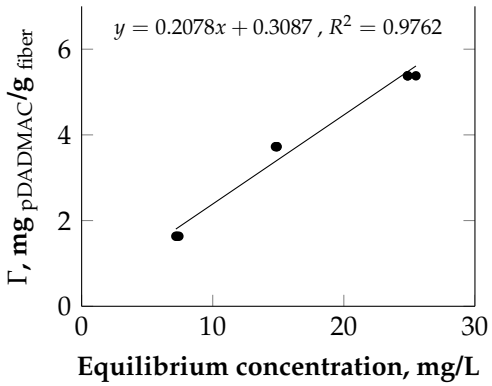

(b) untreated SKPB.

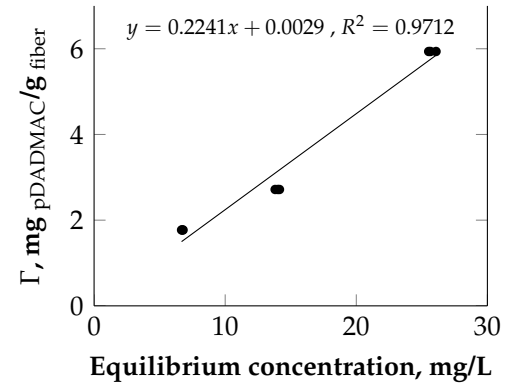

(c) heat-treated SKPB.

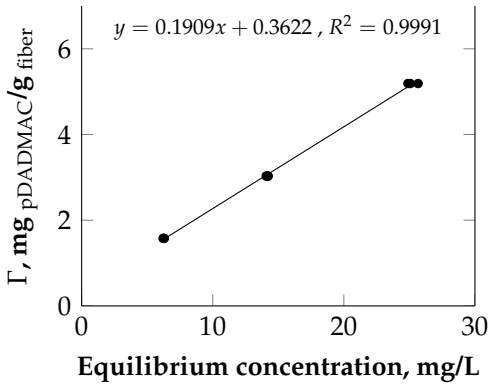

(d) heat-treated SKPB without xylan.

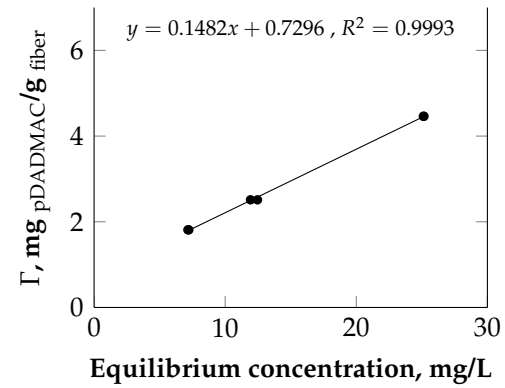

(e) treated with X_1 SKPB.

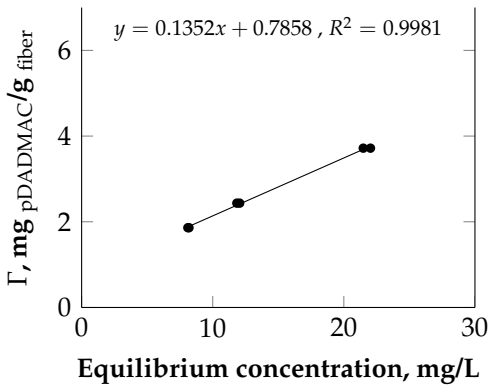

(f) treated with X_2 SKPB.

Figure 4.24 Adsorption isotherms of pDADMAC on: (a) and (b) untreated SKPB fibers, (c) heat-treated SKPB fibers, (d) SKPB fibers treated under the same conditions for adsorption without additional xylan, (e) SKPB fibers treated with X_1, and (f) SKPB fibers treated with X_2. The pDADMAC had a $M_w = 9.2 \times 10^5$ Da and $\xi = 6.19 \times 10^{-3}$ ekv/g.

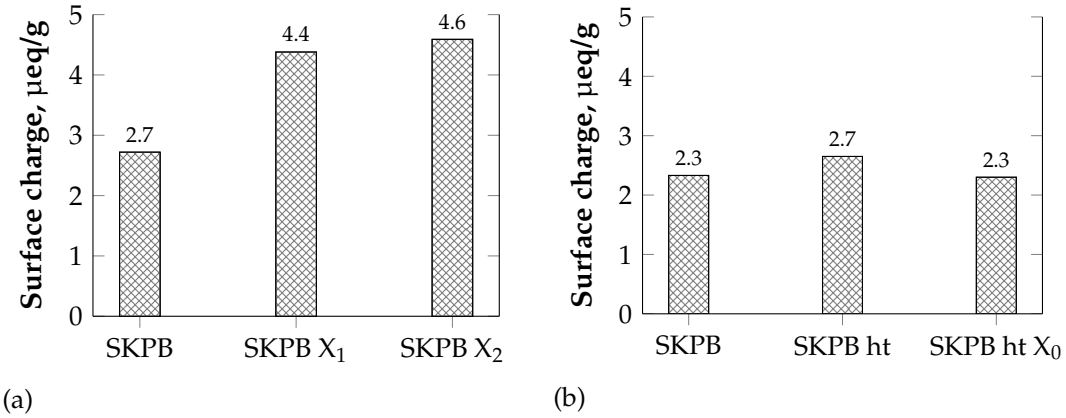

Figure 4.25 Trend of the surface charge of the unrefined samples: (a) SKPB = untreated reference sample, SKPB X1 = softwood kraft pulp treated with X_1, SKPB X2 = softwood kraft pulp treated with X_2, (b) SKPB ht = heat-treatment of softwood kraft pulp in deionized water, and SKPB ht X_0 = softwood kraft pulp treated under the same conditions for adsorption without additional xylan.

Anionic charges cause the fiber to swell, due to the formation of a Donnan equilibrium. Dissociated cations (e.g. Na^+, Ca^{2+}, Mg^{2+}, and Al^{3+}) diffuse in to the cell wall to shield the anionic charges. This leads to a higher concentration of cations in the fiber wall and the fiber takes up more water to dilute the concentration which is similar to an osmotic pressure. Thus, a higher anionic charge of a fiber results in a stronger swelling behavior (Laine et al. 2003). Moreover, swelling makes the fiber more flexible and brings also a jellylike character to the xylan (hydrogel). These parts are softer on the fiber surface (Persson et al. 2013) and within the cell wall. Therefore, higher and homogeneous areas in molecular contact can be achieved between adjacent fibers and additional Van der Waals forces as well as hydrogen bonds can be generated. In addition, a higher surface charge implies that stronger coulomb forces can be generated by the addition of cations between two negatively charged fibers (Laine et al. 2003; Persson et al. 2013; Torgnysdotter et al. 2007). In the end, swelling has an impact on the refining process. The softer and more flexible fibers feature a lower refining resistance, thus strength properties can be achieved with a lower energy demand for refining.

4.4.2 Water retention value

The water retention value (WRV) gives information about the ability of pulp to take up water and the swelling behavior. In a first step, two different xylan conditions were chosen to analyze the impact on the swelling behavior which were: l) I = 1 mol/L, c_x = 8% and h) I = 2 mol/L, c_x = 32%. The other variables during adsorption were kept constant at 80°C, pH 7, and 2.5% pulp consistency for 1 h. The two conditions were performed to investigate different amounts of xylan on the SKPB fiber as presented in section 4.2. Part of the pulp was refined with a PFI mill at

1000 and 3000 revolutions. The WRV was determined from these pulp samples. Handsheets were made and strength properties were analyzed as well, but will be discussed later in section 4.4.3.

A higher surface charge and charge density of the surface of SKPB leads to a stronger swelling behavior. This can be seen in the trend of the water retention value in Figure 4.26. The WRV of the pulp samples with additional X_2 increased faster with refining, compared to the reference sample and to the pulp with additional X_1. The influence of X_1 was quite low or rather the opposite way. Since the surface charge was increased for the pulp with additional X_1, an increased swelling behavior would be expected.

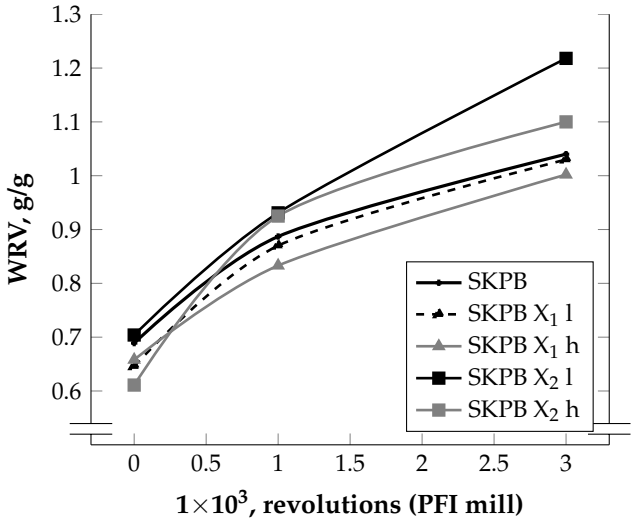

Figure 4.26 Trend of the water retention value of: SKPB = untreated reference sample, SKPB X_1 = softwood kraft pulp treated with X_1, SKPB X_2 = softwood kraft pulp treated with X_2 at two different conditions for xylan adsorption: l) I = 1 mol/L, c_x = 8 %; h) I = 2 mol/L, c_x = 32 %.

The influence of the two xylans on the WRV of the other pulp samples (sulfite pulp, unbleached softwood kraft pulp, and viscose fibers) was measured and compared with the bleached softwood kraft pulp. For all pulps one adsorption condition was chosen (80°C, pH 7, I = 1 mol/L, 2.5% pulp consistency, and 1 h). Additionally, the same procedure was performed with the reference sample, except no xylan was added. As before mentioned, part of the pulp samples were treated with a PFI mill at 1000 and 3000 revolutions and handsheets were made.

The results of the WRV of the different pulp samples is presented in Table 4.5 as well as the beating degree which is an important value for papermaking as it gives information about the drainage behavior of a pulp. The beating degree is increasing for the pulp samples with additional xylan. At the areas when xylan is present, swelling is enhanced and makes it more flexible. Thus, the resistance against mechanical treatment, such as beating, is reduced and consequently the

beating degree increases, also due to the increase in fines concentration and fiber cutting. The beating degree of the unbleached fiber samples is not affected by additional xylan when comparing with the reference sample. This is most probably due to the higher resistance against mechanical treatment. A longer treatment should result in a similar tendency of the beating degree as for the bleached kraft pulp samples. Comparing kraft and sulfite pulps, the refining resistance of sulfite fibers is in generally lower. The chemical decomposition of lignin in the sulfite process starts from the fiber surface in direction to the lumen, whereas in the kraft process it takes place the opposite way. This leads to a completely dissolved primary cell wall and a strongly affected secondary (S1) cell wall in sulfite fibers (Sixta 2006). Therefore, the fiber surfaces from these pulping methods have different characteristics.

In case of the viscose fibers the beating degree and the WRV was not affected by additional xylan. Adsorption of xylan on the VF fibers could not be detected by HPLC (see Table 4.7). In case of the pulp samples, no clear trend regarding an increased WRV for the pulps treated with xylan could be observed. The values varied within a range of 10%. A higher swelling behavior, determined by the WRV, was expected. This could be a result of the amount of xylan. The xylan content may not have been enriched enough to determine a significant increase in the water retention values. The chemical composition of the pulp samples and viscose fibers are presented in Table 4.6 and 4.7.

Table 4.5 Development of the beating degree and the water retention value (WRV) of the different fiber samples. 0 PFI = 0 revolutions; 1000 PFI = 1000 revolutions; and 3000 PFI = 3000 revolutions.

	Beating degree, SR			WRV, g/g		
Sample	0 PFI	1000 PFI	3000 PFI	0 PFI	1000 PFI	3000 PFI
SPB	12.8	14.5	24.8	0.908 ± 0.001	1.271 ± 0.005	1.605 ± 0.033
SPB ht X_0	13.0	15.5	27.3	0.890 ± 0.001	1.272 ± 0.003	1.560 ± 0.017
SPB X_1	13.0	16.0	31.0	0.862 ± 0.002	1.260 ± 0.007	1.599 ± 0.004
SPB X_2	12.0	15.5	30.0	0.895 ± 0.001	1.269 ± 0.003	1.705 ± 0.042
SKPB	13.2	14.8	17.8	0.834 ± 0.013	1.130 ± 0.002	1.396 ± 0.006
SKPB ht X_0	12.8	13.3	17.6	0.870 ± 0.003	1.160 ± 0.009	1.377 ± 0.026
SKPB X_1	12.8	14.0	20.0	0.890 ± 0.020	1.161 ± 0.036	1.479 ± 0.047
SKPB X_2	12.5	13.6	18.8	0.856 ± 0.012	1.114 ± 0.005	1.370 ± 0.033
SKPUB κ42	13.3	14.0	14.8	1.418 ± 0.004	1.381 ± 0.092	1.541 ± 0.010
SKPUB κ42 ht X_0	13.7	13.8	15.3	1.454 ± 0.003	1.481 ± 0.002	1.596 ± 0.005
SKPUB κ42 X_1	14.2	14.0	15.5	1.432 ± 0.008	1.466 ± 0.004	1.611 ± 0.001
SKPUB κ54	13.4	14.6	14.8	1.477 ± 0.144	1.411 ± 0.029	1.624 ± 0.135
SKPUB κ54 ht X_0	13.6	14.1	15.0	1.444 ± 0.014	1.488 ± 0.001	1.595 ± 0.002
SKPUB κ54 X_1	13.3	13.8	15.0	1.413 ± 0.010	1.473 ± 0.004	1.609 ± 0.003
VF	10.2	—	—	0.712 ± 0.002	—	—
VF ht	10.9	—	—	0.728 ± 0.009	—	—
VF ht X_0	11.5	—	—	0.720 ± 0.005	—	—
VF X_1	11.2	—	—	0.705 ± 0.006	—	—
VF X_2	11.3	—	—	0.721 ± 0.012	—	—

Table 4.6 Chemical composition of the fiber samples before and after adsorption of xylan by HPLC: Glu = glucose, Xyl = xylose, Man = mannose, Ara = arabinose, Rha = rhamnose, Gal = galactose, KL = Klason lignin, SL = acid-soluble lignin .

Sample	Glu, %	Xyl, %	Man, %	Ara, %	Rha,%	Gal, %	KL, %	SL, %
SPB	87.5 ± 0.5	5.3 ± 0.0	5.4 ± 0.1	0.0 ± 0.0	0.0 ± 0.0	0.0 ± 0.0	0.06 ± 0.03	1.02 ± 0.01
SPB ht X_0	86.6 ± 1.0	5.2 ± 0.0	5.4 ± 0.1	0.0 ± 0.0	0.0 ± 0.0	0.0 ± 0.0		
SPB X_1	84.3 ± 0.1	7.7 ± 0.1	5.3 ± 0.1	0.0 ± 0.0	0.0 ± 0.0	0.0 ± 0.0		
SPB X_2	86.2 ± 0.2	6.6 ± 0.0	5.3 ± 0.0	0.0 ± 0.0	0.0 ± 0.0	0.0 ± 0.0		
SKPB	80.5 ± 1.2	7.8 ± 0.1	6.2 ± 0.1	0.5 ± 0.0	0.0 ± 0.0	0.2 ± 0.0	0.22 ± 0.01	0.22 ± 0.01
SKPB ht X_0	79.3 ± 1.0	7.8 ± 0.1	6.2 ± 0.1	0.5 ± 0.0	0.0 ± 0.0	0.2 ± 0.0		
SKPB X_1	77.1 ± 1.2	11.1 ± 0.2	5.9 ± 0.0	0.5 ± 0.0	0.0 ± 0.0	0.2 ± 0.0		
SKPB X_2	77.0 ± 1.6	9.4 ± 0.1	6.0 ± 0.1	0.4 ± 0.0	0.0 ± 0.0	0.2 ± 0.0		
SKPUB κ42	77.7 ± 0.4	7.8 ± 0.0	6.1 ± 0.0	0.8 ± 0.0	0.1 ± 0.0	0.5 ± 0.0	6.49 ± 0.06	0.17 ± 0.01
SKPUB κ42 ht X_0	77.9 ± 0.6	7.7 ± 0.1	6.2 ± 0.0	0.8 ± 0.0	0.1 ± 0.0	0.5 ± 0.0		
SKPUB κ42 X_1	76.1 ± 0.8	9.5 ± 0.1	6.0 ± 0.0	0.7 ± 0.0	0.1 ± 0.0	0.5 ± 0.0		
SKPUB κ54	75.2 ± 1.0	7.9 ± 0.1	6.0 ± 0.0	0.8 ± 0.0	0.1 ± 0.0	0.6 ± 0.0	8.04 ± 0.21	0.18 ± 0.01
SKPUB κ54 ht X_0	75.6 ± 0.9	7.8 ± 0.1	6.0 ± 0.1	0.8 ± 0.0	0.1 ± 0.0	0.6 ± 0.0		
SKPUB κ54 X_1	73.4 ± 1.4	9.7 ± 0.1	5.8 ± 0.0	0.8 ± 0.0	0.1 ± 0.0	0.6 ± 0.0		

Table 4.7 Chemical composition of the viscose fiber samples before and after adsorption of xylan by HPLC: Glu = glucose, Xyl = xylose, Man = mannose, Ara = arabinose, Rha = rhamnose, Gal = galactose.

Sample	Glu, %	Xyl, %	Man, %	Ara, %	Rha,%	Gal, %
VF	93.6 ± 0.4	1.2 ± 0.0	0.6 ± 0.0	0.0 ± 0.0	0.0 ± 0.0	0.0 ± 0.0
VF ht	95.0 ± 0.6	1.3 ± 0.0	0.6 ± 0.0	0.0 ± 0.0	0.0 ± 0.0	0.0 ± 0.0
VF ht X_0	95.3 ± 0.4	1.2 ± 0.0	0.6 ± 0.0	0.0 ± 0.0	0.0 ± 0.0	0.0 ± 0.0
VF X_1	95.9 ± 0.4	1.2 ± 0.0	0.6 ± 0.0	0.0 ± 0.0	0.0 ± 0.0	0.0 ± 0.0
VF X_2	95.9 ± 1.2	1.2 ± 0.0	0.6 ± 0.0	0.0 ± 0.0	0.0 ± 0.0	0.0 ± 0.0

4.4.3 Strength properties

Xylans represent an abundant and sustainable source for tailored materials. They are proposed for a use in pharmaceuticals, in wound dressings, and in immunomodulating agents (Daus and Heinze 2010; Kumar and Negi 2012; Petzold-Welcke et al. 2014). However, one of the main suggested areas of applications of xylan is papermaking. Thus, it was of interest , whether xylan does have an impact on the strength properties of paper. Therefore, bleached softwood kraft pulp was modified and tested and compared with other modified pulp samples, such as bleached sulfite pulp and unbleached softwood kraft pulp.

4.4.3.1 Softwood kraft pulp (SKPB)

SKPB pulp was treated with xylan at two different conditions as described earlier in section 4.4.2. After refining at 1000 and 3000 revolutions with a PFI mill, handsheets were made and the tensile and the tear index as well as the breaking strain were evaluated. The results of the strength parameters vs. the PFI revolutions are depicted in Figure 4.27.

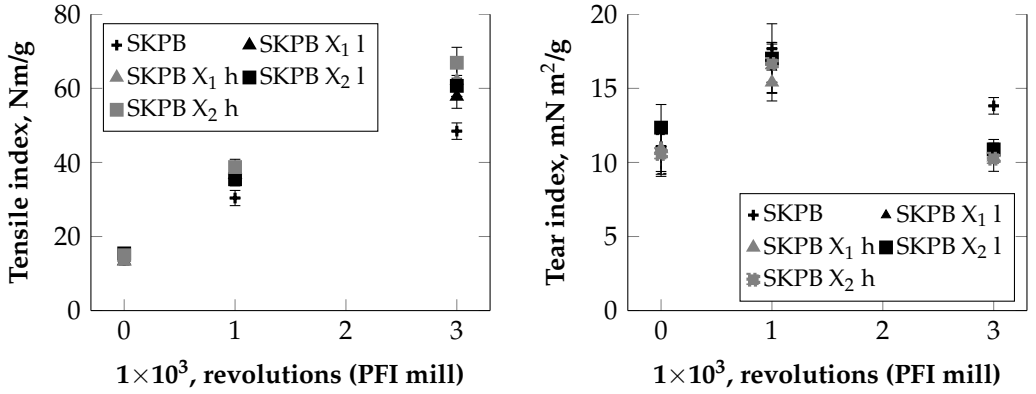

a) Tensile index.

b) Tear index.

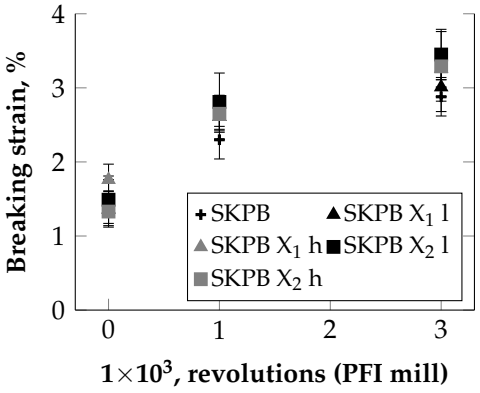

c) Breaking strain.

Figure 4.27 Trend of the tensile index (a), tear index (b), and (c) breaking strain vs. the refining intensity (revolution with a PFI mill) of xylan-modified and unmodified SKPB handsheets at two different adsorption conditions: l) $I = 1\,\mathrm{mol/L}$, $c_x = 80\,\mathrm{mg/g}$; h) $I = 2\,\mathrm{mol/L}$, $c_x = 320\,\mathrm{mg/g}$.

For the unrefined samples, SKPB with additional X_2 at the higher xylan concentration (320 mg/g) possessed an about 13% higher tensile index. The values of the other fiber samples were all in the same range. After refining, the tensile index is stronger increasing for the samples treated with xylan and is further increasing for the samples with a higher xylan content (Figure 4.27a). Upon refining at 3000 revolutions with the PFI mill, the maximum increase in tensile index was 28 % (X_1) and 38 % (X_2), compared to the reference sample. The higher effect of X_2 is most probably due to the higher molecular weight (Hansson and Hartler 1969; Kabel et al. 2007; Meller 1965). However, the mechanical treatment of pulp leads to more flexible and softer fibers, due to internal and external fibrillation. Fibers with a stronger swelling behavior by e.g. a higher xylan content are treated even stronger during refining. Moreover, refining results in the production of fines and cut fibers resulting in shorter fiber lengths (Kerekes 2005). The result is a fiber suspension with a longer drainage behavior. The beating degree is a measure to characterize the drainage behavior of pulp suspension and it is increasing with more intense or

longer mechanical treatment. Additional xylan on the fiber surface could have an influence on the strength properties and contribute to the mechanisms of bonding within the fiber network. The stronger effect on the tensile index could be also the result of more fiber-fiber bonds within the network, due to a higher degree of fibrillation and flexibility of the fibers resulting in higher areas in molecular contact. The latter may be the main effect. By comparing the tear index (Figure 4.27b), the handsheets with additional xylan is decreasing faster. This is most probably the result of a more pronounced fiber cutting during refining, than for the reference sample. The values of the breaking strain (Figure 4.27c) were also higher for the handsheets with additional xylan which may be the result of more fiber-fiber interactions within the network as well. A network with more interactions points (fiber-fiber bonds) can compensate mechanical stress more easily, than a network with fewer fiber-fiber bonds.

4.4.3.2 Comparison between the different pulp samples

Since, the development of the beating degree was more pronounced for the fibers with additional xylan (Table 4.5), the strength properties are related to the beating degree and compared with the other pulp samples in Figure 4.28. The results indicate, that at a similar beating degree, the effect of a higher tensile index is negligible. This is the case for all tested pulp samples.

Comparing kraft and sulfite pulps, the refining resistance of sulfite fibers is generally lower. The chemical decomposition of lignin in the sulfite process starts from the fiber surface in direction to the lumen, whereas in the kraft process it takes place the opposite way. This leads to a completely dissolved primary cell wall and a strongly affected first layer of the secondary cell wall (S1) in sulfite fibers (Sixta 2006). Therefore, the fiber surfaces from these pulping methods have different characteristics. The result of beating is a faster increase in fiber flexibility, but also in fines concentration and fiber cutting. This may be a reason for the lower effect of xylan on paper strength of the sulfite handsheets, as more fines may be generated at a given refining energy. On the other hand, the amount of xylan increased from 5.2% to 6.6% (see Table 4.6). This shows, that the resulting amount of xylan of the sulfite fibers is significantly lower than for the softwood kraft pulps which increased from 7.8% up to 11.1% for the bleached sample. A result could be a harder or stiffer sulfite fiber, by reason of a reduced swelling behavior. Consequently, the surface may have a lower penetration hardness. This will affect the area in molecular contact between adjacent fibers (Persson et al. 2013). Furthermore, the properties and conditions of the fiber surface are different between sulfate and sulfite pulp and could affect the conditions for the precipitation of xylan onto the fibers. These factors will have an influence on the resulting tensile strength of paper. The lower xylan content of sulfite fibers also implies that a lower amount of xylan, due to the

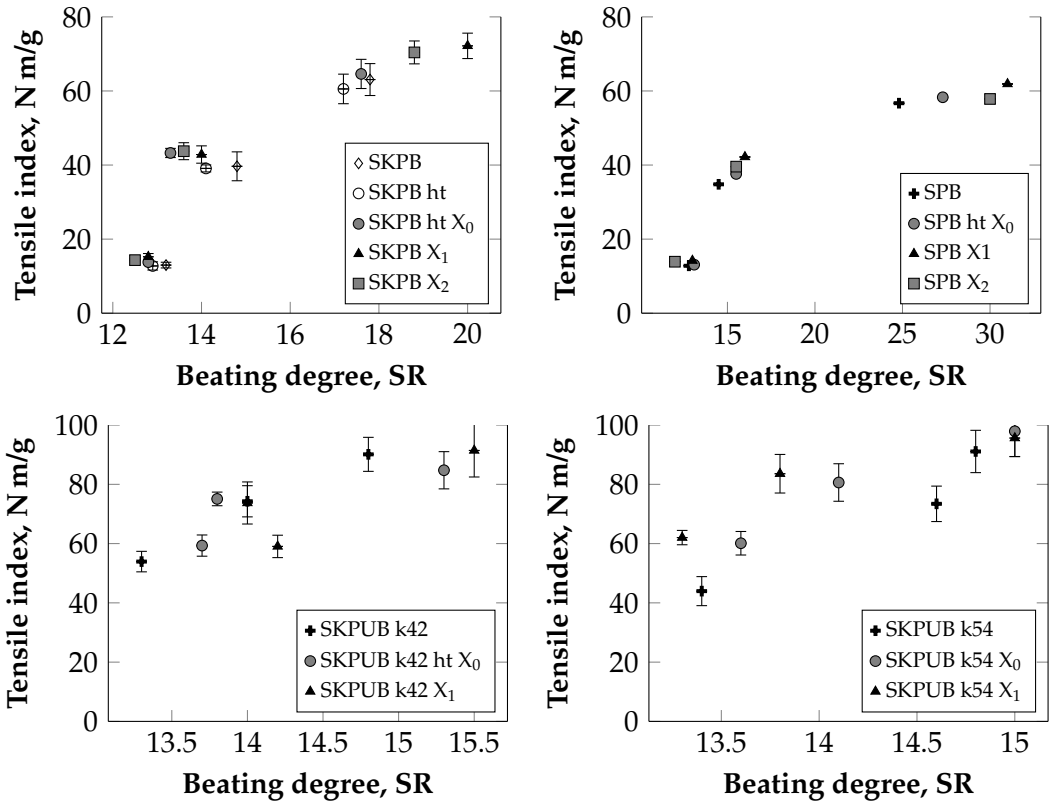

Figure 4.28 Trend of the tensile index vs. the beating degree of: top left = xylan-modified and unmodified bleached softwood kraft handsheets; top right = xylan-modified and unmodified bleached sulfite handsheets; bottom left = xylan-modified and unmodified unbleached softwood kraft handsheets (Kappa 42); and bottom right = xylan-modified and unmodified unbleached softwood kraft handsheets (Kappa 54).

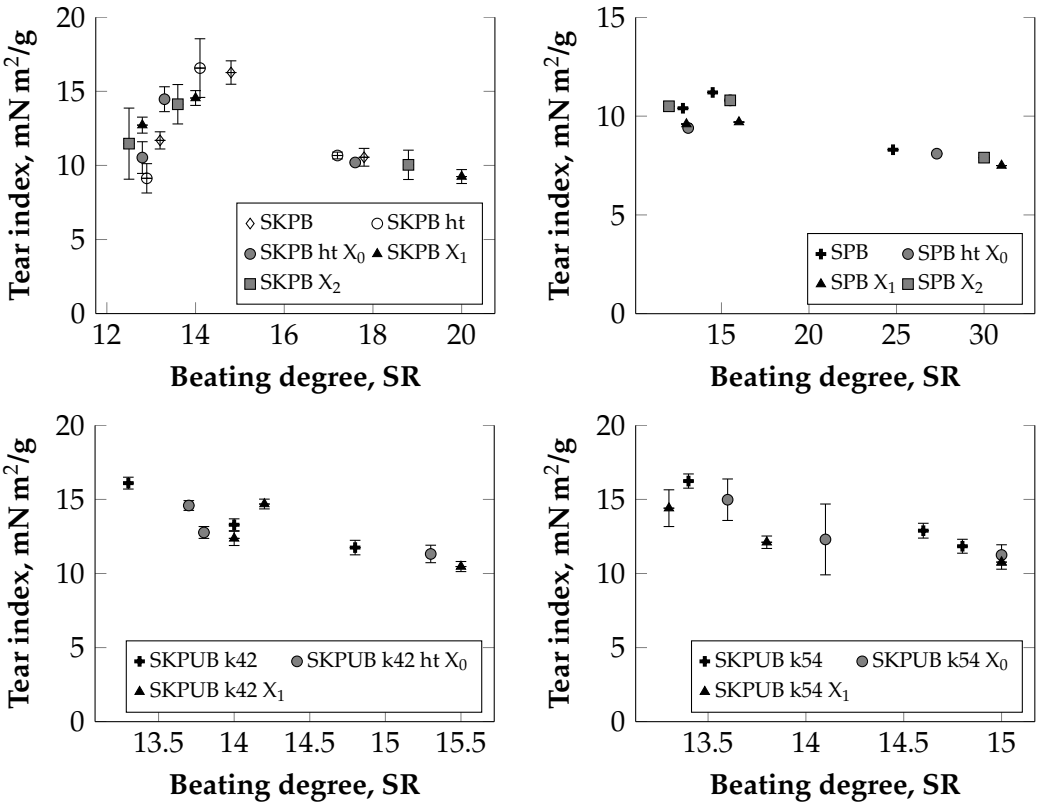

Figure 4.29 Trend of the tear index vs. the beating degree of: top left = xylan-modified and unmodified bleached softwood kraft handsheets; top right = xylan-modified and unmodified bleached sulfite handsheets; bottom left = xylan-modified and unmodified unbleached softwood kraft handsheets (Kappa 42); and bottom right = xylan-modified and unmodified unbleached softwood kraft handsheets (Kappa 54).

missing primary wall, is involved in the bonding mechanisms. The development of the beating degree of the bleached softwood fibers is more pronounced, than for the unbleached fibers. The unbleached fibers still contain a higher amount of lignin (see Table 4.6) which is more resistant against mechanical stress.

A similar trend was obtained by comparing the beating degree vs. the tear index (Figure 4.29) or the strain at break. No significant influence of additional xylan on the pulp fibers was noticeable. The same can be obtained by comparing the tensile index with the sheet density (see Figure G.1 and G.2, Appendix G).

Viscose fibers were investigated whether they could be used as model fibers, as they consist predominantly of cellulose. However, no adsorption or precipitation of xylan onto the VFs could be detected by high pressure liquid chromatography—the xylan content was 1.2% for all samples. On the other hand, xylan did adsorb on the cellulose model films which are built up by cellulose II as well. A reason could be the detection limit of the measurement of the HPLC technique. Although there might be small amounts of xylan present on the surface of VFs, this amount may be too low to have a significant influence on the strength properties of handsheets

made of these fibers as shown in Figure 4.30. The values of the tensile index and the tear index are all in the same range for the xylan-modified VFs and the reference VFs.

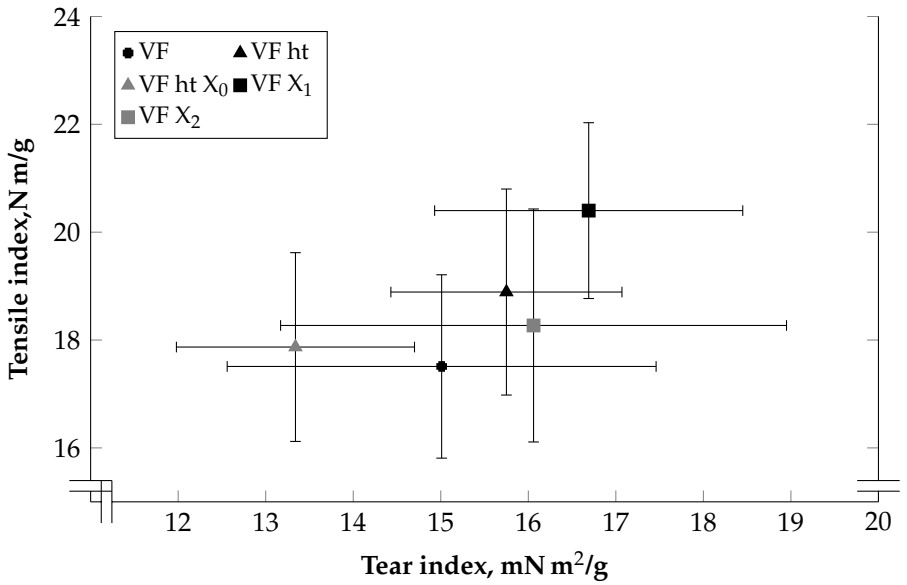

Figure 4.30 Trend of the tensile index vs. tear index of xylan-modified and unmodified VF handsheets.

Rohm et al. (2014) investigated the influence of xylan on the strength of cellulose model films. A set of two films swollen in water were bonded together like a sandwich. After drying, the films were torn apart and the force to separate the films was measured. A higher force was needed when xylan was incorporated between the films and even increased by a higher electrolyte concentration (NaCl). Due to the ability of xylan to take up water, the surface becomes softer and a higher area in molecular contact can be achieved when xylan is incorporated in a bond. Further, the addition of electrolyte suggests that Coulomb forces play a role for the interaction between these surfaces.

Therefore, handsheets of unrefined SKPB fibers were made with an increased salt concentration. This was performed by using a salt concentration equivalent to the salt concentration used during the adsorption step for the washing step. Part of the pulp was treated the same way as for the adsorption of xylan, except no xylan was added. The amount of added xylan during the adsorption step was 80 mg/g. Before handsheet preparation, the conductivity of all pulp suspension was set to 1900 µS/cm. The results are presented in Figure 4.31. The tensile indeces of the four different fiber samples are within the same range. However, the the mean value of the index is the lowest for the heat-treated pulp without additional xylan.

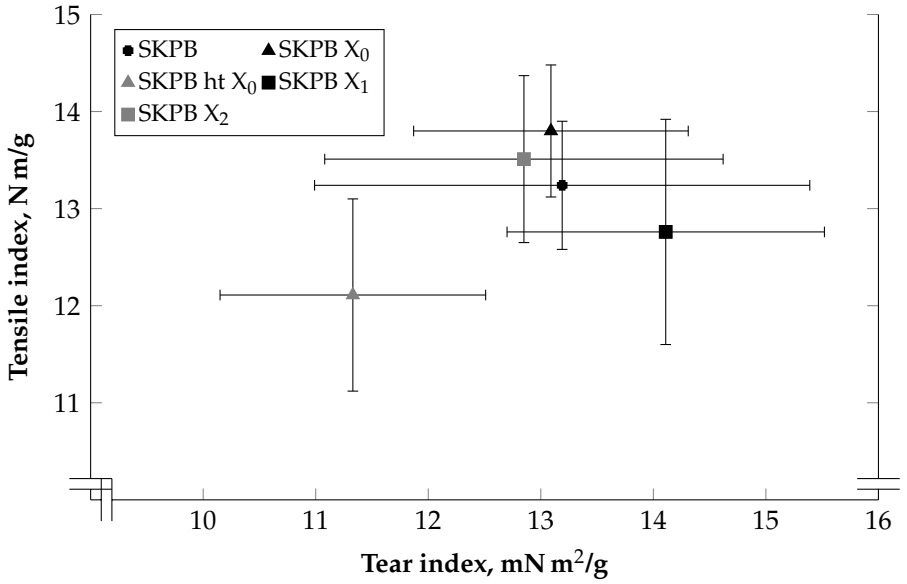

Figure 4.31 Trend of the tensile index vs. tear index of xylan-modified and unmodified SKPB handsheets at a higher salt concentration (conductivity of 1900 µS/cm^2).

4.4.3.3 Summary

The results presented here are in accordance with the other results in literature. A significant effect of xylan was obtained by comparing the strength properties with the refining intensity (Köhnke et al. 2008). indicating a fiber-bonding enhancing effect (Mobarak et al. 1973; Pettersson and Rydholm 1961; Rydholm 1965). However, comparing strength properties with the beating degree no significant difference could be recognized (Köhnke and Gatenholm 2007; Silva et al. 2011). Xylan is able to bind water, thus becoming a hydrogel which make it softer. When xylan is incorporated in a fiber-fiber joint a higher area in molecular contact could be achieved. Moreover, Coulomb forces can be generated due to the existence of carboxylic groups on the backbone. The reason for the negligible effect on strength properties of handsheets could be the result of a nonuniform and heterogeneous distribution of rather small xylan aggregates on the fiber surface (Henriksson and Gatenholm 2001, 2002; Linder et al. 2003). Moreover, a network will always fail at its weakest point. Stronger bonds with incorporated xylan may be present within a fiber network, but weaker bonds will fail first. Thus, xylan-enriched bonds between adjacent fibers may not have a significant influence on the resulting strength properties of handsheets. For this reason, the bond strength of individual fiber-fiber joints was determined and is presented in the next section.

4.5 Influence of xylan on properties of individual fibers

The breaking load of individual fiber-fiber joints and single fiber tensile strength of individual fibers were determined. The chemical composition of the investigated fiber samples is presented in Table 4.8. For the modifications of the fiber samples see section 3.7.1.1.

Table 4.8 Chemical composition (determined by high pressure liquid chromatography) of the fiber samples.

		Sugar amount[1] %			Lignin[2] %
Sample	Name	Glucose	Xylose	Mannose	
A	Ref	80.5	7.8	6.2	1.08
B	X_1 l	77.1	11.1	5.9	
C	X_2 l	77.0	9.5	6.0	
D	X_1 h	77.1	16.1	6.2	
E	X_2 h	77.9	14.6	6.1	
F	KOH	88.1	1.9	6.1	
G	κ42	77.7	7.8	6.1	6.66
H	κ54	75.2	7.9	6.0	8.22

[1] Determined by high pressure liquid chromatography

[2] The lignin content is the sum of Klason lignin and acid-soluble lignin

4.5.1 Individual fiber-fiber joints

Individual fiber-fiber joints were tested to investigate the influence of xylan on the bond strength. This was done to avoid the complication for the fiber network.

The mean values of the breaking load of individual fiber-fiber joints obtained for pulp A and H correspond to values generated in other studies using direct methods. Schniewind et al. (1964) determined a value of 2.26 mN (here 2.85 mN) for once-dried, unrefined, and bleached sulfate pulp (mixture of spruce and pine) at a higher testing speed of 2.54 mm/min. For unbeaten and unbleached softwood kraft pulp the following values were obtained: 6.102 mN (Mayhood et al. 1962), 4.98 mN (Saketi and Kallio 2011), and 6.58 mN (Fischer 2013). In this study, a mean breaking load of 6.01 mN of fiber crossings from unbleached, unbeaten, and never-dried softwood kraft pulp (mixture of spruce and pine) with κ54 was determined.

The results of the force that is needed to break the individual fiber crossings are presented in Figure 4.32. With increasing xylan content of the fibers (pulps B–E), the mean value of the breaking load is generally higher compared to the reference sample (A). At a confidence level of 95%, the mean value of pulp E (X_2 h) is statistically

Table 4.9 P-values of breaking load of the fiber-fiber joints obtained by a t-test against null hyphothesis.

Sample	A	B	C	D	E	F	G	H
A	—	0.708	0.062	0.090	0.036	0.558	0.353	0.013
B	0.708	—	0.274	0.305	0.188	0.859	0.321	0.091
C	0.062	0.274	—	0.878	0.735	0.409	0.075	0.098
D	0.090	0.305	0.878	—	0.889	0.424	0.094	0.262
E	0.036	0.188	0.735	0.889	—	0.292	0.035	0.251
F	0.558	0.859	0.409	0.424	0.292	—	0.267	0.414
G	0.353	0.321	0.075	0.094	0.035	0.267	—	0.071
H	0.013	0.091	0.098	0.262	0.251	0.414	0.071	—

different compared to the reference sample A which means a strong presumption against null hypothesis (see Table 4.9). This is also evident for the unbleached sample H at the same confidence interval of $\alpha = 0.05$. At a confidence level of $\alpha = 0.1$, the mean values of the breaking load of the xylan-treated pulps C (X_1 h) and D (X_2 l) are of low presumption against null hypothesis. The results indicate a strength improving effect of additional xylan on individual fiber-fiber joints. During the adsorption step, xylan adsorbs or precipitates predominantly on the fiber surface. Xylan is able to take up water resulting in a reduced surface hardness and a higher area in molecular contact can be achieved as well as coulomb forces due to the existence of carboxylic groups on the backbone. The results indicate, that xylan could improve joint strength of fiber crossings, but the amount of additional xylan, the chemical and physical properties (e.g. molecular weight), and the distribution on the fiber surface may play the key role in a strength enhancing effect. This may be the reason why no effect was obtained for the fibers with additional X_1 at a lower concentration.

The reduction of the xylan content (pulp F) resulted in a larger variance of the values, but no difference compared to pulp A was found. Alkaline extraction resulted in a reduction in the crystallinity of the fibers from about 50% to 30%. Thus, the surface of the fibers could get softer, resulting in a higher area in molecular contact between adjacent fibers. On the other hand, a significant difference could be noticed for the two unbleached samples, 1.91 mN (pulp G) and 6.01 mN (pulp H) which was confirmed with a t-test. Pulping proceeded longer for pulp G, leading to a lower lignin content, changing the structure of lignin (solubility) and the fiber surface and cell wall itself (e.g. surface area, surface charge, porosity, pore size distribution, and crystallinity). The amount of hemicelluloses was not remarkably affected for the two unbleached fiber sources, as shown in Table 4.8.

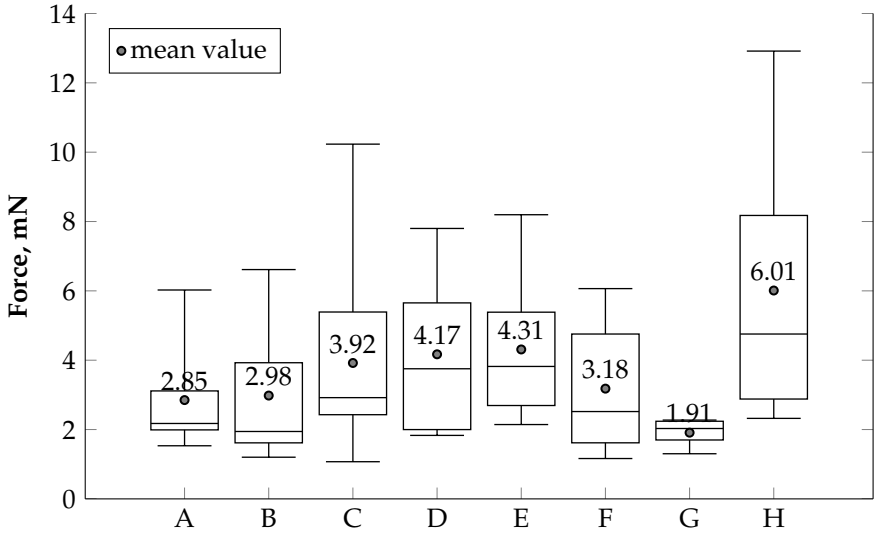

Figure 4.32 Breaking load of individual fiber-fiber joints (n = number of tested crossings) of the fiber samples: (A) Ref (n = 12), (B) X_1 l (n = 7), (C) X_2 l (n = 23), (D) X_1 h (n = 9), (E) X_2 h (n = 10), (F) KOH (n = 7), (G) κ42 (n = 5), and (H) κ54 (n = 7).

The specific bond strength was calculated for each bond by measuring the OBA before testing (section 3.7.1.3). The results are illustrated in Figure 4.33. The values for the samples with additional xylan at higher concentration (pulps D and E), after xylan extraction (pulp F), and the unbleached sample H seem to exhibit a higher specific bond strength, than the other samples. However, the variations are too large for a significant difference. By comparing the OBA of the fiber-fiber joints and its bonding force, no relation was noticed. Only pulps B and C show a higher R^2 of 0.88 (pulp B) and 0.98 (pulp C), as presented in Table 4.10. The reason for this behavior could be, that the OBA gives no information about the area in molecular contact, meaning that the actual contact area is smaller. Besides, the specific bond strength, further joint and fiber parameters are important, such as fiber width, fiber wall thickness, fiber diameter, fibril angle, or crossing angle (Fischer 2013). Thus, it is difficult to obtain a relationship between the bond strength and contact zone of individual fiber-fiber joints. The necessary handling of the samples could also have a certain influence on the bond strength.

Table 4.10 Coefficient of determination (R^2) of linear regression between the bond strength and the optical bonded area of the tested fiber-fiber joints (n = number of tested crossings) of the different pulp samples: (A) Ref (n = 3), (B) X_1 l (n = 6), (C) X_2 l (n = 3), (D) X_1 h (n = 9), (E) X_2 h (n = 9), (F) KOH (n = 7), (G) κ42 (n = 5), and (H) κ54 (n = 6).

Sample	A	B	C	D	E	F	G	H
R^2	0.564	0.883	0.981	0.013	0.013	0.251	0.267	0.004

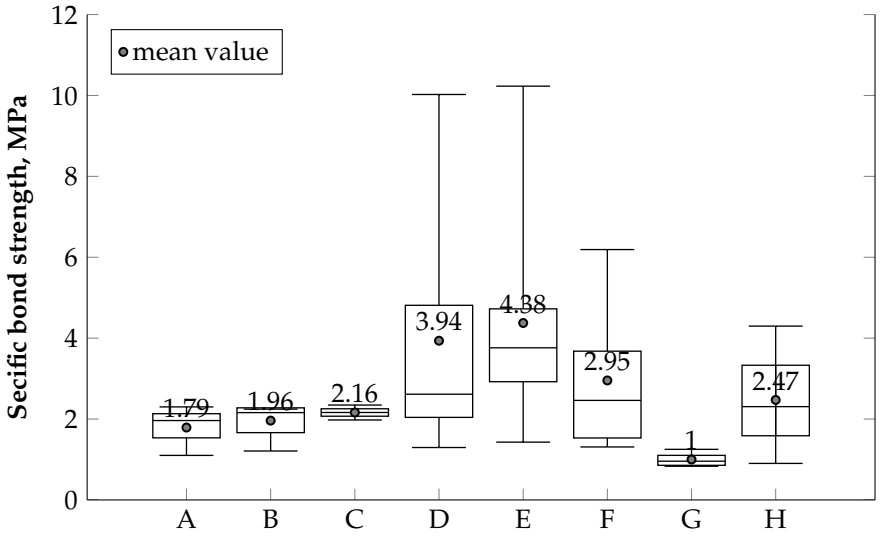

Figure 4.33 Specific bond strength of individual fiber-fiber joints (n = number of tested crossings) of the fiber samples: (A) Ref (n = 3), (B) X_1 l (n = 6), (C) X_2 l (n = 3), (D) X_1 h (n = 9), (E) X_2 h (n = 9), (F) KOH (n = 7), (G) κ42 (n = 5), and (H) κ54 (n = 6).

Nevertheless, the size of the bonded area between adjacent fibers is of fundamental importance for the resulting paper strength. This area is influenced by the contact zone or area in molecular contact which is depending on the fiber morphology. A rougher fiber surface leads to a smaller area in molecular contact while a smoother surface results in a larger contact zone, allowing stronger bonds by hydrogen bonding, Van der Waals linkage, Coulomb forces, interdiffusion, and capillary bridges. Xylan is able to bind water and acts as a hydrogel. Thus, swelling is enhanced in areas where xylan is present. This makes the fiber softer and more flexible, resulting in a lower penetration hardness in these areas (Ganser et al. 2014; Persson et al. 2013). When areas with a lower penetration hardness are getting in close interaction a larger area in molecular contact can be achieved making the bond stronger. To achieve an impact on the bond strength, the distribution of xylan is of great importance. Xylan is most probably heterogeneously and nonuniformly distributed on the fiber surface resulting in these large variations of the breaking load. Moreover, this could be affected by the amount of additional xylan on the fiber surface and by the fiber roughness leading to a lower area in molecular con-

tact. Especially, the surface roughness may have a strong impact on the resulting area in molecular contact, since Rohm et al. (2014) observed higher tensile strength values between two smooth cellulose thin films when xylan was incorporated.

4.5.2 Elastic modulus of individual fibers

Due to the importance of hemicelluloses for the tensile strength of individual fibers (Kersavage 1973; Spiegelberg 1966), the influence of xylan on the tensile strength of single pulp fibers was tested by either adsorption or extraction. The *E*-modulus of single fibers was calculated by measuring the breaking force and the corresponding strain of individual fibers (see section 3.7.2).

The results at constant cross sectional area of the tested fibers are depicted in Figure 4.34a. The mean values are a little bit lower compared to the values from literature but still in the range obtained by Groom et al. (2002) (6.55–27.5 GPa). A strong influence was found between the mean values of the unbleached and bleached fibers which is decreasing from 31.15 GPa (pulp H) to 7.69 GPa (pulp A). The addition of xylan most probably on the fiber surface did not have a significant influence on the *E*-modulus of individual bleached softwood kraft fibers. Only the fiber sample with additional X_2 at the higher concentration (pulp E) exhibited a statistical higher mean value at a confidence level of $\alpha = 0.05$ (see Table 4.12). No significant impact could be observed by alkaline extraction of xylan (pulp F), although the crystallinity was reduced from about 50% to around 30%. Thus, the fibers become less brittle and are less sensitive against to the formation of defects (Kersavage 1973). However, due to the removal of xylan from the fiber wall, defects are induced which may compensate the effect of larger regions with an amorphous character (Spiegelberg 1966).

When calculating the cross sectional area of each tested fiber (shape of an ellipse), the resulting area is two to three times larger (see Table 4.11). Thus, the *E*-modulus is reduced as depicted in Figure 4.34b. However, the trend is similar when comparing with Figure 4.34a, but no significant difference could be observed for the reference sample A and the sample treated with X_2 at the higher concentration (pulp E).

The elasticity of a fiber is dependent on the morphology of the fiber which is changing from fiber to fiber. The most important factors for the *E*-modulus of a fiber are the fibril angle, especially in the secondary (S2) fiber cell wall (Page et al. 1977) which is increasing with decreasing angle as well as the fiber width, cell wall thickness, and fiber thickness. Due to the incorporation of xylan within the fiber cell wall and its amorphous character, it has an impact on the elastic modulus. Chemical puling and bleaching leads to a higher porosity and the introduction of defects within the fiber cell wall. It could be possible, that adsorbed or precipitated

Table 4.11 Mean values of the cross sectional areas of the tested fibers (n = number of tested fibers) for calculating the *E*-modulii. The cross section was assumed to be an ellipse, the fiber width was measured from the images, and the fiber thickness was determined with an aspect ratio of 3.92:1 (Lorbach et al. 2014). (A) Ref (n = 7), (D) X_1 h (n = 6), (E) X_2 h (n = 4), (F) KOH (n = 5), (G) κ42 (n = 8), and (H) κ54 (n = 5).

Fiber source	l_w[1] µm	l_t[2] µm	A[3] µm^2
A	376.6 ± 5.99	9.38 ± 1.53	276.9 ± 90.0
C	41.61 ± 8.34	10.61 ± 2.13	358.5 ± 138.4
D	45.39 ± 9.50	11.58 ± 2.42	426.4 ± 160.5
E	37.12 ± 2.92	9.47 ± 0.74	277.5 ± 45.3
F	43.03 ± 8.93	10.98 ± 2.28	385.0 ± 142.2
G	48.94 ± 5.48	12.48 ± 1.40	484.6 ± 109.5

[1] fiber width [2] fiber thickness

[3] cross sectional area (shape of an ellipse)

Table 4.12 P-values of the elastic modulus of individual fibers (n = number of tested fibers) obtained by a t-test against null hyphothesis. (A) Ref (n = 7), (D) X_1 h (n = 6), (E) X_2 h (n = 4), (F) KOH (n = 5), (G) κ42 (n = 8), and (H) κ54 (n = 5).

Sample	A	D	E	F	G	H
A	—	0.791	0.041	0.958	0.014	0.0004
D	0.791	—	0.116	0.873	0.027	0.001
E	0.041	0.116	—	0.128	0.144	0.016
F	0.958	0.873	0.128	—	0.040	0.003
G	0.014	0.027	0.144	0.040	—	0.477
H	0.0004	0.001	0.016	0.003	0.477	—

Table 4.13 Mean values of the *E*-modulus obtained for different fiber samples in different studies.

Fiber source	mean value, GPa	Literature
loblolly pine earlywood	14.8	Mott et al. (2002)
loblolly pine latewood	19.7	Groom et al. (2002)
white spruce, cypress, Douglas-fir earlywood	25.2	Jayne (1959)
white spruce, cypress, Douglas-fir latewood	35.1	Jayne (1959)
Norway spruce (unbleached)	20.8/26.7	Ehrnrooth and Kolseth (1984)
softwood kraft pulp (unbleached)	20.2/16.8	Lorbach et al. (2014)
unbleached kraft pulp (western Canadian spruce and pine 5:5)	17.3	Kallmes and Perez (1966)
delignified Douglas-fir summerwood	28.9	Kersavage (1973)

xylan can reduce the porosity and compensate defects. However, the addition of xylan did not show any effect on the elasticity of the bleached fibers compared with the reference sample. Alkaline extraction did not have an effect on the elastic modulus as well. The results suggest that additional xylan does not have an impact on the tensile strength properties of individual fibers. This is most probably due to the fact that xylan adsorbs or precipitates predominantly on the fiber surface. This also depends on the quantity of additional xylan on the fiber. A fiber which is completely covered with a film or aggregates of xylan could possess a different tensile strength. Nevertheless, it seems that xylan may have an effect when it is incorporated in the fiber cell wall to support the distribution of stress, especially in the S2 wall.

Large fluctuations of the *E*-modulus could be obtained within one fiber sample. This can be explained by several things. First, the method for testing a fiber may have an influence. During fixation and testing, stresses may occur influencing the tensile strength. Second, as before mentioned pulp fibers exhibit fluctuations in their morphology, due to environmental impacts during growth as well as influences during preparation and production of the fibers. Moreover, the fiber samples were mixtures of spruce and pine (7:3). Therefore, no clear separation between both sources could be achieved resulting in high variations as the tensile strength of spruce fibers may be different, than that of pine fibers. In addition, the samples could be mixtures of earlywood and latewood from each fiber resource. Latewood exhibits in general a higher tensile strength, than earlywood.

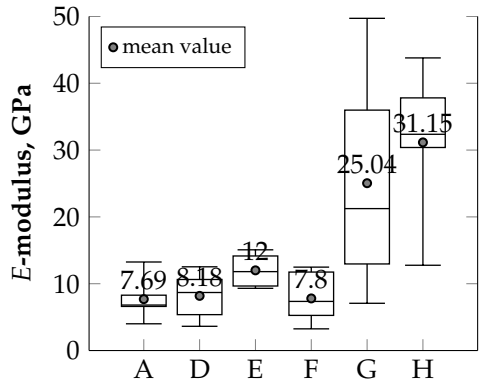

a) *E*-modulus with constant cross sectional area.

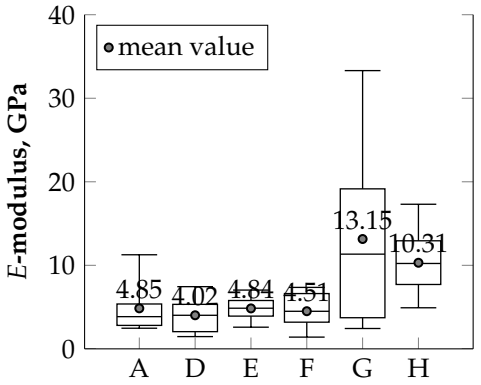

b) *E*-modulus with calculated cross sectional area (ellipse).

Figure 4.34 *E*-modulii of individual fibers (n = number of tested fibers) calculated from single fiber tensile testing: (A) Ref (n = 7), (D) X_1 h (n = 6), (E) X_2 h (n = 4), (F) KOH (n = 5), (G) κ42 (n = 8), and (H) κ54 (n = 5). Figure a) on the left side represent the values with a constant cross sectional area and Figure b) on the right side, the cross sectional area was calculated for each tested fiber. Note that the values of the y-axes are different..

Table 4.14 Mean values of the area of the cross sections of the tested fibers (n = number of tested fibers) for the *E*-modulii. The cross section was assumed to be an ellipse, the fiber width was measured from the images, and the fiber thickness was determined with an aspect ratio of 3.92:1 (Lorbach et al. 2014). (A) Ref (n = 7), (D) X_1 h (n = 6), (E) X_2 h (n = 4), (F) KOH (n = 5), (G) κ42 (n = 8), and (H) κ54 (n = 5).

Fiber source	l_w[1] µm	l_t[2] µm	A[3] µm^2
A	376.6 ± 5.99	9.38 ± 1.53	276.9 ± 90.0
C	41.61 ± 8.34	10.61 ± 2.13	358.5 ± 138.4
D	45.39 ± 9.50	11.58 ± 2.42	426.4 ± 160.5
E	37.12 ± 2.92	9.47 ± 0.74	277.5 ± 45.3
F	43.03 ± 8.93	10.98 ± 2.28	385.0 ± 142.2
G	48.94 ± 5.48	12.48 ± 1.40	484.6 ± 109.5

[1] fiber width [2] fiber thickness [3] cross sectional area (ellipse)

4.5.3 Summary

The breaking load of individual fiber-fiber joints was statistically affected by additional xylan at a confidence level of $\alpha = 0.1$. The distribution of additional xylan could be a main reason for high variations of the values. Furthermore, the chemical structure of lignin and the distribution of charged groups on the fiber surface as well as the morphology could have an influence on the resulting joint strength of individual fibers. No clear trend between the breaking load and the OBA was obtained which is most probably due to the fact, that the OBA gives no information about the area in molecular contact.

The calculated elastic modulus from single fiber tensile strength measurements of individual fibers was not affected by the addition or extraction of xylan. Thus, it seems that xylan could have an influence on the tensile strength when it is incorporated within the fiber wall, especially in the secondary S2 wall, to support the distribution of stresses more homogeneously. However, this highly depends on the morphology, porosity, and the composition of the fiber cell wall.

Chapter 5

Conclusion and Outlook

5.1 Conclusion

The amount of xylan on sulfate and sulfite pulp fibers could be increased by an adsorption step. The temperature and pH had a significant effect on the increase in xylan content. Further, a high ionic strength, pulp consistency, and xylan concentration is favorable to enrich pulp fibers with xylan. However, when increasing the pulp consistency, a sufficient mixing is necessary. An accumulation of xylan on viscose fibers was not observed which could be due to the detection limit of the measurement of the high pressure liquid chromatography technique.

The pulp samples with additional xylan exhibited a stronger increase in the beating degree. Xylan is able to take up water resulting in a stronger fiber swelling and consequently in a higher wet flexibility. Such a fiber features a lower resistance towards mechanical stress as it occurs during refining. This could imply, that less energy is needed in an industrial refining stage to reach a similar beating degree when comparing untreated and xylan-treated pulps. However, the PFI mill (laboratory refiner) holds in general a low impact on the fiber treatment and a high energy demand.

The strength properties of handsheets of the different pulp samples was not affected by additional xylan. An increase in tensile strength was only observed by comparing against the refining input (revolution) during refining. Contrary, the tear index dropped down faster for the xylan-modified samples at longer refining time. However, the reason why the influence of xylan on paper properties is controversially discussed in literature may be due to the fact that paper is a fiber network. A network will always fail at its weakest point. Thus, xylan-enriched bonds between fibers could be present, but they may not be predominant to enhance strength properties.

The investigation of the breaking load of individual fiber-fiber joints exhibited that higher forces are needed to break fiber crossings of xylan-treated fibers. This underlines, that xylan can have an impact on the joint strength. The elastic modulus of the fibers was not affected by additional xylan. The modulus of elasticity is more influenced by the morphology of the fiber wall, especially the secondary S2 wall.

Nevertheless, the distribution of xylan on the fiber surface may have a large impact on the breaking load of individual fiber-fiber-joints. Adsorbed or precipitated xylan is located more heterogeneously and nonuniformly on the fiber surface, determined by attenuated total reflection spectroscopy, X-ray photoelectron spectroscopy, and atomic force microscopy (AFM). The use of OH- and CH_3-functionalized AFM tips is helpful to visualize a clear phase contrast by phase imaging between cellulose and xylan and to determine adhesive forces via force mapping between a functionalized AFM tip and cellulose or xylan. These differences

were expected due to the presence of carboxylic groups on the backbone of xylan which exhibit stronger repulsion (higher negative charge density) than hydroxyl groups. These methods were successfully accomplished on smooth cellulose thin films treated with aqueous solutions of xylan. On untreated and xylan-treated pulp fibers it was not possible to unambiguously verify additional xylan on the fiber surface, although the surface coverage was increased. Untreated fibers featured already areas with a lower adhesive force. Thus, it could not be concluded, if these areas on the fiber samples with additional xylan consist already of xylan or other hemicelluloses. Moreover, lignin which is present on the fiber surface could have an influence on the phase imaging and force mapping. However, this technique could play a key role in analyzing and quantifying the bonding mechanism within paper.

5.2 Outlook

An effect of additional xylan on strength properties of handsheets was not observed. By comparing xylan and Carboxymethyl cellulose (CMC) which features a strength-enhancing effect in paper, CMC possesses a higher molecular weight and charge density. Thus, it would be of interest to further chemically modify xylan regarding a higher amount of charged groups, e.g. carboxylic groups, on the backbone.

Moreover, due to the branched structure of xylans and the size of the polymers, their dissolution behavior can vary between different sources. Therefore, different solvents should be tested on the dissolution behavior and size distribution of xylan. This can be also studied regarding the temperature, pH, and other influencing parameters. Further, the impact of different solvents on the crystallinity and pore size distribution as well as further structural changes of cellulosic fibers need to be investigated.

The size distribution of xylan in aqueous solution has a large influence on the dissolution and precipitation behavior. This should be considered to analyze the self-assembly of xylan on cellulosic surfaces. Moreover, the adjustment of the size distribution of xylan could be investigated by various techniques, such as mechanical, chemical, and physical methods like ultrasound.

Another key aspect is related to the distribution of xylan on cellulosic fibers. Xylan had an strength-enhancing effect on the breaking load of individual fiber-fiber joints. This is most probably influenced by the arrangement of xylan on the fiber surface. Fibers which feature a complete film of xylan on the surface should have different strength properties. Thus, it needs to be investigated, how xylan can be forced to adsorb or precipitate as a film on cellulosic surfaces.

Last but not least, further investigations are necessary concerning the adsorption of xylan by AFM using functionalized tips. Therefore, possible compounds in wood and pulp, i.e. cellulose, hemicelluloses, and lignin should be analyzed with such tips. A higher variety of functionalizations are favorable to study the hydrophilic and hydrophobic character as well as the distribution of charges on cellulosic materials. This AFM technique could have a particularly key role to analyze and quantify the bonding mechanisms within paper. Therefore, phase imaging and force mapping should be performed at different temperatures and relative humidity and in the wet state to determine adhesive forces between functionalized tips and the fiber surface. Additionally, this could allow to investigate the impact of different bonding mechanisms during sheet forming.

References

Åkerholm, M. and Salmén, L. (2001). Interactions between wood polymers studied by dynamic FT-IR spectroscopy. *Polymer*, **42**(3): 963–969.

Almond, A. and Sheehan, J. K. (2003). Predicting the molecular shape of polysaccharides from dynamic interactions with water. *Glycobiology*, **13**(4): 255–264.

Antal, M., Ebringerová, A., and Hromádková, Z. (1997). Struktur und papiertechnische Eigenschaften von Aminoalkylxylanen. *Papier*, **51**(5): 223–226.

Antal, M., Ebringerová, A., and Micko, M. M. (1991). Kationisierte Hemicellulosen aus Espenholzmehl und ihr Einsatz in der Papierherstellung. *Papier*, **45**(5): 232–235.

Askeland, D. R., Fulay, P. P., and Wright, W. J. (2011). *The science and engineering of materials*. Cengage Learning, 6th edition.

Atalla, R. H., Hackney, J. M., Uhlin, I., and Thompson, N. S. (1993). Hemicelluloses as structure regulators in the aggregation of native cellulose. *Int J Biol Macromol*, **15**(2): 109–112.

Atkins, E. D. T. (1992). Three-dimensional structure, interactions and properties of xylan. In *Xylans and Xylanases (J. Visser, G. Beldman, M. A. Kusters-von Someren, A. G. J. Voragen, ed.)* Progress in Biotechnology, Vol. 7, Elsevier, Amsterdam, pages 39–50.

Aurell, R. (1963). The effect of lowered pH at the end of birch kraft cooks. *Svensk Papperstidn*, **66**(11): 437–442.

Aurell, R. (1965). Increasing kraft pulp yield by redeposition of hemicelluloses. *Tappi J*, **48**(2): 80–84.

Aurell, R. and Hartler, N. (1965). Kraft pulping of pine. Part 1. The changes in the composition of wood residue during the cooking process. *Svensk Papperstidn*, **68**(3): 59–68.

Axelsson, S., Croon, I., and Enström, B. (1962). Dissolution of hemicelluloses during sulphate pulpng. Part 1. Isolation of hemicelluloses from the cooking liqour at different stages of birch soda cooking. *Svensk Papperstidn*, **65**(18): 693–697.

Bachner, K., Fischer, K., and Bäucker, E. (1993). Zusammenhang zwischen aufbau der zellwand und festigkeitseigenschaften bei faserstoffen von konventionellen und neuen aufschlussverfahren. *Paper*, 10A: V30–V40.

Back, E. L. (1967). Thermal auto-crosslinking in cellulose material. *Pulp Pap Mag Can*, **68**(4): T165–T171.

Ban, W. and van Heiningen, A. (2011). Adsorption of hemicellulose extracts from hardwood onto celllulosic fibers. I. Effects of adsorption and optimization factors. *Cellul Chem Technol*, **45**: 57–65.

Barakat, A., Winter, H., Rondeau-Mouro, C., Saake, B., Chabbert, B., and Cathala, B. (2007). Studies of xylan interactions and cross-linking to synthetic lignins formed by bulk and end-wise polymerization: a model study of lignin carbohydrate complex formation. *Planta*, **226**: 267–281.

Bartsch, H.-J. (2011). *Mathematischer Formeln für Ingenieure und Naturwissenschaftler*. Hanser Verlag, Leipzig, 22 edition.

Berggren, R., Molin, U., Berthold, F., Lennholm, H., and Lindström, M. (2003). Alkaline degradation of birch and spruce: influence of degradation conditions on molecular mass distributions and fibre strength. *Carbohydr Polym*, **51**(3): 255–264.

Bergman, L. and Schaefer, C. (2004). *Lehrbuch der Experimentalphysik. Band 3 Optik. Wellen- und Teilchenoptik*. Walter de Gruyter & Co, Berlin, 10. Auflage.

Bhaskaran, T. A. and von Koeppen, A. (1970). The degradation of wood carbohydrates during sulphate pulping. *Holzforschung*, **24**(1): 14–19.

Binnig, G., Quate, C., and Gerber, C. (1986). Atomic force microscope. *Phys Rev Lett*, 56:930–933.

Bishop, H. (1966). Some electron backscattering measurements for solid targets. In Castaing, R., Deschamps, P., and Philibert, J., editors, *4th International Conference of X-Ray Optics and Microanalysis*. Hermann, Paris.

Blake, J. D. and Richards, G. N. (1971). Evidence for molecular aggregation in hemicelluloses. *Carbohydr Res*, **18**(1): 11–21.

Bose, S. K., Barber, V. A., Alves, E. F., Kiemle, D. J., and Stipanovic, A. J. (2009). An improved method for the hydrolysis of hardwood carbohydrates to monomers. *Carbohydr Polym*, **78**: 396–401.

Buchert, J., Teleman, A., Harjunpää, V., Tenkanen, M., Viikari, L., and Vuorinen, T. (1995). Effect of cooking and bleaching on the structure of xylan in conventional pine kraft pulp. *Tappi J*, **78**(11): 125–130.

Cao, B. G., Tschirner, U., and Ramaswamy, S. (1998). Impact of pulp chemical composition on recycling. *Tappi J*, **81**(12): 119–127.

Casebier, R. L. and Hamilton, J. K. (1967). Alkaline degradation of xylans. *Tappi J*, **50**(9): 441–449.

Christiernin, M., Henriksson, G., Lindström, M. E., Brumer, H., Teeri, T. T., Lindström, T., and Laine, J. (2003). The effects of xyloglucan on the properties of paper made from bleached kraft pulp. *Nord Pulp Paper Res*, **18**(2): 182–187.

Claesson, P. M., Christenson, H. K., Berg, J. M., and Neuman, R. D. (1995). Interactions between mica surfaces in the presence of cabrohydrates. *J Colloid Interf Sci*, **172**: 415–424.

Clayton, D. and Phelps, G. (1965). Sorption of glucomannan and xylan on alpha-cellulose wood fibers. *J Polym Sci, Part C: Polymer Symposia*, **11**:197–220.

Clayton, D. and Stone, J. (1963). The redeposition of hemicelluloses during pulping. Part I: The use of tritium-labeled xylan. *Pulp Pap Mag Can*, **64**(11):T459–T468.

Clayton, D. W. (1963). The akaline degradation of some hardwood 4-*o*-methyl-d-glucuronoxylans. *Svensk Papperstidn*, **66**(4): 115–124.

Conners, T. and Banerjee, S. (1995). *Surface analysis of paper*. CRC Press.

Contela, G. and Borruso, D. (1967). The influence of hemicelluloses on the beatability of pulps. *Tappi J*, **50**(7): 344–347.

Croon, I. and Enström, B. (1962). The hemicelluloses in sulphate pulps from scot pine. *Svensk Papperstidn*, **65**(16): 595–599.

Croon, I. and Enström, B. F. (1961). The 4-*o*-methyl-d-glucuronic acid groups of birch xylan during sulfate pulping. *Tappi J*, **44**(12): 870–874.

Dahlman, O., Sjöberg, J., Jansson, U. B., and Larsson, P. O. (2003). Effects of surface hardwood xylan on the quality of softwood pulps. *Nord Pulp Paper Res*, **18**(3): 310–315.

Danielsson, S., Kisara, K., and Lindström, M. E. (2006). Kinetics, catalysis, and reaction engineering. Kinetic study of hexenuronic and methylglucuronic acid reactions in pulp and in dissolved xylan during kraft pulping of hardwood. *Industrial & Engineering Chemistry Research*, **45**: 2174–2178.

Danielsson, S. and Lindström, M. E. (2005). Influence of birch xylan adsorption during kraft cooking on softwood pulp strength. *Nord Pulp Paper Res*, **20**(4): 436–441.

Daus, S. and Heinze, T. (2010). Xylan-based nanoparticles: Prodrugs for ibuprofen release. *Macromol Biosci*, **10**(2): 211–220.

Demtröder, W. (2013). *Experimentalphysik 2. Elektrizität und Optik*. Springer-Verlag, 6., überarbeitete und aktualisierte Auflage.

Dixon, M. C. (2008). Quartz crystal microbalance with dissipation monitoring: enabling real-time characterization of biological materials and their interactions. *J Biomolecul Tech*, **18**(3): 151–158.

Dobrynin, A. V. and Rubinstein, M. (2005). Theory of polyelectrolytes in solutions and at surfaces. *Prog Polym Sci*, 30: 1049–1118.

Dobrynin, A. V. A. V., Deshkovski, and Rubinstein, M. (2001). Adsorption of polyelectrolytes at oppositely charged surfaces. *Macromolecules*, 34: 3421–3436.

Doner, L. W. and Hicks, K. B. (1997). Isolation of hemicellulose from corn fiber by alkaline hydrogen peroxide extraction. *Cereal Chem*, **74**: 176–181.

Ebringerová, A. and Heinze, T. (2000). Xylan and xylan derivates - Biopolymers with valuable properties, 1: Naturally occuring xylans structures, isolation procedures and properties. *Macromol Rap Comm*, **21**(9): 542–556.

Ebringerová, A., Hromádkov'a, Z., and Heinze, T. (2005). Hemicellulose. *Adv Polym Sci*, **186**: 1–67.

Ehrnrooth, E. M. L. and Kolseth, P. (1984). The tensile testing of single wood pulp fibers in air and in water. *Wood Fiber Sci*, **16**(4):549–566.

Eklund, D. and Lindström, T. (1991). *Paper chemistry: an introduction*. DT Paper Science Publications, 1st edition.

Eriksson, E. and Samuelson, O. (1962). Isolation of hemicellulose from sulfite cooking liquors. Part 1. Acid sulfite cooking. *Svensk Papperstidning*, **65**(16): 600–605.

Eriksson, E., Samuelson, O., and Viale, A. (1963). Adsorption of hemicellulose isolated from sulfite cooking liquors by cellulose fibers. *Svensk Papperstidn*, **66**(10): 403–406.

Ertl, G. and Küppers, J. (1974). *Low energy electrons and surface chemistry*. Verlag Chemie.

Evans, R., Newman, R., Roick, U., Suckling, I., and Wallis, A. (1995). Changes in cellulose crystallinity during kraft pulping. Comparison of infrared, X-ray diffraction and solid state NMR results. *Holzforschung*, 49: 498–504.

Fahrenfort, J. (1961). Attenuated total reflection: a new principle for the proproduct of useful infra-red reflection spectra of organic compounds. *Spetrochim Acta*, 17: 698–709.

Fengel, D. (1970). Ultrastructure behavior of cell wall polysaccharides. *Tappi J*, **53**(3): 497–503.

Fengel, D. (1992). Möglichkeiten und Grenzen der FTIR-Spektroskopie bei der Charakterisierung von Cellulose. Teil 3. Einfluss von Begleitstoffen auf der IR-Spektrum von Cellulose. *Papier*, 1: 7–11.

Fengel, D., Stoll, M., and Wegener, G. (1978). Studies on milled wood lignin from spruce. Part II. Electron microscopic observations on the milled wood. *Wood Sci Technol*, **12**(2): 141–148.

Fengel, D. and Wenger, G. (2003). *Wood chemistry, ultrastructure, reactions*. Kessel Verlag.

Fernandes Diniz, J. M. B., Gil, M. H., and M.Castro, J. A. A. (2004). Hornification – its origin and interpretation in wood pulps. *Wood Sci Technol*, **37**: 489–494. 10.1007/s00226-003-0216-2.

Fischer, J. W. (2013). *A novel direct method for mechanical testing of individual fibers and fiber to fiber joints*. PhD thesis, Graz University of Technology, Graz, Austria.

Fischer, W. J., Hirn, U., Bauer, W., and Schennach, R. (2012). Testing of individual fibre-fibre joints under biaxial load and simultaneous analysis of deformation. *Nord Pulp Paper Res*, **27**(2): 237–244.

Fischer, W. J., Zankel, A., Ganser, C., Schmied, F., Schroettner, H., Hirn, U., Teichert, C., Bauer, W., and Schennach, R. (2014). Imaging of the formerly bonded area of individual fibre to fibre joints with SEM and AFM. *Cellulose*, **21**(1): 251–260.

Fleer, G., Choen Stuart, M., Scheutjens, J., Cosgrove, T., and Vincent, B. (1993). *Polymers at interfaces*. Chapman & Hall, London, UK.

Frey-Wyssling, A. (1954). The fine structure of cellulose microfibrils. *Science*, **119**(3081): 80–82.

Galván, M. V., Mocchiutti, P., Cornaglia, L. M., and Zanuttini, M. A. (2012). Dual-polyelectrolyte adsorption of poly(allylamine hydrochloride) and xylan onto recycled unbleached kraft pulps. *Bioresources*, **7**(2): 2075–2089.

Ganser, C., Hirn, U., Rohm, S., Schennach, R., and Teichert, C. (2014). AFM nanoindentation of pulp fibers and thin cellulose films at varying relative humidity. *Holzforschung*, 68(1): 53–60.

Gardner, K. H. and Blackwell, J. (1974). The structure of native cellulose. *Biopolymers*, **13**(10): 1975–2001.

Gellerstedt, G. and Lindfors, E.-L. (1984). Structural changes in lignin during kraft pulping. *Holzforschung*, **38**(3): 151–158.

Giancoli, D. C. (2010). *Physik: Lehr- und Übungsbuch*. Person Studium, 3rd edition.

Gilli, E., Horvath, A., Horvath, A., Hirn, U., and Schennach, R. (2009). Analysis of CMC attachment onto cellulosic fibers by infrared spectroscopy. *Cellulose*, 16: 825–832.

Goldstein, J., Newbury, D., Echlin, P., Joy, D., Lyman, C., Lifshin, E., Sawyer, L., and Michael, J. (2003). *Scanning electron microscopy and X-ray microanalysis*. Kluwer Academic / Plenum Publishers, 3rd edition.

Goos, F. and Hänchen, H. (1947). Ein neuer fundamentaler Versuch zur Totalreflexion. *Annalen der Physik*, 436(6): 333–346.

Griffiths, P. R. and de Haseth, J. A. (1986). *Chemical Analysis. A series of monographs on analytical chemistry and its applications*, volume 83. Fourier transform infrared spectrometry. John Wiley & Sons.

Groom, L., Mott, L., and Shaler, S. (2002). Mechanical properties of individual southern pine fibers. part I. determination and variability of stress-strain curves with respect to tree height and juvenility. *Wood Fiber Sci*, **34**(1):14–27.

Gruppen, H., Hamer, R. J., and Voragen, A. G. J. (1992). Water-unextractable cell wall material from wheat flour. 2. Ffractionation of alkali-extracted ppolymer and comparison with water-extractable arabinoxylans. *J Cereal Sci*, **16**: 53–67.

Gullichsen, J. and Paulapuro, H. (2000). *Papermaking science and technology. Chemical pulping*, volume Book 6A. Fapet Oy.

Häggkvist, M., Li, T.-Q., and Ödberg, L. (1998). Effects of drying and pressing on the pore structure in the cellulose fibre wall studied by ^{1}H and ^{2}H NMR relaxation. *Cellulose*, **5**(1): 33–49.

Hannuksela, T., Holmbom, B., Mortha, G., and Lachenal, D. (2004). Effect of sorbed galactoglucomannans and galactomannans on pulp and paper handsheet properties, especially strength properties. *Nord Pulp Paper Res*, **19**(2): 237–244.

Hansson, J.-Å. (1970a). Sorption of hemicelluloses on cellulose fibres, Part 2, Sorption of glucomannan. *Holzforschung*, **24**(3): 77–83.

Hansson, J.-Å. (1970b). Sorption of hemicelluloses on cellulose fibres. Part 3. The temperature dependence on sorption of birch xylan and pine glucomannan at kraft pulping conditions. *Svensk Papperstidn*, **73**(3): 49–53.

Hansson, J.-Å. and Hartler, N. (1968). Alkaline degradation of xylans from birch and pine. *Svensk Papperstidn*, **71**(9): 358–365.

Hansson, J.-Å. and Hartler, N. (1969). Sorption of hemicelluloses on cellulose fibres. Part 1. Sorption of xylans. *Svensk Papperstidn*, **72**(17): 521–530.

Harrick, N. (1960). Surface chemistry from sspectra analysis of tototal ininternal reflected radiation. *J Phys Chem-US*, 64(9): 1110–1114.

Hartler, N. and Lund, A. (1962). Sorption of xylans on cotton. *Svensk Papperstidn*, **65**: 951–955.

Henriksson, Å. and Gatenholm, P. (2001). Controlled assembly of glucuronoxylans onto cellulose fibers. *Holzforschung*, **55**: 494–502.

Henriksson, Å. and Gatenholm, P. (2002). Surface properties of CTMP fibres modified with xylans. *Cellulose*, **9**: 55–64.

Herres, W. and Gronholz, F. (1984). Understanding FT-IR data processing. Part 1. Data acquisition and Fourier transformation. *Computer Applications in the Laboratory*, **2**: 216–220.

Heyn, A. (1966). The microcrystalline structure of cellulose in cell wall of cotton, ramie, and jute fibers as revealed by negative staining of sections. *J Cell Biol*, **29**(2):181–197.

Heyn, A. (1969). The elementary fibril and supermolecular structure of cellulose in soft wood fiber. *J Ultrastruct Res*, **26**(1-2):52–68.

Heyn, A. N. J. (1977). Ultrastructure of wood pulp with special reference to the elementary fibril of cellulose. *Tappi J*, **60**(11): 159–161.

Higgins, H., Stewart, C., and Harrington, K. (1961). Infrared spectra of cellulose and related polysaccharides. *J Polym Sci*, 51: 59–84.

Hindeleh, A. M. and Johnson, D. J. (1974). Crystallinity and crystallite size measurement in cellulose fibres: 2. Viscose rayon. *Polymer*, **15**(11): 697–705.

Höije, A., Sandström, C., Roubroeks, J. P., Andersson, R., Gohil, S., and Gatenholm, P. (2006). Evidence of the presence of 2-*o*-β-D-xylopyranosyl-α-L-arabinofuranose side chains in barley husk arabinoxylan. *Carbohydr Res*, **341**(18): 2959–2966.

Höök, F., Kasemo, B., Nylander, T., Fant, C., Scott, K., and Elwing, H. (2001). Variations in coupled water, viscoelastic properties, and film thickness of a mefp-1 protein film during adsorption and cross-linking: a quartz crystal microbalance with dissipation monitoring, ellipsometry, and surface plasmon resonance study. *Anal Chem*, **73**(24): 5796–5804.

Horvath, A. E. (2003). Appropriate conditions for polyelectrolyte titration to determine the charge of cellulose fibers. Licentiate thesis, KTH Royal Institute of Technology, Stockholm, Sweden.

Horvath, A. E. and Lindström, T. (2007). Indirect polyelectrolyte titration of cellulosic fibers – surface and buld ccharge of cellulosic fibers. *Nord Pulp Paper Res*, **22**(1): 87–92.

Horvath, A. E., Lindström, T., and Laine, J. (2006). On the indirect polyelectrolyte titration of cellulosic fibers. Conditions for charge stoichiometry and comparison with ESCA. *Langmuir*, **22**(2):824–830.

Huber, J. C. K. P. F. K. (1974). Separation of acidic compounds by high-pressure liquid-liquid chromatography involving ion-pair formation. *J Chromatogr A*, 102: 333–351.

Jansson, Z. L. and Brännvall, E. (2011). Characterisation of dissolved spruce xylan in kraft cooking. *Nord Pulp Paper Res*, **26**(4): 380–385.

Janzon, R., Saake, B., and Puls, J. (2008). Upgrading of paper-grade pulps to dissolving pulps by nitren extraction: properties of nitren extracted xylans in comparison to NaOH and KOH extracted xylans. *Cellulose*, 15(1): 161–175.

Jayme, G. and Koburg, E. (1959). Über den elektronisch bestimmten Durchmesser der Mikrofibrillen von Laubholzzellelementen. *Holzforschung*, **13**: 37–43.

Jayne, B. A. (1959). Mechanical properties of wood fibers. *Tappi J*, **42**(6): 461–467.

Johansson, M. and Samuelson, O. (1977). Reducing end groups in birch xylan and their alkaline degradation. *Wood Sci Technol*, **11**:251–263.

Joy, D. and Joy, C. (1996). Low voltage scanning electron microscopy. *Micron*, 27(3-4): 247–263.

Kabel, M. A., van den Borne, H., Vincken, J.-P., Voragen, A. G. J., and Schols, H. A. (2007). Structural differences of xylans affect their interaction with cellulose. *Carbohydr Polym*, **69**(1): 94–105.

Kačuráková, M., Wellner, N., Ebringerová, A., Hromádková, Z., and Wilson, R. (1999). Characterisaiton of xylan-type polysaccharides and associated cell wall components by FT-IR and FT-Raman spectroscopies. *Food Hydrocolloid*, 13: 35–41.

Kallmes, O. J. and Perez, M. (1966). Load/elongation properties of fibers. In *Consolidation of the Paper Web, Volume 1 (F. Bolam, ed.), Technical Section of the British Paper and Board Maker´s Association, London*, pages 507–528.

Kappel, L., Hirn, U., Bbauer, W., and Schennach, R. (2009). A novel method for the determination of the bonded area of individual fiber-fiber bonds. *Nord Pulp Pap Res J*, 24(2): 199–205.

Kappel, L., Hirn, U., Gilli, E., Bauer, W., and Schennach, R. (2010). Revisiting polarized light microscopy for fiber-fiber bond area measurement – part 1: theoretical findamentals. *Nord Pulp Pap Res J*, 25: 65–70.

Kararova, S., Sultanove, N., Ivanov, C., and Nikolov, I. (2007). Analysis of the dispersion of optical plastic materials. *Opt Mater*, 29: 1481–1490.

Katz, S., Beatson, R. P., and Scallan, A. M. (1984). The determination of strong and weak acid groups in sulfite pulps. *Svensk Papperstidn*, **87**(6): R48–R53.

Kerekes, R. J. (2005). Characterization refining action in PFI mills. *Tappi J*, **4**(3): 9–14.

Kerr, A. J. and Goring, D. A. I. (1975). The ultrastructural arrangement of the wood cell wall. *Cell Chem Technol*, **9**: 563–573.

Kersavage, P. C. (1973). Moisture content effect on tensile properties of individual douglas-fir latewood trachaids. *Wood Fiber Sci*, **5**(2):105–117.

Kleinert, T. N. (1966). Mechanisms of alkaline delignification. I. The overall reaction pattern. *Tappi J*, **49**(2): 53–57.

Klungness, J. H. and Caulfield, D. F. (1982). Mechanisms affecting fiber bonding during drying and aging of pulps. *Tappi J*, **65**(12): 94–97.

Knox, J. H. and Pryde, A. (1975). Performance and selected applications of a new range of chemically bonded packing materials in high-performance liquid chromatography. *J Chromatogr*, 112: 171–188.

Köhnke, T., Brelid, H., and Westman, G. (2009). Adsorption of cationized barley husk xylan on kraft pulp fibres: influence of degree of cationization on adsorption characteristics. *Cellulose*, **16**: 1109–1121.

Köhnke, T. and Gatenholm, P. (2007). The effect of controlled glucuronoxylan adsorption on drying-induced strength loss of bleached softwood pup. *Nord Pulp Paper Res*, **22**(4): 508–514.

Köhnke, T., Lund, K., Brelid, H., and Westman, G. (2010). Kraft pulp hornification: A closer look at the preventice effect gained by glucuronoxylan adsorption. *Carbohydr Polym*, **81**(2): 226–233.

Köhnke, T., Pujolras, C., Roubroeks, J., and Gatenholm, P. (2008). The effect of barley husk arabinoxylan adsorption on the properties of cellulose fibres. *Cellulose*, **15**: 537–546.

Köhnke, T., Å. Östlund, and Brelid, H. (2011). Adsorption of arabinoxylan on cellulosic surfaces: Influence of degree of substitution and substitution pattern on adsorption characteristics. *Biomacromol*, **12**: 2633–2641.

Kolpak, F. J. and Blackwell, J. (1976). Determination of the structure of cellulose II. *Macromolecules*, **9**(2): 273–278.

Kontturi, E., Thüne, P. C., and Niemantsverdriet, J. W. (2003). Novel method for preparing cellulose model surfaces by spin coating. *Polymer*, **44**(13): 3621–3625.

Kormelink, F. J. M. and Voragen, A. G. (1993). Degradation of different glucuronoarabinoxylans by a combination of purified xylan-degrading enzymes. *App Microbiol Biothechnol*, **38**: 688–695.

Košiková, B., Joniak, D., and Skamla, J. (1972). Lignin-carbohydrate bonds in beech wood. *Cell Chem Technol*, **6**: 579–588.

Košiková, B., Zákutná, L., and Joniak, D. (1978). Investigations of the lignin-saccharidic complex by electron microscopy. *Holzforschung*, **32**(1): 15–18.

Krässig, H. A. (1968). Characterization of cellulose fibers. In: *Man-Made Fibers, Science and Technology* (Eds: H.F. Mark, S.M. Atlas, and E. Cernia), Vol. II:pp. 133–150, John Wiley & Sons, New York.

Krässig, H. A. (1993). *Cellulose. structure, accessibility and reactivity*. Gordon and Breach Science Publishers. Polymer monographs, Vol. 11.

Kroon-Batenburg, L. J. M., Kroon, J., and Northolt, M. G. (1986). Chain modulus and intramolecular hydrogen bonding in native and regenerated cellulose fibres. *Polym Commun Guildford*, **27**(10): 290–292.

Kumar, S. and Negi, Y. S. (2012). Nanoparticles synthesis from corn cob (xylan) and their potential application as colon-specific drug carrier. *Macromol Symp*, **320**(1): 75–80.

Laine, J., Lindström, T., Bremberg, C., and Glad-Nordmark, G. (2003). Studies on topochemical modification of cellulosic fibres. part 5: comparison of the effects of surface and bulk chemical modification and beating of pulp on paper properties. *Nord Pulp Paper Res*, 18(3): 325–332.

Laine, J. and Stenius, P. (1997). Effect of charge on the fibre and paper properties of bleached industrial kraft pulps. *Pap Puu-Pap Tim*, **79**(4): 257–266.

Larsson, P. T., Hult, E.-L., Wickholm, K., Pettersson, E., and Iversen, T. (1999). Cp/mas 13c-nmr spectroscopry applied to structure and interaction studies on cellulose I. *Solid State Nucl Magn Reson*, **15**: 31–40.

Lawoko, M., Berggren, R., Berthold, F., Henriksson, G., and Gellerstedt, G. (2004). Changes in thelignin-carbohydrate complex in softwood kraft pulp during kraft and oxygen delignification. *Holzforschung*, **58**(6): 603–610.

Lawoko, M., Henriksson, G., and Gellerstedt, G. (2005). Structural differences between the lignin-carbohydrate complexes present in wood and in chemical pulps. *Biomacromol*, **6**: 3467–3473.

Lawoko, M., Henriksson, G., and Gellerstedt, G. (2006). Characterisation of lignin-carbohydrate complexes (lccs) of spruce wood (picea adies l.) isolated with two methods. *Holzforschung*, **60**: 156–161.

Leary, G. J., Sawtell, D. A., and Wong, H. (1983). The formation of model lignin-carbohydrate compounds in aqueous solutions. *Holzforschung*, **37**(1): 11–16.

Leeflang, B. R., van Kuik, J. A., and Kroon-Bratenburg, L. K. J. (2006). Oligosaccharides and cellulose crystal surfaces: computer simulations. In *NMR spectroscopy and computer modelling of carbohydrates (J. F. G. Vliegenthart, R. J. Woods, ed.)* ACS Symposium Series 930, pages 133–155.

Leopold, B. and McIntosh, D. C. (1961). Chemical composition and physical properties of wood fibers. III. Tensile strength of individual fibers from alkali extracted loblolly pine holocellulose. *Tappi J*, **44**(3): 235–240.

Liang, C. and Marchessault, R. (1959). Infrared spectra of crystalline polysaccharides. I. Hydrogren bonds in native cellulose. *J Polym Sci*, **37**:385–395.

Liang, C. Y., Bassett, K. H., McGinnes, E. A., and Marchessault, R. H. (1960). Infrared spectry of crystalling polysacchrides. VII. Thin wood sections. *Tappi J*, **43**: 1017–1024.

Liitiä, T., Maunu, L. S., Hortling, B., Tamminen, T., Pekkala, O., and Varhimo, A. (2003). Cellulose crystallinity and ordering of hemicelluloses in pine and birch pulps as revealed by solid-state nmr spectroscopic methods. *Cellulose*, **10**(4): 307–316.

Lima, D. U., Oliveira, R. C., and Buckeridge, M. S. (2003). Seed storage hemicelluloses as wet-end additives in papermaking. *Carbohydr Polym*, **52**(4): 367–373.

Lin, S. Y. (1992). *Methods in lignin chemistry*. Springer Series in Wood Science.

Linder, Å., Bergmann, R., Bodin, A., and Gatenholm, P. (2003). Mechanism of assenbly of xylan onto cellulose surfaces. *Langmuir*, **19**(12): 5072–5077.

Linder, A. and Gatenholm, P. (2004). Effect of cellulose substrate on assembly of xylans. In Gatenholm, P. and Tenkanen, M., editors, *Hemicelluloses: Science and Technology.* ACS Symposium, 864, pages 236–253.

Lindström, T. (1989). Some fundamental chemical aspects on paper forming. In *Fundamentals in Papermaking, Cambridge 1989, Trans. 9th Fund. Res. Symp. Cambridge, 1989*, volume 1, pages 311–412.

Lindström, T. and Carlsson, G. (1982a). The effect of carboxyl groups and their ionic form during drying on the hornification of cellulose fibers. *Svensk Papperstidn*, **85**(15): R146–R151.

Lindström, T. and Carlsson, G. (1982b). The effect of chemical environment on fiber swelling. *Svensk Papperstidn*, **85**(3): R14–R20.

Lindström, T., Wågberg, L., and Larsson, T. (2005). On the nature of joint strength in paper - a review of dry and wet strength resins used in paper manufacturing. In *Advances in Paper Science and*

Technology Transaction of the 13th Fundamental Research Symposium, (I'Anson, S.J., ed.), pp. 457–562. The Pulp and Paper Fundamental Research Society, Cambridge (UK).

Lisboa, S. A., Evtuguin, D. V., Pascoal Neto, C., and Goodfellow, B. J. (2005). Isolation and structural characterization of polysaccharides dissolved in *Eucalyptus globulus* kraft black liquors. *Carbohydr Polym*, **60**(1): 77–85.

Lorbach, C., Gregorova, W. J. W. J. F., Hirn., U., and Bauer, W. (2014). Pulp fiber bending stiffness in wet and dry state measured from moment of inertia and modulus of elasticity. *Bioresources*, 9(5): 5511–5528.

Luce, J. E. (1964). Radial distribution of properties through the cell wall. *Pulp Pap Mag Can*, **65**(10): T419–T423.

Lundquist, K., Simonson, R., and Tingsvik, K. (1980). Studies on lignin carbohydrate linkages in milled wood lignin preparations. *Svensk Papperstidn*, **83**(16): 452–454.

Marchessault, R., Settineri, W., and Winter, W. (1967). Crystallization of xylan in the presence of cellulose. *Tappi J*, **50**(2):55–59.

Marchessault, R. H. and Sarko, A. (1967). X-ray structure of polysaccharides. *Adv Carbohydr Chem*, **22**: 421–482.

Mayhood, C. H., Kallmes, O. J., and Cauley, M. (1962). The mechanical properteis of paper part II. Measured shear strength of individual fiber to fiber contacts. *Tappi J*, 45(1): 69–73.

Mazeau, K. and Charlier, L. (2012). The molecular basis of the adsorption of xylans on cellulose surface. *Cellulose*, **19**: 337–349.

McIntosh, D. C. (1963). Tensile and bonding strengths of loblolly pine kraft fibers cooked to different yields. *Tappi J*, **46**(5): 273–277.

Meier, H. (1962). On the behaviour of wood hemicelluloses under different pulping conditions. Part 2. Spruce hemicellulose. *Svensk Papperstidn*, **65**(16): 589–594.

Meier, H. and Welck, A. (1965). Über den Ordnungszustand der Hemicellulose in den Zellwänden. *Svensk Papperstidn*, **68**: 878–881.

Meier, H. and Wilkie, K. C. B. (1959). The distribution of polysaccharides in the cell wall of tracheids of pine (Pinus silvestris L.). *Holzforschung*, **13**(6): 177–182.

Meller, A. (1965). The retake of xylan during alkaline pulping. A critical appraisal of the literature. *Holzforschung*, **19**(4): 118–125.

Michell, A. J. and Higgins, H. G. (1965). Conformation and intramolecular hydrogen bonding in glucose and xylose derivates. *Tetrahedron*, **21**: 1109–1120.

Mitikka-Eklund, M. (1996). Sorption of xylans on cellulose fibres. Licentiate thesis, Helsinki University of Technology, Helsinki, Finnland.

Mobarak, F., El-Ashawy, A. E., and Fahmy, Y. (1973). Hemicelluloses as additive in papermaking. Part 2. The role of added hemicellulose in situ on paper properties. *Cellul Chem Technol*, **7**: 325–335.

Mohan, T., Spirk, S., Kargl, R., Doliska, A., Vessel, A., Salzmann, I., Ressel, R., Ribitsch, V., and Stana-Kleinschek, K. (2012). Exploring the rearrangement of amorphous cellulose model thin films upon heat treatment. *Soft Matter*, **8**: 807–9815.

Mora, F., Ruel, K., Comtat, J., and Joseleau, J.-P. (1986). Aspects of native and redeposited xylan at the surface of cellulose microfibrills. *Holzforschung*, **40**(2): 85–91.

Moss, P. A. and Pere, J. (2006). Microscopical study on the effects of partial removal of xylan on the swelling properties of birch kraft pulp fibres. *Nord Pulp Paper Res*, **21**(1): 8–12.

Mott, L., Groom, L., and Shaler, S. (2002). Mechanical properties of individual southern pine fibers. part II. comparison of earlywood and latewood fibers with respect to tree height and juvenility. *Wood Fiber Sci*, **34**(2):221–237.

Muguet, M. C. S., Pedrazzi, C., and Colodette, J. L. (2011). Xylan deposition onto eucalypt pulp fibers during oxygen delignification. *Holzforschung*, **65**: 605–612.

Neuman, R. D., Berg, J. M., and Claesson, P. M. (1993). Direct measurement of surface forces in papermaking and paper coating systems. *Nord Pulp Paper Res*, **8**(1): 96–104.

Nečas, D. and Klapetek, P. (2012). Gwyddion: an open-source software for SPM data analysis. *Cent Eur J Phys*, 10:181–188.

Newman, R. H., Hammingson, J. A., and Suckling, I. D. (1993). Carbon-13 nuclear magnetic resonance studies of kraft pulping. *Holzforschung*, **47**(3): 234–238.

Nieduszynski, I. A. and Marchessault, R. H. (1971). Structure of β-d-(1→4')xylan hydrate. *Nature*, **232**: 46–47.

Niemi, H. and Mahlberg, H. P. P. (2002). Review: application of scanning probe microscopy to wood, fibre and paper research. *Pap Puu-Pap Tim*, 84(6): 389–406.

Nishiyama, Y., Langan, P., and Chanzy, H. (2002). Crystal structure and hydrogen-bonding system in cellulose I_β from synchroton X-ray and neutron fiber diffraction. *J Am Chem Soc*, **124**(31): 9074–9082.

Oksanen, T., Pere, J., Buchert, J., and Viikari, L. (1997). The effect of *Trichoderma reesei* cellulases and hemicellulases on the paper technical properties of never-dried bleached kraft pulp. *Cellulose*, **51**(4): 329–339.

Österberg, M., Laine, J., Stenius, P., Kumpulainen, A., and Claesson, P. M. (2001). Forces between xylan-coated surfaces: Effect of polymer charge density and background electrolyte. *J Colloid Interf Sci*, **242**: 59–66.

Östlund, Å., Köhnke, T., Nordstierna, L., and Nydén, M. (2010). NMR cryoporometry to study the fiber wall structure and the effect of drying. *Cellulose*, **17**(2): 321–328.

Paananen, A., Österberg, M., Rutland, M., Tammelin, T., Saarinen, T., Tappure, K., and Stenius, P. (2004). Interaction between cellulose and xylan: and atomic force microscope and quartz crystal microbalance study. In *Hemicelluloses: Science and Technology (P. Gatenholm, M. Tenkanen, ed.)* ACS Symposium Series 864, pages 269–290.

Paavilainen, L. (1993). Conformability – flexibility and collapsibility – of sulphate pulp fibres. *Pap Puu-Pap Tim*, **75**(9-10): 689–702.

Page, D. H. (1969). A theory for the tensile strength of paper. *Tappi J*, **52**(4): 674–681.

Page, D. H., El-Hosseiny, F., Winkler, K., and Lancaster, A. P. S. (1977). Elastic modulus of single wood pulp fibers. *Tappi J*, **60**(4): 114–117.

Persson, B. N. J., Ganser, C., Schmied, F., Teichert, C., Schennach, R., Gilli, E., and Hirn, U. (2013). Adhesion of cellulose fibers in paper. *J Phys: Condens Matter*, **25**(4): 045002.

Pettersson, S. E. and Rydholm, S. A. (1961). Hemicelluloses and paper properties of pirch pulps. Part 3. *Svensk Papperstidn*, **64**(1): 4–17.

Petzold-Welcke, K., Schwikal, K., Daus, S., and Heinze, T. (2014). Xylan derivatives and their application potential – mini-review of own results. *Carbohydr Polym*, **100**: 80–88.

Pryde, A. and Gilbert, M. T. (1979). *Application of high performance liquid chromatography*. Chapman & Hall, London, UK.

Rahman, A. and Choudhary, M. I. (1996). *Solving problems with NMR spectroscopy*. Academic Press.

Ratcliff, F. T. (1949). The possible correlation between hemicelluloses and the physical properties of bleached kraft pulps. *Tappi J*, **32**(8): 357–367.

Rauvanto, I., Pere, J., and Henricson, K. (2006). Fibre damage in unbleached reinforcement pulp – The effect of hemicelluloses and lignin on the susceptibility of fibres to damage during oxygen delignification. *Nord Pulp Paper Res*, **21**(3): 328–335.

Rebuzzi, F. and Evtuguin, D. V. (2006). Effect of glucuronoxylan on the hornification of *Eucalyptus globulus* bleached pulps. *Macromol Symp*, **232**: 121–128.

Rees, D. A. (1977). *Polysaccharide shapes*. Chapman and Hall, London.

Ren, J.-L., Peng, F., Sun, R.-C., and Kennedy, J. F. (2009). Influence of hemicellulosic derivates on the sulfate kraft pulp strength. *Carbohydr Polym*, **75**(2): 338–342.

Ribe, E. (2010). *Xylan sorption kinetics at industrial conditions*. PhD thesis, Chalmers University of Sweden, Gothenburg, Sweden.

Robyt, J. F. (1998). *Essentials of carbohydrate chemistry*. Springer-Verlag New York, Inc.

Rohm, S., Hirn, U., Ganser, C., Teichert, C., and Schennach, R. (2014). Thin cellulose films as a model system for paper fibre bonds. *Cellulose*, **21**(1): 237–249.

Ruel, K., Joseleau, J. P., Comtat, J., and Barnoud, F. (1976). Ultrastructural localization of xylans in the developing cell wall of graminae fibers by the use of an endoxylanase. *J Appl Polym Sci*, **28**: 971–981.

Russo, V. A. (1959). *Sorption studies of a modified locust bean gum on a bleached sulfite pulp*. PhD thesis, The Institute of Paper Chemistry, Allpleton, Wisconsin, USA.

Rydholm, S. A. (1965). *Pulping processes*, volume 1. New York: John Wiley & Sons, Ltd.

Saake, B., Kruse, T., and Puls, J. (2001). Investigations on molar mass, solubility and enzymatic fragmentation of xylans by multi-detected SEC chromatography. *Bioresour Technol*, **80**: 195–204.

Saarnio, J. and Gustafsson, C. (1953). On the dissolving and destruction of carbohydrates during the sulfate cook. *Pap Puu-Pap Tim*, **35**(3): 65–66,78.

Saha, B. C. and Bothast, R. J. (1999). Pretreatment and enzymatic saccharification of corn fiber. *Appl Biochem Biotechnol*, **76**: 65–77.

Saketi, P. and Kallio, P. (2011). Measuring bond strength of individual paper fibers using micro-robotics. In *Progress in Paper Physics Seminar, 2011 (U. Hirn, ed.)*, pages 199–203. Verlag der Technischen Univsersität Graz.

Sauerbrey, G. (1959). Verwendung von Schwingquarzen zur Wägung dünner Schichten und zur Mikrowägung. *Z Phys*, **155**: 206–222.

Scallan, A. M. (1974). The structure of cell wall of wood – a consequence of anisotropic inter-microfibrillar bonding? *Wood Sci*, **6**(3): 266–271.

Schmied, F. J., Teichert, C., Kappel, L., Hirn, U., and Schennach, R. (2012). Analysis of precipitated lignin on kraft pulp fibers using atomic force microscopy. *Cellulose*, **19**(3): 1013–1021.

Schniewind, A. P., Nemeth, L. J., and Brink, D. L. (1964). Fiber and pulp properties. I. shear strength of single fiber crossings. *Tappi J*, 47(4): 244–248.

Schönberg, C., Oksanen, T., Suurnäkki, A., Kettunen, H., and Buchert, J. (2001). The importance of xylan for the strength properties of spruce kraft pulp fibres. *Holzforschung*, **55**(6): 639–644.

Schwikal, K., Heinze, T., Saake, B., Puls, J., Kaya, A., and Esker, A. R. (2011). Properties of spruce sulfite pulp and birch kraft pulp after sorption of cationic birch xylan. *Cellulose*, **18**: 727–737.

Siegbahn, K., Nordling, C., Fahlman, A., Nordberg, R., Hamrin, K., Hedman, J., Johansson, G., Bergmark, T., Karlson, S., Lindgren, I., and Lindberg, B. (1967). ESCA [Electron Spectroscopy for Chemical Analysis]. Atomic, molecular, and solid state structure studied by means of electron spectroscopy. *Nova Acta Regiae Societatis Scientiarum Upsaliensis*, 20: 1–282.

Silva, T. C. F., Colodette, J. L., Lucia, L. A., de Oliveira, R. C., Oliveira, F. N., and Silva, L. H. M. (2011). Adsorption of chemically modified xylans on eucalyptus pulp and its effect on the pulp physical properties. *Ind Eng Chem Res*, **50**: 1138–1145.

Simão, J. P. F., Egas, A. P. V., Baptista, C. M. S. G., and Carvalho, M. G. (2005a). Evolution of methylglucuronic and hexenuronic acid contents of *Eucalyptus globulus* pulp during kraft delignification. *Ind Eng Chem Res*, **44**(9): 2997–3002.

Simão, J. P. F., Egas, A. P. V., Baptista, C. M. S. G., and Carvalho, M. G. (2005b). Heterogeneous kinetic model for the methylglucuronic and hexenuronic acid reactions during kraft pulping of *Eucalyptus globulus*. *Ind Eng Chem Res*, **44**(9): 2997–3002.

Simonson, R. (1963). The hemicellulose in the sulfate pulping process. Part 1. The isolation of hemicellulose fractions from pine sulfate cooking liquors. *Svensk Papperstidn*, **66**(20): 839–845.

Simonson, R. (1965). The hemicellulose in sulfate pulping process. Part 3. The isolation of hemicellulose fractions from birch sulfate cooking liquors. *Svensk Papperstidn*, **68**(8): 275–280.

Simonson, R. (1971a). The hemicellulose in sulfate pulping process. *Svensk Papperstidn*, **74**(21): 691–700.

Simonson, R. (1971b). Sorption of hemicellulose-lignin compounds on cotton. *Svensk Papperstidn*, **74**(17): 519–520.

Sinha, S., Sirota, E., Garoff, S., and Stanley, H. (1988). X-ray and neutron scattering from rough surfaces. *Phys Rev B*, 38:2297–2311.

Sixta, H. (2006). *Handbook of pulp*, volume 1. Wiley-VCH.

Sixta, H., Schelosky, N., Milacher, W., Baldinger, T., and Röder, T. (2001). Characterization of alkalisoluble pulp fractions by chromatography. In *proc. 11th International Symposium on Wood and Pulping Chemistry*, pages 655–658, Nice, France.

Sjöberg, J., Kleen, M., Dahlman, O., Agnemo, R., and Sundvall, H. (2004). Fiber surface composition and its relations to papermaking properties of soda-anthraquinone and kraft pulps. *Nord Pulp Paper Res*, **19**(3): 392–396.

Sjöström, E. (1977). The behavior of wood polysaccharides during alkaline pulping processes. *Tappi J*, **60**(9): 151–154.

Sjöström, E. (1989). The origin of charge on cellulose fibers. *Nord Pulp Paper Res*, **4**: 90–93.

Sjöström, E. (1993). *Wood chemistry: fundamentals and applications*. Academic Press, Inc., San Diego, 2nd edition.

Sjöström, E. and Enström, B. (1967). Characterization of acidic polysaccharides isolated from different pulps. *Tappi J*, **50**(1): 32–36.

Smook, G. A. (1982). *Handbook for pulp & paper technologies*.

Spiegelberg, H. L. (1966). The effect of hemicelluloses on the mechanical properties of individual pulp fibers. *Tappi J*, **49**(9): 388–396.

Stone, J. E. and Scallan, A. M. (1967). The effect of component removal upon the porous structure of the cell wall of wood. II. Swelling in water and the fiber saturation point. *Tappi J*, **50**(10): 496–501.

Stone, J. E. and Scallan, A. M. (1968). The effect of component removal upon the porous structure of the cell wall of wood. Part III. A comparison between the sulphite and kraft processes. *Pulp Pap Mag Can*, **69**(6): T288–T293.

Stothers, J. (1972). *Organic chemistry. A series of monographs. Carbon-13 NMR spectroscopy*, volume 24. Academic Press.

Ström, G., Barla, P., and Stenius, P. (1982). The effect of pine xylan on the use of some polycations as retention and drainage aids. *Svensk Papperstidn*, **85**(12): R100–R106.

Sullivan, J. D. (1968). Wood cellulose protofibrils. *Tappi J*, **51**: 501–507.

Surewicz, W. (1962). The sorption of organic components from cooking liquor by cellulose fibers; Its relation to the "dangerous cooking crest" in alkaline pulping (I). *Tappi J*, **45**(7): 570–578.

Suumäkki, A., Heijensson, A., Buchert, J., Westermark, U., and Viikari, L. (1995). Characterization of kraft pulp fibers by mechanical and enymatic peeling. In *8th Int Symp on Wood and Pulping Chem, Helsinki, 1995, Vol III*, pages 237–242.

Suurnäkki, A., Oskanen, T., Kettunen, H., and Buchert, J. (2003). The effect of mannan on physical properties of ECF bleached softwood kraft fibre handsheets. *Nord Pulp Paper Res*, **18**(4): 429–435.

Takahashi, N. and Koshijima, T. (1988a). Ester linkages between lignin and glucuronoxylan in a lignin-carbohydrate complex from beech (*Fagus crenata*) wood. *Wood Sci Technol*, **22**: 231–241.

Takahashi, N. and Koshijima, T. (1988b). Molecular properties of lignin-carbohydrate complexes from beech (*Fagus crenata*) and pine (*Pinus densiflora*) wood. *Wood Sci Technol*, **22**: 177–189.

Tammelin, T., Paananen, A., and "Osterberg, M. (2009). Hemicelluloses at interfaces: some aspects on the interactions. In *The nanoscience and technology of renewable biomaterials (L. A. Lucia, O. J. Rojas, ed.)* Wiley-Blackwell, pages 149–172.

Teichert, C. (2002). Self-organization of nanostructures in semiconductor heteroepitaxy. *Phys Rep*, 365:335–342.

Teleman, A., Harjunpää, V., Tenkanen, M., Buchert, J., Hausalo, T., Drakenberg, T., and Vuorinen, T. (1995). Characterisation of 4-deoxy-β-l-*threo*-hex-4-enopyranosyluronic acid attached to xylan pine kraft pulp and pulping liquor by ^{1}H and ^{13}C NMR spectroscopy. *Carbohydr Res*, **272**: 55–71.

Teleman, A., Larsson, P. T., and Iversen, T. (2001). On the accessibility and structure of xylan in birch kraft pulp. *Cellulose*, **8**(3): 209–215.

Teleman, A., Nordström, M., Tenkanen, M., Jacobs, A., and Dahlman, O. (2003). Isolation and characterisation of o-acetylated glucomannans from aspen and birch wood. *Carbohydr Res*, **338**: 525–534.

Tenkanen, M., Kroon, J., Gilli, G., Larsson, T., and Biely, P. (2000). *The strength of wood fibres. Association between hemicellulose and cellulose at the molecular level*. Final report FAIR CT96-1624.

Terayama, H. (1952). Method of colloid titration (a new titration between polymer ions). *J Polym Sci*, **8**(2): 243–253.

Thygesen, A., Oddershede, J., Lilholt, H., Thomson, A. B., and Ståhl, K. (2005). On the determination of crystallinity and cellulose content in plant fibres. *Cellulose*, **12**(6): 563–576.

Torgnysdotter, A., Kulachenko, A., Gradin, P., and Wågberg, L. (2007). The link between the fiber contact zone and the physical properties of paper. A way to control paper properties. *J Compos Mater*, **41**(13): 1619–1633.

Torgnysdotter, A. and Wågberg, L. (2003). Study of the joint strength between regenerated cellulose fibres and its influence on the sheet strength. *Nord Pulp Paper Res*, **18**(4): 455–459.

Uhlin, K. I., Atalla, R. H., and Thompson, N. S. (1995). Influence of hemicelluloses on the aggregation ppattern of bacterial cellulose. *Cellulose*, **2**(2): 129–144.

Voinova, M. V., Rodahl, M., Jonson, M., and Kasemo, B. (1999). Viscoelastic acoustic response of lalayer polymer films at fluid-solid interfaces: continuum mechanics appraoach. *Phys Scripta*, **59**: 391–396.

Wakelin, J. H., Virgin, H. S., and Crystal, E. (1959). Development and comparison of two X-ray methods determining the crystallinity of cotton cellulose. *J Appl Phys*, **30**(11): 1654–1662.

Walker, E. F. (1965). Effects of the uronic acid carboxyls on the sorption of 4-*o*-methylglucuronoarabinoxylans and their influence on papermaking properties of cellulose fibers. *Tappi J*, **48**(5): 298–303.

Wang, X., Maloney, T. C., and Paulapuro, H. (2003). Internal fibrillation in never-dried and once-dried chemical pulps. *Appita J*, **56**(6): 455–459.

Weber, F. (2014). *Viscose fibres – a model system to investigate the influence of charges on the properties of handsheets and fibre-fibre joints*. PhD thesis, Graz University of Technology, Graz, Austria.

Weber, F., Koller, G., Schennach, R., Bernt, I., and Eckhart, R. (2013). The surface charge of regenerated cellulose fibres. *Cellulose*, pages 1–11.

Weise, U. and Paulapuro, H. (1999). Effect of drying and reswelling cycles on fibre swelling. *J Pulp Pap Sci*, **25**(5): 163–166.

Westbye, P., Köhnke, T., Glasser, W., and Gatenholm, P. (2007). The influence of lignin on the self-assembly behaviour of xylan rich fractions from birch (*Betula pendula*). *Cellulose*, **14**: 603–613.

Wigell, A., Brelid, H., and Theliander, H. (2007). Degradation/dissolution of softwood hemicelluloses during alkaline cooking after different temperatures and alkali concentrations. *Nord Pulp Paper Res*, **22**(4): 488–494.

Wikström, R. (1967). An investigation of the acidic precipitation of xylan from an alkaline extract of birch wood. *Svensk Papperstidn*, **70**(23): 819–821.

Wilke, C. R. and Chang, P. (1955). Correlation of diffusion ceufficients in dilute solutions. *Amer Inst Chem Eng J*, 1(2): 264–270.

Winter, H., Barakat, A., Cathala, B., and Saake, B. (2006). Preparation of arabinoxylan and its sorption on barcterial cellulose during cultivation. *Macromol Symp*, 232: 74–84.

Winter, L., Wågberg, L., Ödberg, L., and Lindström, T. (1986). Polyelectrolytes adsorbed on the surface of cellulosic materials. *J Colloid Interf Sci*, **111**: 537–543.

Yllner, S. and Enström, B. (1956). Studies of the adsorption of xylan on cellulose fibres during the sulphate cook. Part I. *Svensk Papperstidn*, **59**(6): 229–232.

Yllner, S. and Enström, B. (1957). Studies of the adsorption of xylan on cellulose fibres during the sulphate cook. Part 2. *Svensk Papperstidn*, **60**(15): 549–554.

Yundt, A. P. (1951). Crystalline hemicelluloses. II. Crystalline xylan from paper birch. *Tappi J*, **34**(2): 91–92.

Zankel, A., Kraus, B., Poelt, P., Schaffer, M., and Ingolic, E. (2009). Ultramicrotomy in the ESEM, a versatile method for materials and life science. *J Microsc*, 233(1): 144–148.

Zhao, Y., Wang, G., and Lu, T. (2001). *Characterization of amorphous and crystalline rough surface: principles and applications*. Academic Press, San Diego.

Appendix

A High pressure liquid chromatography

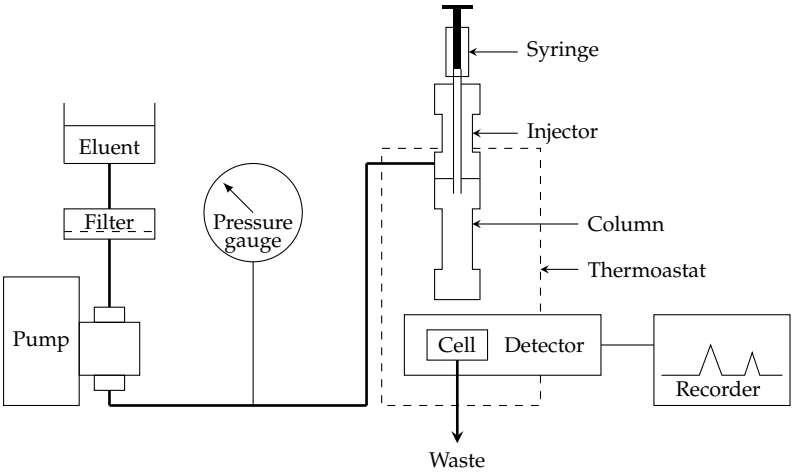

Figure A.1 Components of a HPLC (adopted from Pryde and Gilbert 1979).

The components of a HPLC are depicted in Figure A.1. The column capacity ratio k', indicating the solute retention, is measuring the ratio of the time spent by the solute in the stationary phase to the time spent in the mobile phase and can be calculated from (Pryde and Gilbert 1979)

$$k' = \frac{t_r - t_0}{t_0} \tag{A.1}$$

where t_r is the retention time of the given peak and t_0 is the retention time of the unretained (or solvent) peak at constant flow rates.

The number of theoretical plates N to which the column is equivalent is identifying the efficiency of a chromatography by measuring the amount of spreading of a solute as it travels down the column and given by (Pryde and Gilbert 1979)

$$N = 16 \left(\frac{t_\mathrm{r}}{W} \right)^2 \tag{A.2}$$

or

$$N = 5.54 \left(\frac{t_\mathrm{r}}{W_\mathrm{HH}} \right)^2 \tag{A.2}$$

where W is the base width of the peak which is extrapolated of the tangents at the points of inflection to the baseline and W_HH is the width of the peak at half height. A high value of N characterizes an efficient system.

The plate height H or the height equivalent to a theoretical plate is calculated from (Pryde and Gilbert 1979)

$$H = \frac{L}{N} \tag{A.3}$$

where L is the length of the column. Further, H depends on the mean particle size d_p and varies with the linear velocity of the eluent u (Pryde and Gilbert 1979)

$$u = \frac{L}{t_0}\,. \tag{A.4}$$

To reduce the plate height and fluid velocity as well as to overcome the dependence of H on d_p it is favorable to calculate the dimensionless parameter h and ν (Pryde and Gilbert 1979), where

$$h = \frac{H}{d_\mathrm{p}} \tag{A.4}$$

and

$$\nu = \frac{u\,d_\mathrm{p}}{D_\mathrm{m}} \tag{A.4}$$

with the diffusion coefficient of the solute in the mobile phase D_m which is estimated form the Wilke-Chang equation (Wilke and Chang 1955). The value of h gives a ratio of the plate height to the particle size and the ν value measures the ratio of the rate of diffusion of the solute within the particle to the rate of flow outside the particle. An improved relation between h and ν is given by (Knox and Pryde 1975)

$$h = \frac{B}{\nu} + A\,\nu^{0.33} + C\,\nu \tag{A.5}$$

where the term A represents the goodness of packing of the column, with $A < 1$ in the best case, B reflects axial diffusion geometry, with $B \sim 2$, and C determines the efficiency of mass transfer, with typical values between 0.05...0.1.

The column resistance parameter ϕ' measures the resistance to the eluent flow which is caused by the column and can be calculated from (Pryde and Gilbert 1979)

$$\phi' = \frac{\Delta P\,d_\mathrm{p}^2}{u\,\eta\,L} \tag{A.6}$$

where ΔP is the pressure drop down the column and η is the eluent viscosity.

Finally, the separation is determined by the resolution R_s of two chromatographic peaks and calculated from (Pryde and Gilbert 1979)

$$R_\mathrm{s} = 2\,\frac{t_2 - t_1}{W_1 + W_2} \tag{A.7}$$

where t_1 and t_2 are the distances of retention and W_1 and W_2 the peak base widths of peaks 1 and 2. By putting Equation A.1 and A.2 into A.7 a general equation may be derived which relates to the column selectivity $\alpha = k'_2/k'_1$ by (Pryde and Gilbert 1979)

$$R_s = \frac{1}{4}\frac{(\alpha - 1)}{\alpha} \cdot \frac{k'_2}{1 + k'_2} \cdot \sqrt{N} \,. \tag{A.8}$$

The three factors can be optimized by changing the temperature, the nature of the stationary and mobile phases, by increasing the column length, decreasing the mean particle size or working closer to the minimum in the plate height curve (Huber 1974; Pryde and Gilbert 1979).

B Nuclear magnetic resonance spectroscopy

Certain nuclei, such as ^{1}H, ^{2}H, ^{13}C, ^{15}N, and ^{19}F, feature a spin angular momentum, a corresponding magnetic momentum μ is given by (Rahman and Choudhary 1996)

$$\mu = \frac{\gamma h [I(I+1)]^{1/2}}{2\pi} \tag{B.1}$$

where h is Planck's constant, γ is the magnetogyric ratio, and I is the spin quantum. In a magnetic field B_0 along the z-axis, the nuclei adopt one of $(2I+1)$ quantized orientations which corresponds to a certain energy level (Rahman and Choudhary 1996)

$$E = -\mu_z B_0 = \frac{m_1 \gamma h B_0}{2\pi} \tag{B.2}$$

where m_1 is the magnetic quantum number of the nucleus. ^{1}H and ^{13}C nuclei have the advantage, that they have an I of $1/2$ and only two quantized orientations are allowed. The alignment can be either parallel (lower energy orientation) or antiparallel (higher energy orientation) to the external B_0. Adsorption of Rf radiation of the correct frequency can result in transitions from the lower energy level to the higher energy level. This energy difference ΔE is proportional to B_0 and defined by (Rahman and Choudhary 1996)

$$\Delta E = \frac{\gamma h B_0}{2\pi} \tag{B.3}$$

and corresponds to (Rahman and Choudhary 1996)

$$v_0 = \frac{\gamma B_0}{2\pi}\,. \tag{B.4}$$

Without applying a magnetic field, the nucleus is spinning on its axis. An external magnetic field provokes a characteristic wobbling motion (*precession*) of the nucleus. When applying a Rf field in a direction perpendicular to the external B_0 and at a frequency that exactly matches the precessional frequency (*Larmor* frequency) of the nucleus, adsorption of energy will occur. This forces the nucleus suddenly to go to the higher energy state, where the magnetic moment is aligned in the opposite direction of the external magnetic field. Afterwards, it can relax back to the lower energy level through *spin–lattice relaxation*, or by *spin–spin relaxation*. In the first case, the energy is transferred to the assembly of surrounding molecules (*lattice*), while the latter involves transfer of energy to the neighboring nucleus. The relaxation causes a change in the impedance of the oscillator coils. The transition between excitation and relaxation establishes an equilibrium state after a certain amount of time. This is measured as a signal (*free induction decay)*

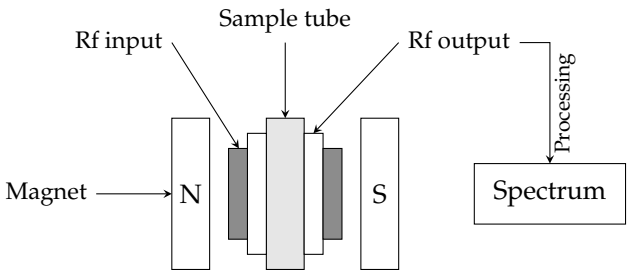

Figure B.1 Illustration of the principle set-up of a NMR spectrometer, adopted from Stothers (1972).

and converted into the *frequency* domain by Fourier transformation to the conventional NMR spectrum. No NMR signal would be measured, if the amount of nuclei in the upper and lower energy level were equal, since no energy difference between the two magnetogyric states of the nucleus would exist. However, at equilibrium a slight difference in the populations (*Boltzmann excess*) between the lower energy state and the upper energy state is causing a NMR signal. The principle set-up of a NRM spectrometer is illustrated in Figure B.1.

C Infrared spectroscopy

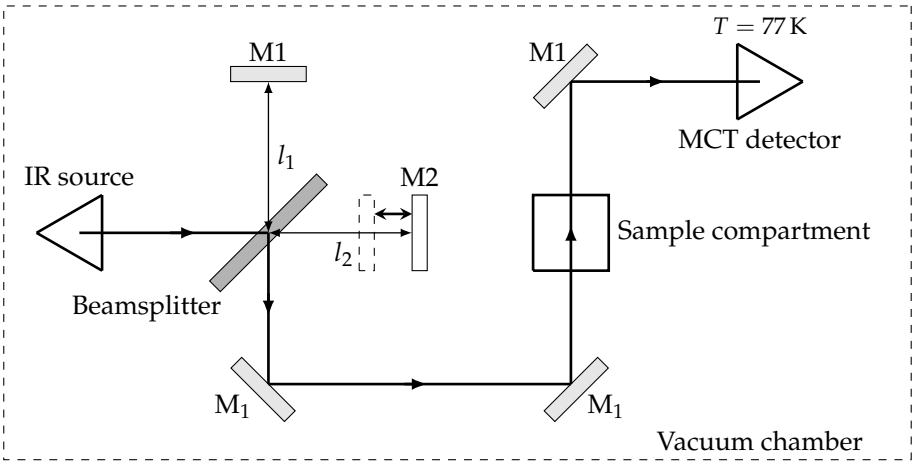

Figure C.1 Schematic diagramm of a Michelson interferometer. M_1 = fixed mirror, M_2 = translation mirror.

The interferometer consists mainly of a beam splitter, some fixed mirrors (M_1), a movable mirror (M_2), and is placed in a vacuum chamber at a pressure of about 2 mbar during operation. Half of the IR beam, from a SiC-globar, is getting reflected at the beam splitter (KBr coated with Ge) and the other half is able to pass through. The reflected light is getting again reflected at M_1 in direction to the beam splitter. The light which could pass through the beam splitter is getting reflected at M_2. Since the position of M_2 is not fixed, the distances l_1 between the beam splitter and M_1 as well as between the beam splitter and M_2 (l_2) are different. This results in spatially coherent and interfering beams, when recombined. In the sample compartment, the partial beams being adsorbed by the substrate, resulting in characteristic vibrational excitations of the bonds in the sample, e.g. C−C, C−OH, or C=O. Then, the beam is focused on the mercury cadmium telluride ($Hg_{(1-x)}Cd_xTe$) detector. In the mid-wave IR only a very small amount of excitation energy is necessary. In order to sense this small amount of energy, the detector needs to be cooled with liquid nitrogen ($T = 77$ K). Otherwise, electrons can be lifted to a higher energy level by thermal agitation of the solid resulting in a larger noise ratio of the signal (Griffiths and de Haseth 1986).

During the measurement of a FTIR spectrum, an interferogram of a reference sample is measured and transformed by FT to the so-called single channel reference spectrum $R(\nu)$. In a next step, the same procedure is done with the sample obtaining the so-called single channel sample spectrum $S(\nu)$. The final transmittance spectrum $T(\nu)$ can be calculated from (Herres and Gronholz 1984)

$$T(\nu) = \frac{S(\nu)}{R(\nu)}\,. \tag{C.1}$$

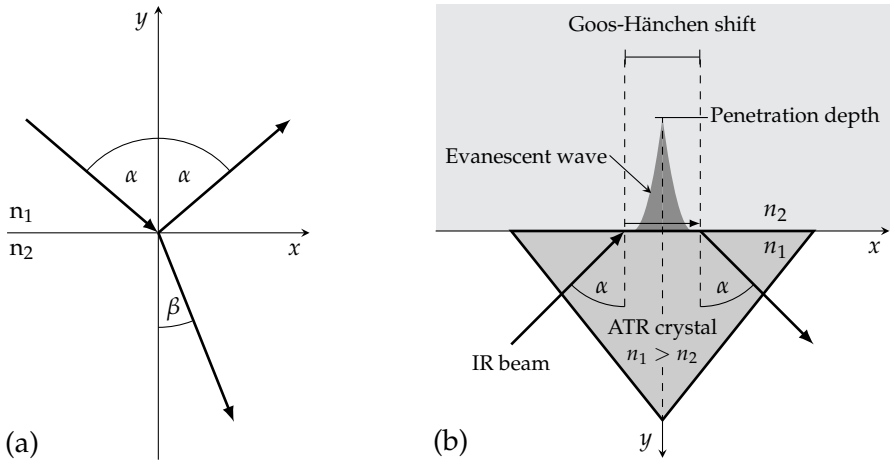

Figure C.2 Principle of ATR measurement: (a) Reflection of a light beam at an interface, replotted from (Bergman and Schaefer 2004); (b) The path of the IR beam.

Attenuated total reflection spectroscopy

Figure C.2a depicts the reflection and transmission of a light beam impinging with the angle α at an interface between two media with different optic densities.

When a light beam is impinging from a medium with a refractive index n_1 entering into a medium with a lower refractive index n_2, the following equation holds (Demtröder 2013)

$$\sin\alpha = \frac{n_2}{n_1} \cdot \sin\beta \tag{C.2}$$

due to the Snell's law for the angle α. Because $\sin\beta$ cannot be > 1, the following expression has to be valid for the angle α to enter into medium 2 (Demtröder 2013)

$$\sin\alpha \leq \frac{n_2}{n_1}\,. \tag{C.3}$$

All of the light beam will be reflected at the interface, when $\sin\alpha > n_2/n_1$. The so-called *critical angle* of the total reflection is given by (Demtröder 2013)

$$\sin\alpha_c = \frac{n_2}{n_1} \tag{C.4}$$

for $\alpha > \alpha_c$ and $n_1 > n_2$. When the light beam is approaching the interface of a medium with a lower refractive index ($n_1 > n_2$), the amplitude does not immediately decline down to zero, due to the $\alpha_{\text{incident}} > \alpha_{\text{critical}}$. This is illustrated in Figure C.2b. The light wave is rather entering into the medium and exponentially declining, also known as *evanescent wave*, while the energy of the wave travels parallel to the surface of the medium until the evanescent wave is reflected and entering again into the medium with the higher refractive index. This results in a lateral displacement in wave direction, the so-called *Goos-Hänchen shift* (Goos and Hänchen

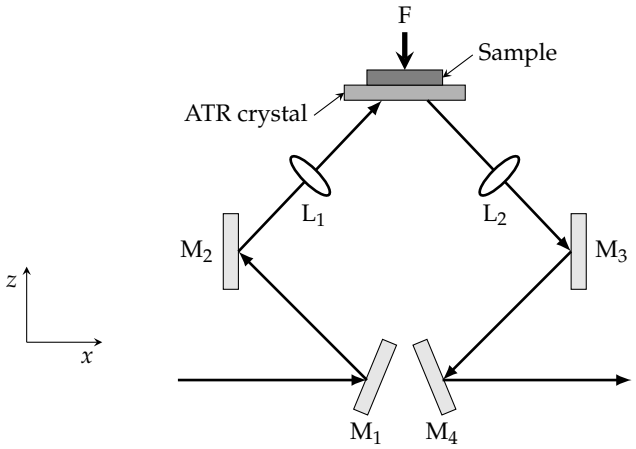

Figure C.3 Schematic view of the direction of the IR beam in the Specac MKII Golden Gate Single Reflection ATR unit. $M_{1...4}$ = mirrors and $L_{1...2}$ = lenses.

1947). The reversal point of the evanescent wave is also the penetration depth d of the wave into the medium and can be calculated from (Griffiths and de Haseth 1986)

$$d = \frac{\lambda}{2\pi n_1 \left(\sin^2 \alpha - n_{21}^2\right)^{1/2}} \tag{C.5}$$

where λ is the wavelength, n_1 is the refractive index of the ATR crystal, α is the incident angle of the IR beam, and $n_{21} = n_2/n_1$ where n_2 is the refractive index of the sample. A schematic view of the direction of the IR beam in the ATR unit is shown in Figure C.3

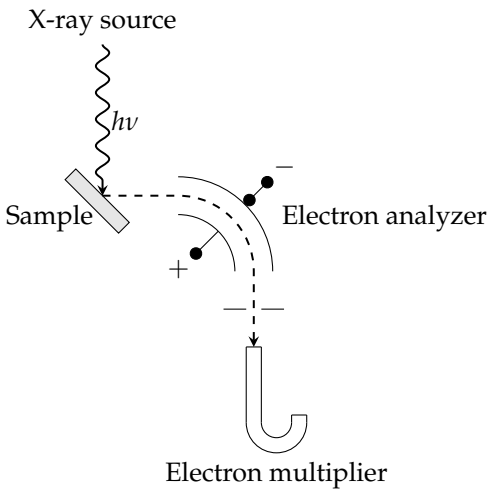

Figure D.1 Schematic arrangement of a XPS system (Ertl and Küppers 1974).

D X-ray photoelectron spectroscopy

The main components of a XPS device are the X-ray source, the electron energy analyzer, and a system for the detection of the electron energy. A schematic diagram is illustrated in Figure D.1 (Ertl and Küppers 1974). X-ray tubes are most commonly used as a light source, which are vacuum tubes that use a high voltage to accelerate the electrons and emit monochromatic X-ray photons at a high velocity. The characteristic radiation is provided by a Al or Mg anode which can be also combined (switchable twin-anode) to separate fixed energies of photoemitted electrons or Auger electrons. A main disadvantage of such sources is the limited resolution in energy due to the inherent energy width of the lines. Thus, the excitation energy has to be narrowed by a monochromator. As a consequence, the intensity is reduced, and therefore a multichannel detection system is necessary.

The kinetic energy (E_{kin}) of an expelled electron from a molecular bond by a photon can be calculated from (Conners and Banerjee 1995)

$$E_{\mathrm{kin}} = h\nu - E_{\mathrm{b}} \tag{D.1}$$

where $h\nu$ is the energy of the incident photon and E_{b} the bond energy of the electron in its orbital. The binding energy can be obtained by the existence of the work function ϕ_{sp} of the detector since the electrons are extracted with respect to the vacuum level as illustrated in Figure D.2 for a metal surface. An electron absorbs the energy of the incident photon $h\nu$ at an energy level E_{b} below the total chemical potential for electrons E_{F} (*Fermi level*). By measuring E_{kin} the bond energy E_{b} is given

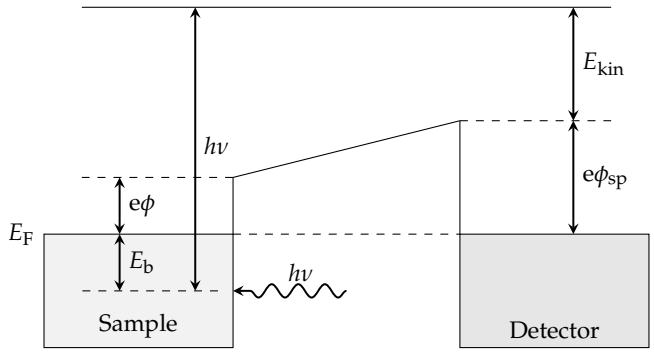

Figure D.2 Energy level diagram for XPS (Ertl and Küppers 1974).

by (Ertl and Küppers 1974)

$$E_b = h\nu - E_{kin} - \phi_{sp} \,. \tag{D.2}$$

Figure D.2 represents the energy level diagram for a metal surface, where the sample and the spectrometer are electrically connected, Fermi energies are at the same level for both of them. The value of E_F can be easily obtained by the onset of the electron emission at the highest E_{kin}. In case of semicunductors the electron emission takes place at the valence band edge and not at E_F. This results in building-up charges in paper and other insulating materials, thus shifting the energy scale, and the spectra needs to be calibrated.

The penetration depth is set by the mean free path of the emitted electrons which ranges between 0.5–10 nm for paper (Conners and Banerjee 1995). For the investigation, a high vacuum is necessary due to the low E_{kin} (0...1500 eV) of the ejected electron. Further, scattering on air molecules needs to be prevented by a clean vacuum since scattered electrons comprise the background. Hence, photoelectrons originated from the sample without a loss in E_{kin} can contribute to a peak (Conners and Banerjee 1995).

The surface analysis by XPS is based on the ionization probability of a core level which is nearly independent of the investigated element in the valence status (Ertl and Küppers 1974). Thus, the number of atoms in the obtained area is proportional to the integrated area below a certain peak (C 1s or O 1s).

E Fiber charge

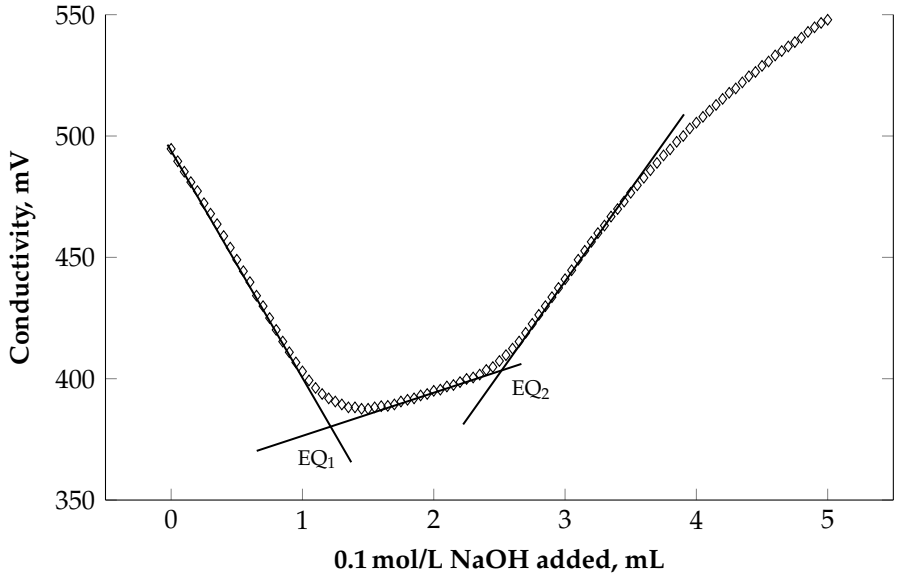

Figure E.1 Determination of the two inflections points EQ_1 and EQ_2 by the tangent method: untreated SKPB.

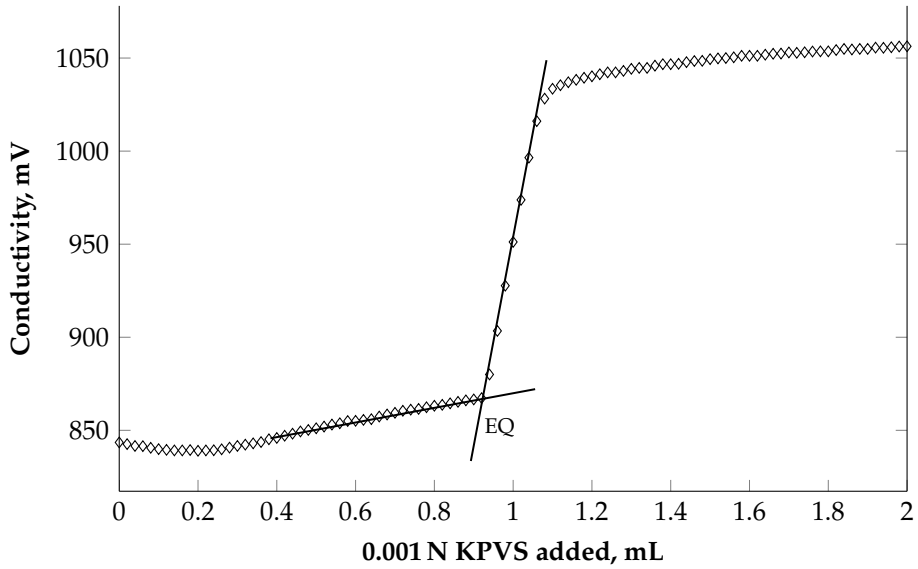

Figure E.2 Determination of the inflection points EQ by the tangent method: untreated SKPB. The KPVS had a charge density of $\xi = 1 \times 10^{-1}$ kev/g.

F QCM-D measurements

Substrate cleaning

The film preparation is was performed in accordance with Kontturi et al. (2003); Mohan et al. (2012). Before spin coating, the QCM-D Au sensors (QSX303 from LOT-Oriel, Germany) were soaked into a mixture of H_2O/H_2O_2 (30 wt%)/NH_4OH (5:1:1; v/v/v) for 10 min at 70°C. Afterwards, the sensors were immersed in a (*piranha*) solution containing H_2O_2 (30 wt%)/H_2SO_4 (1:3; v/v) for 40 s, and then rinsed with MQ-water from a Millipore water purification system (Millipore, USA, resistivity of 18.2 $\Omega^{-1}\,cm^{-1}$) and finally blow dried with N_2 gas.

Film production

A solution of TMSC (1 wt%) was obtained by first dissolution in toluene by heating to 60°C, followed by cooling down to room temperature, and afterwards filtered through a 5 µm PTFE filter. 50 µL of the TMSC solution was deposited onto the QCM sensors and rotated for 60 s at a spinning speed of 4000 rpm and an acceleration of 2500 rpm/s. The TMSC films were then transferred into pure amorphous cellulose by placing the films in a polystyrene petri-dish (5 cm in diameter) containing 3 mL of 10 wt% hydrochloric acid (HCl). The dish was covered with its cap and the TMSC films were exposed to the vapors of HCl for 15 min. The regeneration of cellulose from TMSC coated films was verified by water contact angle, and ATR-IR measurements as reported elsewhere (Kontturi et al. (2003); Mohan et al. (2012)).

QCM-D measurements

For the measurements a QCM-D device (model E4) from Q-Sense (Gothenburg, Sweden) was utilized. The resonance frequency Δf and the energy dissipation ΔD are simultaneously detected and recorded when the mass of an oscillating piezoelectric crystal changes. Changes in the mass occur due to increase/decrease in the mass of the crystal surface as a result of the addition/reduction of mass. Dissipation also refers to the frictional losses leading to damping in the oscillation depending on the viscoelastic properties of the adsorbent. For a rigid adsorbed layer which is fully coupled to the oscillating crystal, the change in the mass Δm of the crystal due to the adsorbed layer is given by the Sauerbrey equation (Sauerbrey 1959)

$$\Delta m = \frac{C}{\mathrm{n}} \Delta f_{\mathrm{n}} \tag{F.1}$$

where Δf is the observed frequency shift, C is the Sauerbrey constant which is $-17.7\,ng/Hz\,cm^2$ for a 5 MHz crystal, and n is the overtone number. For a soft

or viscoelastic film the Sauerbrey relation is not valid since the film is not fully coupled to the oscillation and energy is dissipated in the film during oscillation. The dissipation of damping D is calculated from (Dixon 2008)

$$D = \frac{E_{\text{diss}}}{2\pi E_{\text{stor}}} \tag{F.2}$$

where E_{diss} is the dissipated energy and E_{stor} is the total energy stored in the oscillator during one cycle.

The values of Δf and ΔD were used for the calculation of the adsorbed mass by viscoelastic modelling, according to the Voigt model (Höök et al. 2001; Voinova et al. 1999). The adsorbed layer was treated as a viscoelastic layer between the crystal and a semi-infinite Newtonian liquid layer. The different overtones were used to determine the adsorbed mass Γ_{QCM} which is given by (Sauerbrey 1959)

$$\Gamma_{\text{QCM}} = d\rho \tag{F.3}$$

where d is the film thickness and ρ is the density. The latter values varied between 1000–1400 kg/m^3. Moreover, the viscosity η and the elastic shear modulus μ can be calculated. The model was fitted with $\eta = 1 \times 10^{-4}$–$1 \times 10^{-1}\,\text{N s/m}^2$, $\mu = 1 \times 10^{4}$–$1 \times 10^{8}\,\text{N/m}^2$, and $d = 1 \times 10^{-10}$–$1 \times 10^{-6}\,\text{m}$. The calculations were done with the software QTools 3.0.12 (Q-Sense).

G Strength properties vs. sheet density

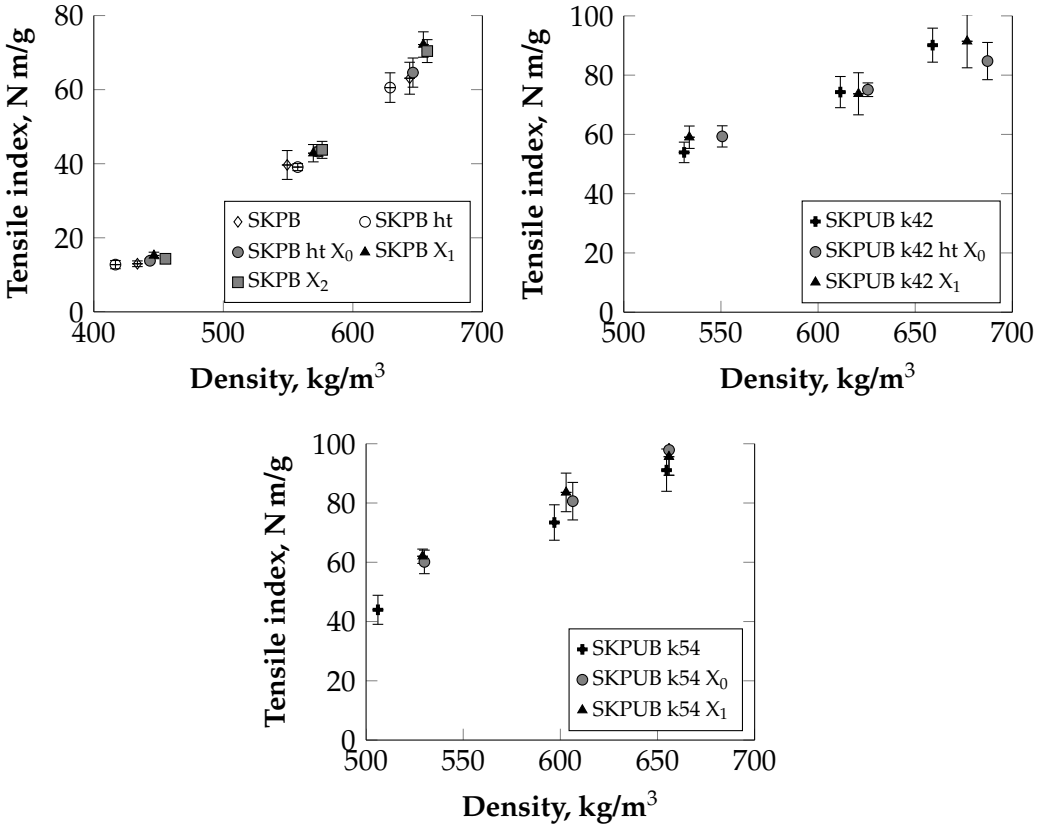

Figure G.1 Trend of the tensile index vs. the sheet density of: top left = xylan-modified and unmodified bleached softwood kraft handsheets; top right = xylan-modified and unmodified bleached sulfite handsheets; bottom left = xylan-modified and unmodified unbleached softwood kraft handsheets (Kappa 42); and bottom right = xylan-modified and unmodified unbleached softwood kraft handsheets (Kappa 54).

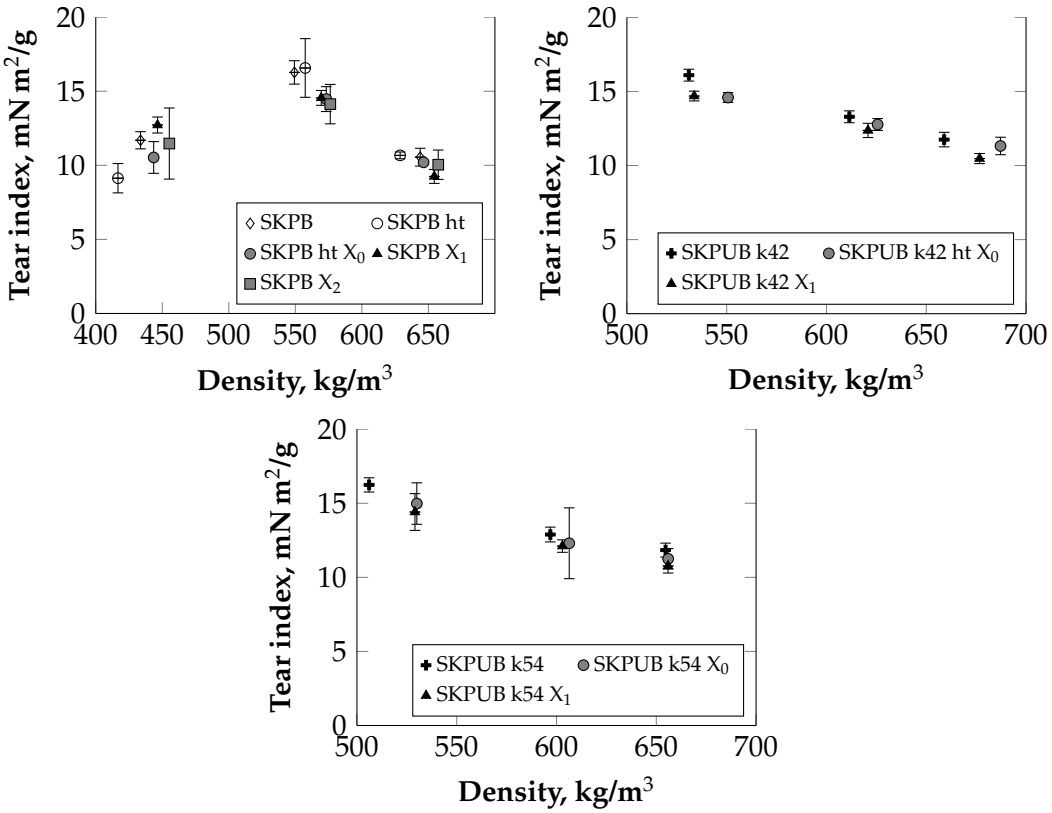

Figure G.2 Trend of the tear index vs. the sheet density of: top left = xylan-modified and unmodified bleached softwood kraft handsheets; top right = xylan-modified and unmodified bleached sulfite handsheets; bottom left = xylan-modified and unmodified unbleached softwood kraft handsheets (Kappa 42); and bottom right = xylan-modified and unmodified unbleached softwood kraft handsheets (Kappa 54).

H Fiber-fiber joint

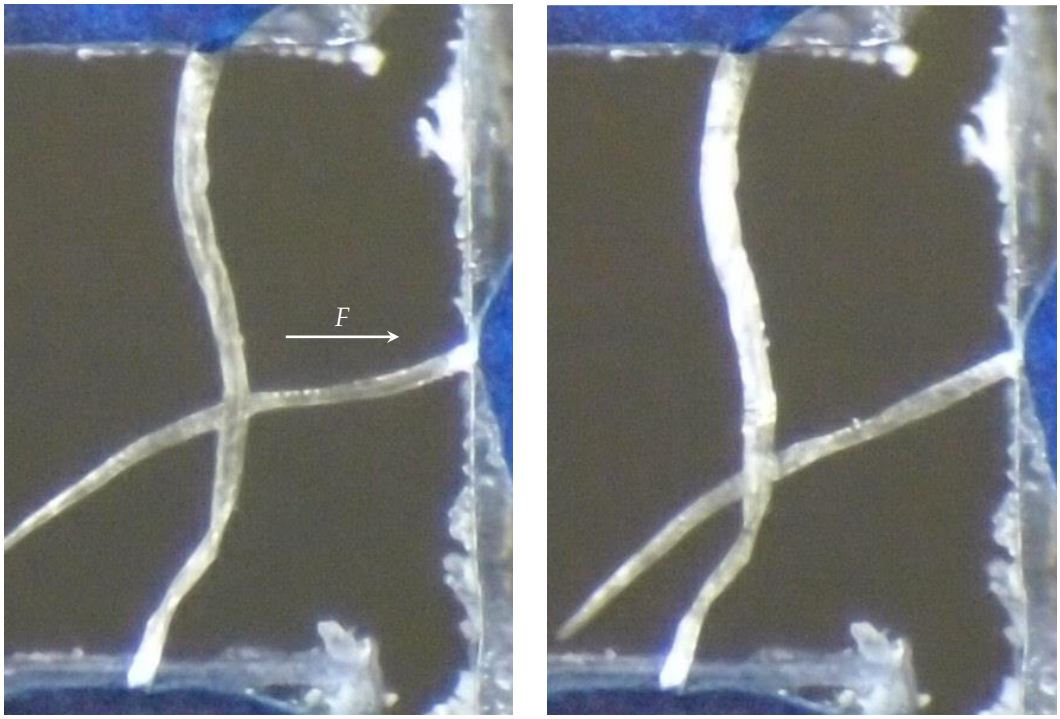

(a) FFJ during testing.

(b) FFJ after testing.

Figure H.1 Images of an individual fiber-fiber joint (a) during testing and (b) after the rupture of the bond.

List of Figures

Chapter 1: Introduction

1.1 Responsibilities within the Christian Doppler Laboratory 3

Chapter 2: Background

2.1 Structure of the cellulose chain 9
2.2 Hydrogen bonds in cellulose I and cellulose II 10
2.3 Chemical structure of a hardwood xylan chain 13
2.4 Chemical structure of a softwood xylan chain 13
2.5 Structure of barley husk xylan 14
2.6 Model of the cell wall structure of wood fibers 17
2.7 Distribution of main chemicals in the cell wall layers 18
2.8 Models of the association of the cell wall components 18
2.9 Model of the cell wall components between two cellulose fibrils 18
2.10 Model of the swelling process of the cell wall 28
2.11 Bonding mechanisms between single fibers 33
2.12 Schematic diagram of a capillary bridge between adjacent fibers 34

Chapter 3: Experimental part

3.1 Work flow of adsorption and chemical analysis 39
3.2 Schematic illustration of the interior of a SEM chamber 45
3.3 Operating mode of AFM in the (xz) plane 47
3.4 Set-up of a functionalized AFM tip 48
3.5 Principle of phase imaging 50
3.6 Principle of force mapping 51
3.7 General view of the micro bond tester 54
3.8 Fixation of an individual fiber-fiber joint on a sample holder 56
3.9 Mounting and positioning of a sample holder 57
3.10 Preloading and breaking an individual fiber-fiber joint 57
3.11 Testing the tensile strength of a single fiber 58
3.12 Elongation of a single fiber during tensile testing 60

Chapter 4: Results and Discussion

4.1 Dependence of temperature on adsorption 64
4.2 Dependence of pH on adsorption 65
4.3 Adjustment of pH for adsorption 66
4.4 Dependence of ionic strength on adsorption 66
4.5 Dependence of consistency on adsorption 67
4.6 Dependence of xylan input on adsorption 67
4.7 Retention of xylan 68
4.8 Comparison between HPLC and NMR 69
4.9 ATR spectra of pure X_1 and X_2 71
4.10 ATR spectra of SPKB handsheets with additional X_1 71
4.11 ATR spectra of SPKB handsheets with additional X_2 72
4.12 SEM images generated in the conventional mode 74
4.13 SEM images generated in the low voltage mode 77
4.14 Images of the topography of cellulose model films 79
4.15 Phase contrast images of cellulose model films using OH-tips 81
4.16 Phase contrast images of cellulose model films using CH_3-tips 81
4.17 Images of force mapping of cellulose model films 83
4.18 Rel. surface coverage on cellulose model films 84
4.19 Images of the topography of SKPB fibers 86
4.20 Images of the phase contrast of SKPB fibers 87
4.21 Images of force mapping of SKPB fibers 88
4.22 Rel. surface coverage on pulp fibers 89
4.23 Trend of the total charge 91
4.24 Adsorption isotherm of pDADMAC on SKPB fibers 92
4.25 Trend of the surface charge 93
4.26 Trend of the WRV of SKPB 94
4.27 Tensile and tear index vs refining intensity 99
4.28 Influence of xylan on tensile index 101
4.29 Influence of xylan on tear index 102
4.30 Tensile index vs. tear index of VFs 103
4.31 Tensile index vs. tear index at higher salt concentration 104
4.32 Breaking load of individual fiber-fiber joints 107
4.33 Specific bond strength of individual fiber-fiber joints 108
4.34 *E*-modulii of individual fibers from different samples 112

Appendix

A.1 Components of a HPLC (adopted from Pryde and Gilbert 1979) 130
B.1 Illustration of the principle set-up of a NMR spectrometer 134
C.1 Schematic diagramm of a Michelson interferometer 135
C.2 Principle of ATR measurement 136
C.3 Schematic view of the direction of the IR beam in the ATR unit 137

D.1 Schematic arrangement of a XPS system 138
D.2 Energy level diagram for XPS 139
E.1 Tangent method for total charge 140
E.2 Tangent method for surface charge 140
G.1 Influence of xylan on tensile index 143
G.2 Influence of xylan on tear index 144
H.1 Individual fiber-fiber joint during testing 145

List of Tables

Chapter 2: Background

2.1 Fiber dimensions of some wood species 8
2.2 Main substances of some cellulose-containing materials 8

Chapter 3: Experimental part

3.1 Molecular weight and chemical composition of the used xylans 37
3.2 Set values of the variables during adsorption 38

Chapter 4: Results and Discussion

4.1 Chemical properties of the pulp samples 63
4.2 Analysis of metals in the pulp samples 63
4.3 Binding energies and atomic concentration of handsheets (XPS) 73
4.4 Roughness analysis of fiber samples 85
4.5 Impact of xylan on beating degree and WRV 96
4.6 Chemical composition of pulp samples for paper testing 97
4.7 Chemical composition of viscose fibers for paper testing 98
4.8 Chemical composition of tested individual fibers 105
4.9 Statistical analysis of the fiber-fiber joints 106
4.10 Correlation between OBA and bond strength 108
4.11 Calculated cross sectional areas of individual fibers 110
4.12 Statistical analysis of individual fibers (*E*-modulus) 110
4.13 *E*-modulii of fibers reported in literature 111
4.14 Area of the cross sections 112